Clustering Behaviour in Networks with Time Delayed All-to-all Coupling

by

Zhen Wang

A thesis
presented to the University of Waterloo
in fulfillment of the
thesis requirement for the degree of
Doctor of Philosophy
in
Applied Mathematics

Waterloo, Ontario, Canada, 2017

Examining Committee Membership

The following served on the Examining Committee for this thesis. The decision of the Examining Committee is by majority vote.

External Examiner	Victor LeBlanc Professor
Supervisor(s)	Sue Ann Campbell Professor
Internal Member	Brain Ingalls Associate Professor
Internal-external Member	Xuemin Shen Professor
Other Member(s)	Xinzhi Liu Professor

Author's Declaration

I hereby declare that I am the sole author of this thesis. This is a true copy of the thesis, including any required final revisions, as accepted by my examiners.

I understand that my thesis may be made electronically available to the public.

Abstract

Networks of coupled oscillators arise in a variety of areas. Clustering is a type of oscillatory network behavior where elements of a network segregate into groups. Elements within a group oscillate synchronously, while elements in different groups oscillate with a fixed phase difference. In this thesis, we study networks of N identical oscillators with time delayed, global circulant coupling with two approaches.

We first use the theory of weakly coupled oscillators to reduce the system of delay differential equations to a phase model where the time delay enters as a phase shift. We use the phase model to determine model independent existence and stability results for symmetric cluster solutions. We show that the presence of the time delay can lead to the coexistence of multiple stable clustering solutions.

We then perform stability and bifurcation analysis to the original system of delay differential equations with Z_N symmetry. We first study the existence of Hopf bifurcations induced by coupling time delay, and then use symmetric Hopf bifurcation theory to determine how these bifurcations lead to different patterns of symmetric cluster oscillations. We apply our results to two specific examples: a network of FitzHugh-Nagumo neurons with diffusive coupling and a network of Morris-Lecar neurons with synaptic coupling. In the case studies, we show how time delays in the coupling between neurons can give rise to switching between different stable cluster solutions, coexistence of multiple stable cluster solutions and solutions with multiple frequencies.

Acknowledgements

I would like to thank first and foremost my supervisor, Sue Ann Campbell. This work would not have been possible without her wise guidance and patient support.

I would also like to thank my committee members, Prof. Brain Ingalls and Prof. Xinzhi Liu for all their helpful suggestions and the meetings.

I would also like to express my sincere thanks to my friends that I have met over the last five years at Waterloo: Wilten Nicola, Matthew Kloosterman, Keegan Keplinger.

Dedication

This is dedicated to my husband, Chen Zhang.

Table of Contents

List of Tables

List of Figures

Chapter 1

Introduction

In this thesis we investigate the clustering behavior of networks of identical oscillators with time delayed, circulant coupling. Networks of coupled oscillators arise in a variety of areas, for example neural networks [59, 69], laser arrays [118, 119], flashing of fireflies [83], and movement of a slime mold [112]. A fundamental question about these systems is whether the elements will phase-lock, i.e., oscillate with some fixed phase difference, and how the physical parameters affect the answer to this question. Clustering is a type of phase locking behavior where the oscillators in a network separate into groups. Each group consists of fully synchronized oscillators, and different groups are phase-locked with nonzero phase difference. Symmetric clustering refers to the situation when all the groups are the same size while non-symmetric clustering means the groups have different sizes. The main subject of this thesis is to show that clustering behavior is a common feature shared by a wide class of delayed, circulant coupled networks.

While clustering solutions are important in many applications. Experimental evidence shows neural systems use cluster states to process environmental information and perform neurocomputation [92]. That is, a group of neurons transiently act together to achieve a particular purpose, which is called neural assembly. It has been proposed that neural assemblies are formed not just due to external inputs of the system, but also due to the intrinsic dynamics of the network. Mathematically, the intrinsic dynamics of the network should support solutions with multiple different grouping of neurons, with different neurons able to participate in multiple groupings. Further, switching between different groupings should be able to be achieved by changing the inputs to the network. Thus, the study of clustering behavior is a good candidate for this intrinsic dynamics in the formation of neural assembly [48].

The behaviour of coupled systems cannot be determined by simply understanding in-

dividual elements. The interaction between these elements may give rise to rich dynamical systems. Examples include, in neuron systems the dynamics of a single neuron (its structure, the evolution of the membrane potential and the ion transport) is well understood, and can be represented by a mathematical system of ordinary differential equations (ODEs). For instance, the Hodgkin-Huxley, Morris-Lecar, FitzHugh-Nagumo models [63, 84, 43, 85]. Moreover, the coupling of neurons can also be incorporated into the mathematical system directly, or by adding ODEs to describe the chemical/electrical processes. However, the interactions and collections of coupled neurons can present complex dynamics such as clustering, quasi-periodic solutions, chaos or even coexistence of the above solutions [91, 92, 93]. All such studies suggest that the system of globally coupled oscillators can exhibit unexpected rich behavior in spite of its simple form.

In these modelings, signal transmission is often considered to be instantaneous. In this thesis, we consider the signal transmission between different elements is not instantaneous, and include the propagation time, as a time delay. This results in delay differential equations (DDEs). Over the past decades, it has been shown that time delays are a fundamental reality for modeling of realistic biological and physical systems. Dynamically, time delays can lead to instability and occurrence of cluster solutions, and they can also stabilize unstable equilibrium points or cluster solutions, or even lead to multi-stability.

Phase models are one of the popular approaches used in the study of clustering in networks of oscillators. By assuming weak coupling, we are able to exploit an powerful analytic technique, phase model reduction. The phase models can be used to predict clustering behaviors in networks with any form of coupling. The phase model method allows one to reduce the dimension of differential equations for each element to a single differential equation which describes its phase. The phase equations take the form of a convolution of the input to the neuron via coupling and the neuron's infinitesimal phase response curves. The phase resetting curve measures the response to a small perturbation and acts like an impulse response function for the oscillating elements [39]. In particular, the effect of time delay can be neglected if the delay has the same magnitude as the period of oscillation [65], which greatly simplifies the analysis. However, the phase model method has its limits. To apply the phase model reduction, we need that the individual elements are intrinsically oscillatory, and the coupling between each elements must be "weak" for the prediction to be enough accurate.

With strong coupling if some of the elements in a network are not intrinsically oscillatory, stability and bifurcation analysis is another useful approach. This approach enables us to derive exact and explicit conditions of how the time delays affect the stability of equilibrium points, existence, stability and patterns of bifurcating cluster solutions.

This thesis is organized into six chapters, which are listed and summarized as follows.

Chapter 1. Introduction

A general introduction of this thesis.

Chapter 2. Biological Preliminaries

In this chapter, we will introduce the typical structure of neurons and synapses, and various ways of modeling single neurons, synapses, and networks of neurons. We will also introduce the Morris-Lecar and FitzHugh-Nagumo models. We will apply the theoretical analysis to those two models in chapters 4 and 5.

Chapter 3. Brief review of delay differential equations

In this chapter, we will introduce the mathematical prerequisites required in this thesis. In particular, we introduce some important results about the Hopf bifurcation and phase model reduction which will be required in later analysis.

Chapter 4. Phase models and clustering

In this chapter, we will apply the phase model analysis, and investigate the effect of time delayed coupling on the clustering behavior of oscillator networks with circulant coupling. Existence and stability of symmetric cluster solutions are determined. Moreover, a particular application, a network of Morris-Lecar oscillators, is considered theoretically and numerically.

Chapter 5. Symmetry, Hopf bifurcation and clustering

In chapter 5, we will investigate the Hopf bifurcations induced by the time delay in networks with time delay and circulant coupling. Analytically, we derive the conditions of Hopf bifurcation and patterns of bifurcating cluster solutions, and stability of bifurcating cluster solutions for specific models (networks of Morris-Lecar and FitzHugh-Nagumo oscillators).

Chapter 6. Conclusion and future directions

This chapter summarizes the results presented above, and outline some possible directions for future research.

Chapter 2

Biological Preliminaries

In this chapter, we present the biological background which is necessary in understanding the problems that we study. In section 2.1, we introduce neurons and their general functions. In section 2.2, we introduce a number of popular approaches that are used in modeling neurons. Further, we discuss the modeling of synapses that couple neurons together in section 2.3. From there, we develop the modeling for networks of neurons. As the neurons couple together, it is inevitable that time delays arise in the connection. Therefore, we introduce how to incorporate time delays in networks of neurons in section 2.4.

2.1 Neurons and synapses

The central nervous system of a human consists of two parts: the brain and the spinal cord, The brain itself consists of neurons and glial cells. Neurons are the basic signaling units of the nervous system, and glial cells are supportive units that maintain the health and function of neurons. Neurons are coupled together at junctions called synapses or gap junctions which are highly specialized for generating and transmitting action potentials in response to chemical and other inputs. Although neurons come in incredible variety of sizes and shapes, they share a typical structure (see Figure 2.1). The structure of a neuron can be divided into three parts: the dendrites, the soma and the axon. The dendrites branching out in a tree receive signals from other neurons, while the axon typically leaves the soma and branches out in order to connect to other neurons.

The action potential represents the change in the neuron's membrane potential, and is initialized at the soma, propagates along the axon to axon terminal boutons, then synaps-

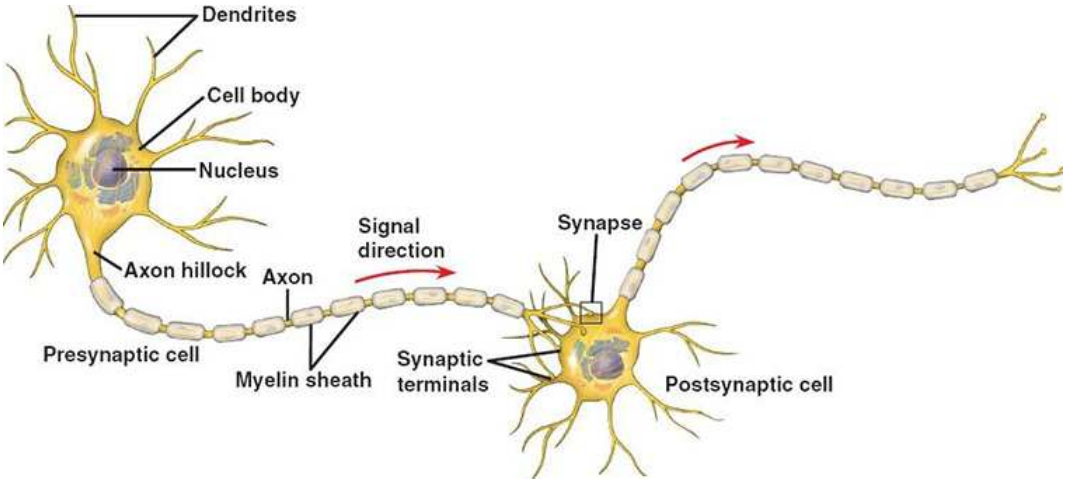

Figure 2.1: Typical structure of a neuron and a synapse. Figure is taken from [98].

es onto the dendritic arbors of other neurons. Synapses may be chemical or electrical. A chemical synapse consists of presynaptic and postsynaptic parts which are separated by a synaptic cleft (see Figure 2.2). When an action potential reaches the axon terminal, it triggers a chain of chemical reactions which lead to a release of a chemical substance, neurotransmitter, into the synaptic cleft. The neurotransmitter then diffuses across the synaptic cleft, combines with receptors of the postsynaptic neurons, and causes a change of membrane potential of the postsynaptic neuron An electrical synapse is more straightforward. The presynaptic and postsynaptic neurons are connected physically through special proteins, called gap junctions. The gap junction is a channel which allows ions to pass through it if it is open.

2.2 Modeling neurons

Conductance based models have a long and important history in the study of neuroscience, and are the most common formulation in neural modeling. They describe the initialization and propagation of action potentials on neurons based on an equivalent circuit representation of a cell membrane.

Consider each component of a cell as an electrical component. For example, the lipid bilayer are represented as a capacitance (C_m). Voltage-gated ion channels are represented by electrical conductances with conductance $\bar{g}_n$, where n represents the specific ions (like

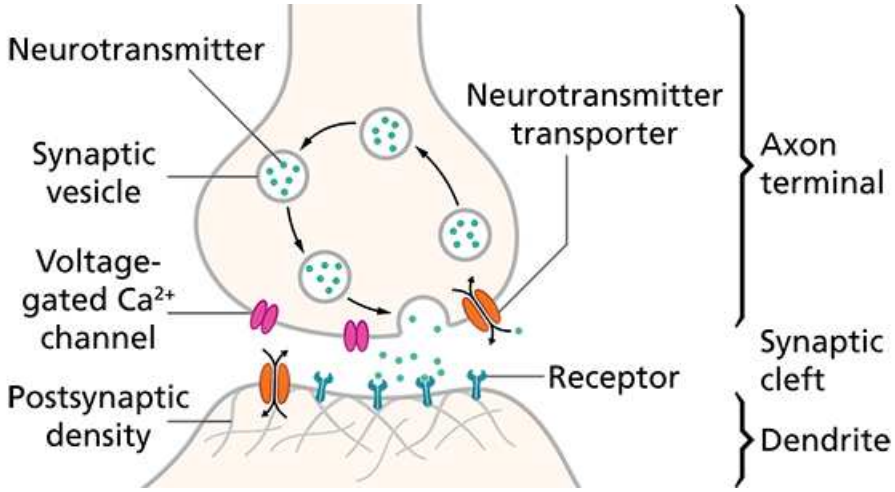

Figure 2.2: Typical structure of a chemical synapse. Figure is taken from [108].

Na^+, K^+, Ca^{2+}, or Cl^-). Denote V_m as the membrane potential. Therefore, the total membrane current $I_m(t)$ is the sum of the capacitive current and the ionic current

$$I_m(t) = I_C(t) + I_{ionic}(t).$$

Here I_C is the current flowing through the lipid bilayer and can be described as

$$I_C(t) = C_m \frac{dV_m}{dt}$$

and the current through an ion channel is

$$I_{ionic}(t) = \bar{g}_n(V_m - V_n),$$

where V_n is the reversal potential of the "n" ion channel.

Based on the study of the squid giant axon where Hodkgin and Huxley carried out a series of experiments and assuming there are voltage-gated K^+ and Na^+ channels and a

leak current, they [63] proposed a model consisting of four differential equations:

$$\begin{aligned} C_m\frac{dV_m}{dt} &= I_{app} - I_{Na} - I_K - I_L \\ &= I_{app} - \bar{g}_{Na}m^3h(V_m - V_{Na}) - \bar{g}_k n^4 h(V_m - V_k) - \bar{g}_L(V_m - V_L) \\ \frac{dm}{dt} &= \phi[\alpha_m(V_m)(1-m) - \beta_m(V_m)m] \\ \frac{dh}{dt} &= \phi[\alpha_h(V_m)(1-h) - \beta_h(V_m)h] \\ \frac{dn}{dt} &= \phi[\alpha_n(V_m)(1-n) - \beta_n(V_m)n] \end{aligned} \tag{2.1}$$

where m, n, h represent the activation and inactivation variable of the corresponding ion channels, and $\alpha(V_m), \beta(V_m)$ are voltage-dependent rate constants for different ions. ϕ is referred to as a temperature factor.

The Morris-Lecar model is a two dimensional "reduced" model developed by Morris and Lecar [84] in the study of the muscle fiber of the giant barnacle. There are two voltage-gated currents, Na^+ and Ca^{2+}. Assuming the calcium current depends instantaneously on the voltage, the Morris-Lecar equation have the form

$$\begin{aligned} C_m\frac{dV_m}{dt} &= I_{app} - \bar{g}_K M(V_m - V_k) - \bar{g}_{Ca}C_\infty(V_m)(V_m - V_{Ca}) - \bar{g}_L(V_m - V_L), \\ \frac{dM}{dt} &= \phi(M_\infty(V_m) - M)\lambda(V_m). \end{aligned} \tag{2.2}$$

where

$$\begin{aligned} C_\infty(V) &= \frac{1}{2}(1 + \tanh\frac{V-\nu_1}{\nu_2}), \\ \lambda_\infty(V) &= \cosh^{-1}(\frac{V-\nu_3}{2\nu_4}), \\ M_\infty(V) &= \frac{1}{2}(1 + \tanh(\frac{V-\nu_3}{\nu_4})). \end{aligned}$$

Here ν_1, ν_2, ν_3 and ν_4 are parameters chosen to fit voltage clamp data.

The Morris-Lecar equation generates action potentials, there is a threshold for firing and there are several mechanisms for the generation of oscillatory behavior. Considering the nullclines of (2.2) (see Figure 2.3 for examples), the V_m-nullcline has a cubic shape, while the m nullcline is a monotonically increasing function. Fitzhugh and Nagumo [43, 85]

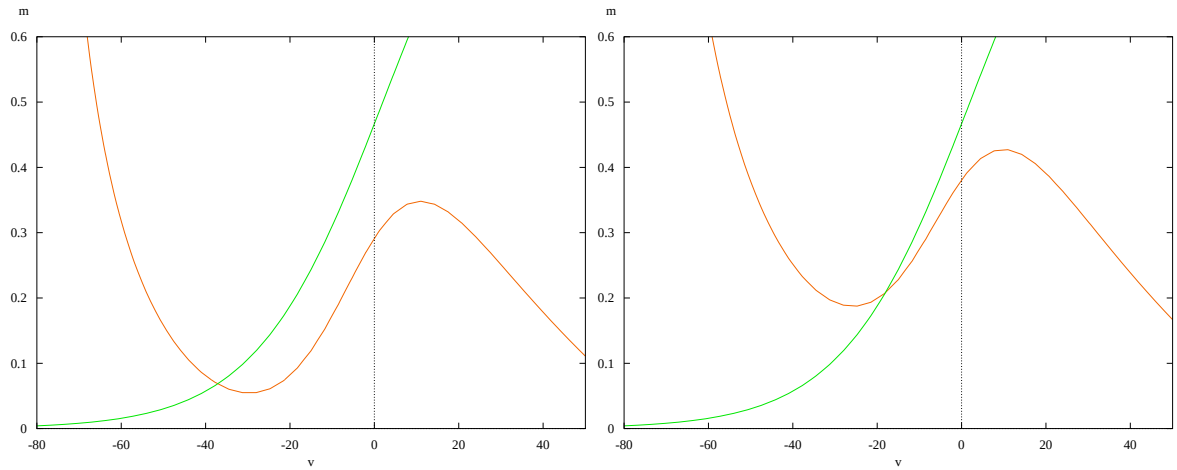

(a) $I_{app} = 60$ (b) $I_{app} = 120$

Figure 2.3: Nullclines for the Morris-Lecar model for (a) $I_{app} = 60$, (b) $I_{app} = 120$. The other parameters are as in [41, Table 3.1].

captured the essence of the cubic properties of the V_m nullclines and many other more complicated behaviors of (2.1) and (2.2), proposed the model:

$$\mu \frac{dx}{dt} = x - x^3 - y + I_{app},$$
$$\frac{dy}{dt} = x - a - by.$$

Here μ is a time scale parameter corresponding to fast activation variable V and slow variable m when choosing μ to be small.

Beside the ones above, other conductance based models include the Connor-Stevens model [25], the Wang-Buzsaki model [114] and Hindmarsh-Rose model [62]. A great advantage of the conductance based model is that one can incorporate many ion channels. Furthermore, all the parameters inside can be fitted experimentally to a specific neuron. These enable us to model a neuron accurately. However, the conductance based models also have some draw backs. As the number of ion channels increases, the model becomes difficult to analyze, therefore, to understand the dynamics.

2.3 Modeling synapses and networks of neurons

To extend the modeling from a single neuron to networks, we need to understand and model the synaptic current, I_{syn}. Therefore, any kind of synapse between neurons could then be modeled as adding I_{syn} in the voltage equation of the post-synaptic neurons. We introduce the modeling of synapses for chemical synapses and gap junction, respectively. Finally, we state the full network equations.

2.3.1 Modeling of chemical synapses

A chemical synapse involves a sequence of chemical reactions in both the presynaptic and postsynaptic neurons. See Figure 2.2. The simplest (and quite commonly used) model considers the synapse as another ion channel on the membrane of the postsynaptic neuron with a gating variable that depends on the voltage of the presynaptic neuron. Thus, the synaptic current could be expressed as

$$I_{syn} = g_{syn} s(t)(V_m - V_{syn}), \tag{2.3}$$

where g_{syn} represents the maximum conductance of the synapse, $s(t)$ is the time-dependent proportion of open channels, and V_{syn} is the reversal potential for the synapse. Therefore, $s(t)$ is between $[0, 1]$, and is zero if the presynaptic neuron is not firing.

Consider a network of N neurons, the total synaptic current the ith postsynaptic neuron receives can be written as

$$I_{syn,i} = \sum_{j=1}^{N} g_{syn,ij} s_{ij}(t)(V_{m,j} - V_{syn,ij}) \tag{2.4}$$

where $g_{syn,ij}$ is the maximum synaptic conductance of the synapse connecting neuron i and neuron j. For more details of the modeling of $s_{ij}(t)$, see [41].

2.3.2 Modeling of gap junctions

Considering the gap junction as a resistor connecting the presynaptic and post-synaptic neurons, the gap junction current can be modeled by

$$I_{gap} = g_{gap}(V_{post} - V_{pre}), \tag{2.5}$$

where g_{gap} is the conductance, and $V_{post} - V_{pre}$ is the voltage difference of the postsynaptic and presynaptic neurons.

Therefore, in a network of N neurons, the total synaptic current the ith neuron receives can be written as

$$I_{gap,i} = \sum_{j=1}^{N} g_{gap,ij}(V_{m,j} - V_{m,i}) \tag{2.6}$$

where $g_{syn,ij}$ is the maximum synaptic conductance of the synapse connecting neuron i and neuron j. For more details of the modeling of $s_{ij}(t)$, see [41].

We now can state the general form of a network of neurons

$$C_{m,i}\frac{dV_{m,i}}{dt} = I_{app,i} - I_{ionic} - I_{syn,i}(\text{ or } I_{gap,i}). \tag{2.7}$$

2.4 Time delay in networks of neurons

Time delay is an inevitable and important factor in the modeling of biophysical models. In particular, it plays an important role in improving our understanding of neural networks. Considering the dynamical behavior, time delay may lead to oscillation, or destroy an oscillation, or change stability of an existing oscillation. Campbell [16] gave a detailed discussion of how to incorporate the time delay into models by delay differential equations. We briefly summarize the results here.

We first formulate the general model for a network of N neurons:

$$x_i'(t) = f_i(x_i(t)) + \sum_{j=1}^{N} f_{ij}(x_i(t), x_j(t)),\ i = 1, \ldots, N. \tag{2.8}$$

where x_i represents all the variables that describes the state of the i^{th} neuron in the network, and f_{ij} is the coupling function which describes the dynamics between the i^{th} neuron and j^{th} neuron. In model (2.8), the transmission of signals between different neurons is simultaneous. That is, when an action potential is generated in neuron j, it is immediately felt by all other neurons that connect to it. However, in reality, the action potential must travel along the presynaptic neuron, and cross the synapse/gap junction to reach the postsynaptic neuron, which are the two main sources of time delays in the neural network.

First, the axonal conduction delay is the time required for an action potential to travel from its initiation site near the neuronal soma to the axon terminals [111]. To incorporate

this aspect into the model, a simple way is to include a time delay in the coupling term. Thus, the coupling function becomes

$$f_{ij}(x_i(t), x_j(t - \tau_j)), \tag{2.9}$$

where $\tau_j > 0$ represents the time taken for the action potential to propagate along the axon of the j^{th} neuron.

Processing delay is the time delay due to the transmission of signals through the synapse, that is, the time difference between the action potential of neuron j reaches the synapse and an action potential is felt by neuron i. There are two ways of modeling the processing delay. One way is to add an equation into the model equation to describe the dynamical properties of the synapse as discussed in the previous section; another way is to simply add another delay into (2.10), which can be achieved by adding another delay term τ_{ij} in (2.10)). That is, the coupling function becomes

$$f_{ij}(x_i(t), x_j(t - (\tau_j + \tau_{ij}))), \tag{2.10}$$

In above, we assume that the delays, τ_j, τ_{ij}, are fixed constants. However, in reality, they may vary slightly every time an action potential is propagated from neuron j to neuron i even for identical neurons. Therefore, we may consider time dependent delays, $\tau_j(t)$, $\tau_{ij}(t)$ with $0 \leq \tau_j(t), \tau_{ij}(t) \leq \tau_{ij}$ for some constant $\tau_{ij} > 0$.

Chapter 3

Brief review of delay differential equations

In this chapter, we introduce some important mathematical prerequisites needed to understand the rest of the thesis. In sections 3.1 we define delay differential equations (DDEs) and the corresponding initial value problem, then state existence and uniqueness theorems. We then focus on DDEs with discrete delays, present the local and global stability results for equilibrium points in section 3.2, and introduce concepts of stability for periodic solutions in section 3.3. A general Hopf bifurcation theorem is provided in section 3.4. Furthermore, Hopf bifurcation for networks with symmetry is introduced in section 3.5. Finally, we present the weakly connected theory for phase model reduction.

3.1 Definition, initial value problem, existence and uniqueness theorem

A delay differential equation is a differential equation which has the past dependence through the state variables and not the derivative of the state variables.

In order to state the formal definition of a DDE, we first introduce some terminology. Let $\mathcal{C} = C([-\tau, 0], \mathbb{R}^N)$ denote the Banach space of continuous functions mapping the interval $[-\tau, 0]$ into $\mathbb{R}^N$ with supremum norm, i.e., for $\phi \in \mathcal{C}$, $||\phi|| = \max_{-\tau \leq s \leq 0} |\phi(s)|$ with $|\cdot|$ the Euclidean norm in $\mathbb{R}^N$. Suppose $x(t) \in C([-\tau, A], \mathbb{R}^N)$. Then for any $t \in [0, A]$, define $x_t(\theta) = x(t + \theta)$, $\theta \in [-\tau, 0]$. It is easy to see that since $x(t)$ is continuous from $[-\tau, A]$, then x_t is a continuous function of t for $t \in [0, A]$ [57]. For $D \subset \mathbb{R}^N$, let $\mathcal{C}_D = C([-\tau, 0], D)$ denote the set of continuous functions mapping $[-\tau, 0]$ into D.

A general type of DDE is in the following form

$$x'(t) = f(t, x_t). \tag{3.1}$$

In particular, a general equation with n discrete delays can be written as

$$x'(t) = f(t, x(t), x(t-\tau_1), x(t-\tau_2), \cdots, x(t-\tau_n)).$$

In this case, the above $\tau = \max\{\tau_1, \tau_2, \cdots, \tau_n\}$.

For a given $t_0 \in J \subset \mathbb{R}$ and $\phi_0 \in \mathcal{C}_D$, the initial value problem associated with (3.1) is

$$\begin{aligned} x'(t) &= f(t, x_t), \ t > t_0, \\ x_{t_0} &= \phi_0. \end{aligned} \tag{3.2}$$

Definition 1. *A function $x(t)$ is said to be a solution of (3.2) on $[t_0 - \tau, \beta]$ if there are $t_0, \beta \in \mathbb{R}$ such that $x \in C([t_0-\tau, \beta], D)$, $[t_0-\tau, \beta] \subset J$ and $x(t)$ satisfies (3.2) on $[t_0-\tau, \beta]$.*

Theorem 1. *[58, Lemma 1.1, section 2.1] Finding a solution of the IVP (3.2) is equivalent to solving the integral equation*

$$\begin{aligned} x(t) &= \phi_0(0) + \int_{t_0}^{t} f(s, x_s)ds, \ t_0 \le t \le \beta, \\ x_{t_0} &= \phi_0. \end{aligned} \tag{3.3}$$

Definition 2. *Let $f : J \times \mathcal{C}_D \to \mathbb{R}^N$ and let $S \subset J \times \mathcal{C}_D$. Then f is Lipschitz on S if there exists a constant $L \ge 0$ such that*

$$|f(t, \phi) - f(t, \psi)| \le L||\phi - \psi|| \tag{3.4}$$

whenever (t, ϕ), $(t, \psi) \in S$. f is called locally Lipschitz if for each given $(\bar{t}, \bar{\psi})$ there exists numbers $a > 0, b > 0$ such that $\mathcal{E} = ([\bar{t} - a, \bar{t} + a] \cap J) \times \{\psi \in \mathcal{C}_D, ||\psi - \bar{\psi}|| < b\}$ is a subset of $J \times \mathcal{C}_D$, and f is Lipschitz in $\mathcal{E}$.

Theorem 2 (Local Existence)**.** *[58, Theorem 2.1, section 2.2] Assume $J \times \mathcal{C}_D$ is an open set in $\mathbb{R} \times \mathcal{C}$, and $f : J \times \mathcal{C}_D \to \mathbb{R}^N$ is continuous on its domain. If $(t_0, \phi_0) \in J \times \mathcal{C}_D$, then there exists a solution of the initial value problem (3.2) passing through (t_0, ϕ_0) on $[t_0 - \tau, t_0 + \delta)$ for some $\delta > 0$.*

Theorem 3 (Uniqueness)**.** *[58, Theorem 2.2, section 2.2] Suppose $J \times \mathcal{C}_D$ is an open set in $\mathbb{R} \times \mathcal{C}$, and $f : J \times \mathcal{C}_D \to \mathbb{R}^N$ is continuous and Lipschitz on each compact set of $J \times \mathcal{C}_D$. If $(t_0, \phi_0) \in J \times \mathcal{C}_D$, then there exists a unique solution of the initial value problem (3.2) passing through (t_0, ϕ_0).*

Definition 3 (Non-continuable solutions). *[58, section 2.3] Define $x(t) \in (t_0 - \tau, \beta_1)$ and $y(t) \in (t_0 - \tau, \beta_2)$ be two solutions for (3.2). If $\beta_2 > \beta_1$, and $x(t) = y(t)$ for $t \in [t_0 - \tau, \beta_1)$, we say that y is a continuation of $x(t)$. A solution is non-continuable if it has no continuation.*

Theorem 4 (Global Existence). *[58, Theorem 3.3, section 2.3] Let $f : (t_0, \alpha) \times \mathcal{C} \to \mathbb{R}^N$ be continuous and locally Lipschitz. If $|f(t, \phi)| \leq M(t) + N(t)||\phi||$ on $[t_0, \alpha) \times \mathcal{C}$. Here M and N are continuous, positive functions on $[t_0, \alpha)$. Then the unique non-continuable solution of (3.2) exists on the entire interval $[t_0, \alpha)$.*

3.2 Equilibrium, linearization, characteristic equation

An equilibrium point of (3.1) is a constant solution $x(t) = x^*$ for all $t \in \mathbb{R}$ that satisfies

$$f(t, x^*) = 0, \text{ for all } t \in \mathbb{R}.$$

Since all the systems that we consider in this thesis are autonomous, that is,

$$x'(t) = f(x_t). \tag{3.5}$$

we give the stability results for autonomous systems only. Therefore, without loss of generality we drop the dependence on t_0, and denote the solution of (3.5) passing through (t_0, ϕ_0) by $x(t; \phi_0)$.

Definition 4. *Assume x^* is an equilibrium point of (3.5).*

1. *x^* is said to be stable if for any $\epsilon > 0$, there is a $\delta = \delta(\epsilon)$ such that $||\phi_0 - x^*|| < \delta$ implies $|x(t; \phi_0) - x^*| < \epsilon$ for all $t \geq t_0$. Otherwise, it is called unstable.*
2. *x^* is said to be asymptotically stable if it is stable and there is a $b = b(\delta) > 0$ such that $||\phi_0 - x^*|| < b$ implies $\lim_{t\to\infty} |x(t; \phi_0) - x^*| = 0$.*
3. *x^* is called globally asymptotically stable if all solutions $x(t; \phi_0)$ tend to x^* as $t \to \infty$.*

The general form of a linear autonomous DDE is

$$x'(t) = L(x_t). \tag{3.6}$$

where $L : \mathcal{C} \to \mathbb{R}^N$ is continuous and linear. According to the Riesz Representation Theorem, (3.6) can be represented as

$$x'(t) = \int_{-\infty}^{0} [d\eta(\theta)]x(t+\theta), \tag{3.7}$$

where η is an $N \times N$ matrix of functions of bounded variation on $(-\infty, 0]$ and the integral is a Riemann-Stiltjes integral.

Definition 5. *[109, Definition 1.4] The function given by*

$$\Delta(\lambda) = Det(\lambda I - \int_{-\infty}^{0} e^{\lambda\theta} d\eta(\theta)). \tag{3.8}$$

is the characteristic function corresponding to the linear autonomous system (3.6), where I is the $N \times N$ identity matrix.

For example, consider the discrete DDE

$$x'(t) = Ax(t) + Bx(t-\tau), \tag{3.9}$$

where A and B are $N \times N$ matrices. The characteristic equation of (3.9) is

$$\Delta(\lambda) = \mathrm{Det}(\lambda I - A - Be^{-\lambda\tau}) = 0$$

The behavior of solutions of (3.5) in a neighborhood of equilibrium point x^* can be determined by the stability of zero equilibrium of the corresponding linearized system. See Theorem 5 below.

The behavior of solutions of (3.6) can be more complicated than for linear ordinary differential equations (ODEs) even when $n = 1$. This is because (3.6) may have infinitely many linearly independent solution $e^{\lambda t}$ with λ being an eigenvalue, i.e., a root of the characteristic equation (3.8). In particular, the infinite-dimensional problem (3.6) leads to a transcendental equation (3.8) rather than a polynomial as occurs for the ODE case. Therefore, (3.8) may have multiple roots on the imaginary axis which will lead to complicated critical cases. On the other hand, note that the number of zeros of the characteristic equation on the imaginary axis must be finite.

In the rest of this chapter, we let (3.6) denote the linearization equation of (3.5) at equilibrium x^*.

Theorem 5. *[72, Theorem 4.1, section 2.4] In equation (3.8), if* $\sup\{Re(\lambda) : \Delta(\lambda) = 0\} < 0$, *then* x^* *is asymptotically stable. If* $Re(\lambda) > 0$ *for some* λ *satisfying (3.8), then* x^* *is unstable. Moreover, if* $\Delta(\lambda)$ *has a non-simple root with zero real part, then* x^* *is also unstable.*

The above theorem shows us how to determine the local stability of an equilibrium point. We next introduce a result which uses the method of Liapunov functional to determine global stability of an equilibrium point of autonomous system (3.5). For simplicity, we further assume that the equilibrium point is $x^* = 0$.

Suppose f in (3.5) is completely continuous and solutions of (3.5) depend continuously on the initial condition. Let $V : \mathcal{C} \to \mathbb{R}$ be continuous, and define the derivative of V along the solutions of (3.5) as

$$\dot{V} = \dot{V}(\phi) = \lim_{h \to 0^+} \sup \frac{1}{h}(V(x_h(\phi)) - V(\phi)).$$

Definition 6. *[57, Definition 3.1, section 5.3] We say* $V : \mathcal{C} \to \mathbb{R}$ *is a Liapunov functional on a set* G *in* $\mathcal{C}$ *relative to equation (3.5) if* V *is continuous on* CLG, *the closure of* G *and* $\dot{V} \leq 0$ *on* G. *Let*

$$\begin{aligned} S &= \{\phi \in CLG : \dot{V}(\phi) = 0\}, \\ M &= \textit{Largest set in } S \textit{ which is invariant with respect to (3.5).} \end{aligned} \tag{3.10}$$

Theorem 6. *[57, Theorem 3.1, section 5.3] If* V *is locally Lipschitz, and is a Liapunov functional on* G *and* $x(t; \phi_0)$ *is a bounded solution of (3.5) which remain in* G, *then* $x(t; \phi_0) \to M$ *as* $t \to \infty$.

Theorem 7 (Global asymptotic stability for autonomous systems)**.** *[57, Corollary 3.1, section 5.3] Suppose* f *is completely continuous, and* x^* *is an equilibrium point of (3.5). Suppose there exist nonnegative functions* $w(s)$, $u(s)$ *such that* $w(s), u(s) > 0$ *for* $s \neq 0$ *and* $w(0) = u(0) = 0$. *If there exists a continuous and locally Lipschitz functional* $V : \mathcal{C} \to \mathbb{R}$, *such that*

1. $u(|\phi(0)|) \leq V(\phi)$, *for any* $\phi \in \mathcal{C}$,
2. $\dot{V}(\phi) \leq -w(|\phi(0)|)$, *for any* $\phi \in \mathcal{C}$
3. $u(s) \to \infty$ *as* $s \to \infty$.

Then every solution of (3.5) approaches $x^* = 0$ *as* $t \to \infty$, *that is, the equilibrium solution* $x^* = 0$ *of (3.5) is globally asymptotically stable.*

3.3 Orbital stability of periodic solutions

In this section, we introduce the concept of orbital stability for periodic solutions. We begin by defining a distance function $d_1 : \mathbb{R}^N \times 2^{\mathbb{R}^N} \to \mathbb{R}$ between a set $A_1 \subset \mathbb{R}^N$ and a point $x \in \mathbb{R}^N$ with respect to the Euclidean metric,

$$d_1(x, A_1) = \inf_{y \in A_1} |x - y|. \tag{3.11}$$

We call this the point-to-set distance. Similarly, we define a distance function d_2 between a set $A_2 \subset \mathcal{C}$ and $\psi_0 \in \mathcal{C}$ as the point-to-set distance with respect to the supremum norm, that is

$$d_2(\psi_0, A_2) = \inf_{y \in A_2} ||\psi_0 - y||. \tag{3.12}$$

A solution $X(t)$ of the DDE (3.5) is called a periodic solution if it is not an equilibrium point and there exists a $T > 0$ such that $X(t + T) = X(t)$ for all t. Let $X_t(\theta) = X(t + \theta)$, $\theta \in [-\tau, 0]$. Denote the orbit, $\{X(t) : t \in [0, T]\}$, associated with a periodic solution $X(t)$ as $\hat{X}$, and $\{X_t(\theta) : t \in [0, T]\}$ as $\hat{X}_t$.

Definition 7. *(Orbital stability)[42, Definition 5.1.1] Let $X(t)$ be a periodic solution of (3.5) with orbit $\hat{X}$. The periodic orbit $\hat{X}$ is orbitally stable, if for every $\epsilon > 0$, there exists a $\delta(\epsilon) > 0$ such that $d_2(\psi_0, \hat{X}_t) < \delta$ implies $d_1(x(t; \psi_0), \hat{X}) \leq \epsilon$, $\forall t \geq 0$.*

Definition 8. *(Asymptotic orbital stability)[42, Definition 5.1.2] Let $X(t)$ be a periodic solution of (3.5) with orbit $\hat{X}$. The periodic orbit $\hat{X}$ is asymptotically orbitally stable if it is orbitally stable and there is a $\delta > 0$ such that $d_2(\psi_0, \hat{X}_t) \leq \delta$ implies $\lim_{t\to\infty} d_1(x(t; \psi_0), \hat{X}) = 0$.*

Definition 9. *(Exponential asymptotic orbital stability) Let $X(t)$ be a periodic solution of (3.5) with orbit $\hat{X}$. The periodic orbit $\hat{X}$ is exponentially asymptotically orbitally stable if there exist constants c_1, c_2, $\delta \geq 0$ such that $d_2(\psi_0, \hat{X}_t) \leq \delta$ implies that $d_1(x(t; \psi_0), \hat{X}) < d_2(\psi_0, \hat{X}_t) c_1 e^{-c_2 t}$.*

3.4 Hopf bifurcation for DDEs

In this section, we present the well-known method of establishing non-constant periodic solutions of autonomous DDEs - the so-called Hopf bifurcation. We consider a one parameter family of DDEs in the form

$$x'(t) = f(x_t, \alpha), \tag{3.13}$$

where $f(\phi, \alpha)$ has continuous first and secondary derivatives in ϕ, α for $\phi \in \mathcal{C}$ and $\alpha \in \mathbb{R}$. For simplicity, we assume $x^* = 0$ is an equilibrium point of (3.13), that is, $f(0, \alpha) = 0$.

Define $L : \mathcal{C} \times \mathbb{R} \to \mathbb{R}^N$ where $L(\alpha)$ is the linear operator at $x^* = 0$ of (3.13). Define $R(\phi, \alpha) = f(\phi, \alpha) - L(\alpha)\phi$.

Theorem 8 (Hopf bifurcation theorem)**.** *[72, Theorem 9.1, section 2.9]*

Assume $f(\phi, \alpha)$ has continuous first derivatives with respect to ϕ and α, $f(0, \alpha) = 0$ for all α, and

(H1) The linear system $x'(t) = L(\alpha_0)x_t$ has a simple pair of purely imaginary eigenvalues $\lambda_0^{\pm} = \pm i\omega_0 \neq 0$ and all other eigenvalues λ_j satisfies $\lambda_j \neq m\lambda_0^{\pm}$ for any integer m.

(H2) $Re\big(\frac{d\lambda}{d\alpha}|_{\alpha=\alpha_0}\big) \neq 0$.

Then there exists an $\epsilon > 0$ such that for $a \in \mathbb{R}$, $|a| \leq \epsilon$, there are functions $\alpha(a) \in \mathbb{R}$, $\omega(a) \in \mathbb{R}$ and an $\omega(a)$-periodic function $x^*(a)$ with all functions being continuously differentiable with $\alpha(0) = \alpha_0$, $\omega(0) = \omega_0$ and (3.13) has a $2\pi/\omega(a)$-periodic solution $x^*(a)(t)$. Furthermore, for $\alpha - \alpha_0 < \epsilon$, $2\pi/\omega(a) - 2\pi/\omega_0 < \epsilon$, every $2\pi/\omega(a)$-periodic solution $x(t)$ of (3.13) with $x(t) < \epsilon$ must be of this type except for a translation in phase. That is, there exists $a \in (-\epsilon, \epsilon)$ and $b \in \mathbb{R}$ such that $x(t) = x^*(a)(t + b)$ for all $t \in \mathbb{R}$.

We refer to the conclusions stated in this theorem as the Hopf bifurcation theorem. We next present a normal form analysis of the standard Hopf bifurcation. Normal form theory is a powerful tool in the study of nonlinear dynamical systems. In particular in the stability and bifurcation analysis. The basic idea of normal form theory is using successive near-identity nonlinear transformations that lead to a differential equation in a simpler form which is quantitatively equivalent to the original system in the vicinity of an equilibrium point. Please refer to [72, 56] for details of the development of the normal form for Hopf bifurcation of DDEs. Here, we state the result with respect to the normal form of Hopf bifurcation in polar coordinates directly:

$$\begin{aligned} r' &= \alpha(a)r + \beta_1(a)r^3 + \mathcal{O}(r^5), \\ \theta' &= \omega(a) + \beta_2(a)r^2 + \mathcal{O}(r^4). \end{aligned} \tag{3.14}$$

where $\alpha(0) = \alpha_0$ and $\omega(0) = \omega_0$. Since we are interested in the dynamics near $a = 0$, it is natural to Taylor expand the right hand side of (3.14) at $a = 0$. Neglecting the higher order parts, we have

$$\begin{aligned} r' &= d_1 ar + d_2 r^3, \\ \theta' &= \omega_0 + d_3 a + d_4 r^2. \end{aligned} \tag{3.15}$$

where $\alpha'(0) = d_1$, $\beta_1(0) = d_2$, $\omega'(0) = d_3$, $\beta_2(0) = d_4$.

Theorem 9. *[117, section 20.2] Depending on the signs of d_1, d_2, system (3.15) has the following behaviors.*

1. *$d_1 > 0, d_2 > 0$. The equilibrium point is unstable when $a > 0$ and asymptotically stable for $a < 0$ with an unstable periodic orbit for $a < 0$.*
2. *$d_1 > 0, d_2 < 0$. The equilibrium point is asymptotically stable when $a < 0$ and unstable when $a > 0$ with an asymptotically stable periodic orbit for $a > 0$.*
3. *$d_1 < 0, d_2 > 0$. The equilibrium point is unstable when $a < 0$ and asymptotically stable for $a > 0$ with an unstable periodic orbit for $a < 0$.*
4. *$d_1 < 0, d_2 < 0$. The equilibrium point is asymptotically stable when $a < 0$ and unstable for $a > 0$ with an asymptotically stable periodic orbit for $a < 0$.*

3.5 Hopf bifurcation for symmetric DDEs

In this section, we briefly introduce results determining patterns of Hopf bifurcating periodic solutions for DDEs with symmetry. We first write the DDE in the following form

$$x'(t) = f(x_t, \alpha) = L(\alpha)x_t + R(x_t, \alpha); \tag{3.16}$$

where $R(0, \alpha) = 0$ and $\frac{\partial}{\partial \phi} R(0, \alpha) = 0$ for $\alpha \in \mathbb{R}$ and $\phi \in \mathcal{C}$.

It is well-known that [58] for each fixed α, the linear system (3.6) generates a strongly continuous semigroup of linear operators with the infinitesimal generator $A(\alpha)$ given by

$$A(\alpha)\phi = \dot{\phi}, \ \phi \in \ \mathrm{Dom}(A(\alpha)),$$
$$\mathrm{Dom}(A(\alpha)) = \{\phi \in \mathcal{C} : \dot{\phi} \in \mathcal{C}, \ \dot{\phi}(0) = L(\alpha)\phi\}.$$

Moreover, the spectrum of $A(\alpha)$ consists of eigenvalues which are solutions of the following characteristic equation

$$\mathrm{Det}\Delta(\lambda, \alpha) = 0 \tag{3.17}$$

with $\Delta(\lambda, \alpha)$ the characteristic matrix which can also be rewritten as

$$\Delta(\lambda, \alpha) = \lambda I - L(\alpha)(e^{\lambda} I) \tag{3.18}$$

Assume that

(A1) The characteristic matrix is continuously differentiable in $\alpha \in \mathbb{R}$ and there exist $\alpha_0 \in \mathbb{R}$ and $\omega_0 > 0$ such that

(i) $A(\alpha_0)$ has eigenvalues $\pm i\omega_0^{\pm}$;

(ii) The generalized eigenspace, denoted by $U_{i\omega_0}(A(\alpha_0))$, of these eigenvalues $\pm i\omega_0^{\pm}$, consists of eigenvectors of $A(\alpha_0)$;

(iii) All other eigenvalues of $A(\alpha_0)$ are not integer multiple of $\pm i\omega_0^{\pm}$.

(A2) There exists a compact Lie group Γ acting on $\mathbb{R}^N$ such that f is Γ-equivariant, i.e. $f(\gamma\phi, \alpha) = \gamma f(\phi, \alpha)$ for $(\alpha, \gamma, \phi) \in \mathbb{R} \times \Gamma \times \mathcal{C}$. Here $\gamma\phi \in \mathcal{C}$ is given by $(\gamma\phi)(s) = \gamma\phi(s)$ for $s \in [-\tau, 0]$.

(A3) There exists an m-dimensional absolutely irreducible representation V of Γ such that $\mathrm{Ker}\Delta(i\omega_0, \alpha_0)$ is isomorphic to $V \oplus V$. Here a representation V of Γ is absolutely irreducible if the only linear mapping that commutes with the action of Γ is a scalar multiple of the identity.

(A4) $\mathrm{Re}\big(\frac{d\lambda}{d\alpha}|_{\alpha=\alpha_0}\big) \neq 0$.

Denote $\mathcal{T} = \frac{2\pi}{\omega_0}$. Denote $P_{\mathcal{T}}$ the Banach space of all continuous $\mathcal{T}$-periodic mappings $x : \mathbb{R} \to \mathbb{R}^N$. Then $\Gamma \times S^1$ acts on $P^{\mathcal{T}}$ by

$$(\gamma, \theta)x(t) = \gamma x(t + \theta), \ (\gamma, \theta) \in \Gamma \times S^1, \ x \in P_{\mathcal{T}}.$$

Denote by $SP_{\mathcal{T}}$ the subspace of $P_{\mathcal{T}}$ consisting of all $\mathcal{T}$ periodic solutions of (3.16) when $\alpha = \alpha_0$. Then for each subgroup $\Sigma \subset \Gamma \times S^1$, the fixed point set

$$\mathrm{Fix}(\Sigma, SP_{\mathcal{T}}) = \{x \in SP_{\mathcal{T}} : \ (\gamma, \theta)x = x, \ \text{for all } (\gamma, \theta) \in \Sigma.\}$$

is a subspace.

Theorem 10. *[120, Theorem 2.1] Assume that (A1)-(A4) are satisfied and dim Fix$(\Sigma, SP_{\mathcal{T}}) = 2$ for some $\Sigma \subset \Gamma \times S^1$. Then for a chosen basis ϵ_1, ϵ_2 of Fix$(\Sigma, SP_{\mathcal{T}})$ there exist constants $a_0 > 0$, $a_0^* > 0$, $\sigma_0 > 0$, functions $\alpha : \mathbb{R}^2 \to \mathbb{R}$, $\mathcal{T}^* : \mathbb{R}^2 \to \mathbb{R}$ and a continuous function $x^* : \mathbb{R}^2 \to \mathbb{R}^N$, with all functions being continuously differentiable in $a \in \mathbb{R}^2$ with $|a| \leq a_0$, such that $x^*(a)(t)$ is a $\mathcal{T}^*(a)$-periodic solution of (3.16) with $\alpha = \alpha(a)$, and*

$$\gamma x^*(a)(t) = x^*(a)(t - \frac{\mathcal{T}^*(a)}{\mathcal{T}}\theta), \ (\gamma, \theta) \in \Sigma,$$
$$x^*(0) = 0, \ \mathcal{T}^*(0) = \mathcal{T}, \ \alpha(0) = \alpha_0.$$

Furthermore, for $|\alpha - \alpha_0| < \alpha_0^*, |\mathcal{T}^* - \mathcal{T}| < \sigma_0$, every $\mathcal{T}^*$-periodic solution of (3.16) with $||x_t|| < \sigma_0$, $\gamma x(t) = x(t - \frac{\mathcal{T}^*}{\mathcal{T}}\theta)$ for $(\gamma, \theta) \in \Sigma$, $t \in \mathbb{R}$, must be of the above type.

3.6 Phase model reduction

In this section, we consider weakly connected networks of oscillators, which usually can be written as

$$X_i' = F_i(X_i) + \varepsilon G_i(X_1, \ldots, X_N),\ i = 1, \ldots, N. \tag{3.19}$$

where $X_i \in \mathbb{R}^m$, and ε is a small parameter. When $\varepsilon = 0$, we obtain N uncoupled systems

$$X_i' = F_i(X_i),\ i = 1, \ldots N. \tag{3.20}$$

Assume that each subsystem of (3.20) has an exponentially orbitally stable limit cycle attractor σ_i with period T_i which is the minimum positive number such that $\sigma_i(t) = \sigma_i(t + T_i)$ for all $t \in \mathbb{R}$. $\Omega_i = 2\pi/T_i$ is called the natural frequency of limit cycle σ_i.

Note that the limit cycle σ_i is a closed periodic solution, and any solution $X_i(t)$ of the i^{th} subsystem of (3.20) with initial condition $X_i(0) \in \sigma_i$ stays on σ_i forever. Moreover, we can parameterize the limit cycle by a single variable, the phase, in the phase space. Let $X_i(t)$ be any solution of the i^{th} subsystem of (3.20) with initial condition $X_i(0) = X_{i0} \in \sigma_i$. Since the limit cycle σ_i is a T_i-periodic solution, for any $t_0 \in [0, T_i)$, there exists a unique point, $p \in \sigma_i$ such that $p = X_i(t_0)$. Based on that, we then define a map: $\theta_i : [0, 2\pi) \to \mathbb{R}^m$ as that $\theta_i(0) = X_{i0}$, and $\theta_i(t) = X_i(\theta_i(t)/\Omega)$ (see Figure 3.1). As θ_i travels between 0 and 2π, the points with coordinates $X_i(\theta/\Omega)$ makes one full trip along the limit cycle σ_i. By similar analysis for all the other subsystems of (3.20), we have that system (3.20) is equivalent to the next N scalar equations along the limit cycles:

$$\begin{aligned}
\theta_1(t) &= \theta_1^0 + \Omega_1 t,\ \mod 2\pi \\
\theta_2(t) &= \theta_2^0 + \Omega_2 t,\ \mod 2\pi \\
&\vdots \\
\theta_N(t) &= \theta_N^0 + \Omega_N t,\ \mod 2\pi
\end{aligned}$$

Notice that in the definition of map θ_i, the initial value X_{i0} is arbitrary. Therefore, we can choose appropriate X_{i0} such that $\theta_i^0 = 0$, $i = 1, \ldots, N$.

By the assumption that the limit cycles are exponentially orbitally stable, a limit cycle still exists for the full system (3.19) under small perturbation (ε is sufficiently small) [64],

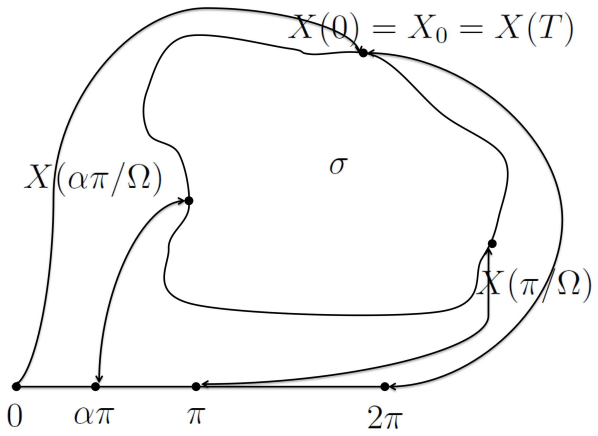

Figure 3.1: The parametrization of the limit cycle σ by the points in an interval $[0, 2\pi)$

but with phase deviation

$$\begin{aligned} \theta_1(t) &= \Omega_1 t + \vartheta_1(t), \\ \theta_2(t) &= \Omega_2 t + \vartheta_2(t), \\ &\vdots \\ \theta_N(t) &= \Omega_N t + \vartheta_N(t), \end{aligned}$$

where $\vartheta_i(t)$ is the phase deviation of the i^{th} subsystem from its natual phase due to the influence from other connected oscillators. To write the system in the form of a differential equation, we have

$$\begin{aligned} \theta_1' &= \Omega_1 + \varepsilon g_1(\theta_1, \ldots, \theta_N) \\ \theta_2' &= \Omega_2 + \varepsilon g_2(\theta_1, \ldots, \theta_N) \\ &\vdots \\ \theta_N' &= \Omega_N + \varepsilon g_N(\theta_1, \ldots, \theta_N) \end{aligned} \tag{3.21}$$

Hoppensteadt and Izhikevich [64] summarized the above discussion into the next theorem and gave a detailed theoretical proof based on the invariant manifold reduction.

Theorem 11. ([64, Theorem 9.1, section 9.2])

Consider a family of weakly connected systems (3.19) such that each equation in the uncoupled system (3.20) has an exponentially orbitally stable limit cycle attractor $\sigma_i \subset \mathbb{R}^m$

having natural frequency $\Omega_i \neq 0$. *Then the dynamical system (3.21) defined on the* N*-torus* $T^N = S^1 \times S^1 \times \cdots \times S^1$ *is a local model for (3.19). That is, there is an open neighborhood* W *of* $M = \sigma_1 \times \sigma_2 \times \cdots \times \sigma_N \in \mathbb{R}^{mN}$ *and a continuous function* $h : W \to T^N$ *that maps solutions of (3.19) to those of (3.21).*

Remark 1. *Since in the thesis research, we consider mainly the case that all the neurons inside a network are identical, we then have* $F_1 = F_2 = \cdots = F_N \equiv F$. *Furthermore, we have* $\sigma_1 = \sigma_2 = \cdots = \sigma_N \equiv \sigma$, $T_1 = T_2 = \cdots = T_N \equiv T$, *and* $\Omega_1 = \Omega_2 = \cdots = \Omega_N \equiv \Omega$.

Consider the weakly connected network of N identical neurons with time delay:

$$X_i'(t) = F(X_i(t)) + \varepsilon G_i(X_1(t-\tau_1), \ldots, X_N(t-\tau_N)),\ i = 1, \ldots, N. \tag{3.22}$$

Assume that each subsystem $X_i'(t) = F(X_i(t))$, $X_i \in \mathbb{R}^m$, has an exponentially orbitally stable limit cycle σ with natural frequency $\Omega = 2\pi/T$. The next two results are originally taken from the main result and its proof in [65], and give an explicit formula for computation of the phase models.

Theorem 12. ([64, Theorem 9.2, section 9.2.1], [68, Theorem 3.2.1])

Assume that there exists $\varepsilon > 0$, *such that the normally hyperbolic invariant manifold* $M = \sigma \times \cdots \times \sigma \subset \mathbb{R}^{mN}$ *of system (3.22) persists for all* ε *such that* $0 < |\varepsilon| < \varepsilon_0$. *Let* $\rho = \Omega t$ *denote a scaled time variable,* $\alpha = |\varepsilon|\rho = |\varepsilon|\Omega t$ *denote the corresponding slow scaled time variable, and let functions* $\theta_i(\alpha)$, $i = 1, \ldots, N$, *denote the phase deviations of* θ_i *from its natural phase* Ωt *mod* 2π. *Then*

$$\frac{d\theta_i}{d\alpha} = H_i(\theta_1(\alpha - \zeta_1) - \eta_1 - \theta_i(\alpha), \ldots, \theta_N(\alpha - \zeta_N) - \eta_N - \theta_i(\alpha)) + O(\varepsilon),\ i = 1, \ldots, N, \tag{3.23}$$

where $\zeta_i = |\varepsilon|\Omega\tau_i$ *and* $\eta_i = \Omega\tau_i$. *The functions* $H_i(\cdot)$ *have the following form:*

$$\begin{aligned} &H_i(\theta_1(\alpha - \zeta_1) - \eta_1 - \theta_i(\alpha), \ldots, \theta_N(\alpha - \zeta_N) - \eta_N - \theta_i(\alpha)) \\ &= \frac{1}{2\pi}\int_0^{2\pi} Q^T(s) G_i(\sigma[\theta_1(\alpha - \zeta_1) - \eta_1 - \theta_i(\alpha)], \ldots, \sigma[s], \\ &\qquad \ldots, \sigma[s + \theta_N(\alpha - \zeta_N) - \eta_N - \theta_i(\alpha)])ds, \end{aligned} \tag{3.24}$$

where $\sigma[s]$ *stands on the* i^{th} *position, and* $Q(t) \in \mathbb{R}^m$ *is the unique nontrivial* 2π *periodic solution to the linear system*

$$\frac{dQ}{dt} = -\frac{1}{\Omega} DF(\sigma[\rho])^T Q,$$

satisfying the normalization condition

$$\frac{1}{2\pi}\int_0^{2\pi} Q_i^T(s) F(\sigma[s]) da = 1.$$

Using perturbation analysis, [65] proved that weakly connected networks with explicit delays do not lead to phase models with time delays even when the delay is of the same order of magnitude as the period of oscillators. Instead, it is appropriate to include the time delay as a phase shift in the interaction function.

Theorem 13. ([65, Corollary 2], [68, Corollary 3.2.1])

There exists $\eta_0 > 0$, such that for $\eta_i < \eta_0$, $i \in \{1, \ldots, N\}$, the delay terms in system (3.23) can be neglected, and (3.23) takes form

$$\frac{d\theta_i}{d\alpha} = H_i(\theta_1 - \eta_1 - \theta_i, \ldots, \theta_N - \eta_N - \theta_i) + O(\varepsilon), \tag{3.25}$$

where all phase deviations are computed at the point α, and the function H_i is defined by integral in (3.24)

Chapter 4

Phase models and clustering

4.1 Introduction

Assuming weak connection, a phase model represents each oscillator in a network with a single variable. A differential equation for each phase variable indicates how the phase of the oscillator changes in time:

$$\frac{d\theta_i}{dt} = \Omega_i + H_i(\theta_1, \theta_2, \ldots, \theta_N)$$

Here Ω_i is the intrinsic frequency of the i^{th} oscillator and the functions H_i described how the coupling between oscillators influences the phases. Phase models have been used to study the behaviour of networks of coupled oscillators beginning with the work of [73]. Phase models are sometimes *posed* as models for coupled oscillators [83, 73, 91, 76]. When the coupling between oscillators is sufficiently weak, however, a phase model representation of a system can be *derived* from a higher dimensional differential equation model, such as one obtained from a physical or biological description of the system [41, 64, 70, 104]. The low dimensional phase model can then be used to predict behaviour in the original high dimensional physical model. This approach has proved useful in studying synchronization properties of many different neural models [59, 8, 26, 37, 47, 60, 81, 126]. Phase models can be linked to experimentally derived phase resetting curves [41, 104], thus this approach has also been used to make predictions about synchronization properties of experimental preparations [81].

[1, 91] were the first to use phase models to study clustering behaviour. Using the theory of equivariant differential equations [1] studied a general network of identical oscillators of

arbitrary size with symmetric, weak coupling, corresponding to the symmetry groups S_n, Z_n, and D_n. They determined which type of solutions are forced to exist by the symmetry in each case. For the case of S_n symmetry they gave conditions for the stability of several types of solutions, including symmetric cluster solutions, and determined which bifurcations are forced by symmetry to occur. They also studied the existence of heteroclinic cycles and tori for some special cases. By direct analysis of the phase model, [91] studied the following network with global homogeneous coupling, (S_n symmetry)

$$\theta_i'(t) = \Omega + \frac{1}{N}\sum_{j=1}^{N} H(\theta_i - \theta_j). \tag{4.1}$$

He established general criteria for the stability of all possible symmetric cluster solutions as well as some nonsymmetric cluster solutions. Using numerical simulations, [91] further showed that these results give a good prediction of stability for a variety of model networks. More recently, [10] considered the existence and stability of cluster solutions and fixed tori for phase models corresponding to networks with global homogeneous coupling. They also considered the effect of additional absolute-phase product coupling. Using a similar approach as [91] stability results have been obtained for inhibitory neural networks with nearest-neighbour coupling [82]. Phase model analysis has also been extensively used to study phase-locking in pairs of model and experimental neurons [70, 101, 81]. More recently it has been used to study clustering in larger neural networks [66, 48]. A more comprehensive review of the analysis of phase models and their application to the study of synchronization is given in [31].

In many systems there are time delays in the connections between the oscillators due to the time for a signal to propagate from one element to the other. In neural networks this delay is attributed to the conduction of electrical activity along an axon or a dendrite [26, 70]. Much work has been devoted to the study of the effect of time delays in neural networks. However, the majority of this work has focussed on systems where the neurons are excitable not oscillatory, (e.g., [14, 15, 13, 27, 95, 102]), the networks have only a few neurons (e.g., [76, 18, 70, 77, 103]) or focussed exclusively on synchronization (e.g., [26, 78, 92, 93, 95]). Extensive work has been done on networks of Stuart-Landau oscillators with delayed diffusive coupling (e.g., [24, 28]) where the model for the individual oscillators is the normal form for a Hopf bifurcation and thus the system is often amenable to theoretical analysis. Numerical approaches to study the stability of cluster solutions in delayed neural oscillator networks have also been developed [93, 94]. We note that there is a vast literature on time delays in artificial neural networks which we do not attempt to cite here.

Initial studies of phase models for systems with delayed coupling considered models where the delay occurs in the argument of the phases [103, 78, 67, 90, 121]. However, it has

been shown [70, 36, 65] that for small enough time delays it is more appropriate to include the time delay as phase shift in the argument of the coupling function. Crook et al. [26] use this type of model to study a continuum of cortical oscillators with spatially decaying coupling and axonal delay. Bressloff and Coombes [8, 9] study phase locking in chains and rings of pulse coupled neurons with distributed delays and show that distributed delays result in phase models with a distribution of phase shifts. They consider phase models derived from integrate and fire neurons and the Kuramoto phase model.

In this chapter, we consider a network of N identical oscillators with time delayed, and circulant coupling. Our work draws on the previous works, however, extends their work to more general cases. [1, 91, 10, 82, 70, 101, 81]. considered weakly connected networks without time delay. In particular, [91] considered networks with global homogeneous coupling and [82] mainly focused on networks with nearest neighborhood coupling and second nearest neighborhood coupling. In this chapter, we consider networks with time delayed and circulant coupling. Specifically, we discuss the special case of bi-directional coupling and global homogeneous coupling. Our work is also an extension to [26, 78, 92, 93, 95] since we determine not only the existence and stability of synchronizations, but also all possible symmetric cluster solutions.

The plan for the rest of this chapter is as follows. In the next section we will review how a general network model with delayed coupling may be reduced to a phase model. In section 4.3 we use the phase model to determine conditions for existence and stability of symmetric cluster solutions in a network with a circulant coupling matrix, extending some prior results [1, 91, 82] to systems with time delays and more general coupling. In section 4.4 we consider a particular application: a network of Morris-Lecar oscillators. We derive the particular phase model for this system and compare the predictions of the phase model theory to numerical continuation and simulation studies to determine when the weak coupling assumption breaks down. We show that the time delay can induce multistability between different cluster solutions and explore how changing the coupling matrix affects this. In section 4.5 we explore the effects of breaking the symmetry of the connection matrix and introducing multiple time delays on our results. In section 4.6 we discuss our work.

4.2 The model and phase model reduction

In this chapter, we consider the following network of identical oscillators with all-to-all, time-delayed coupling

$$\frac{dX_i}{dt} = F(X_i(t)) + \epsilon \sum_{j=1}^{N} w_{ij} G(X_i(t), X_j(t - \tau_{ij})), \ i = 1, \cdots, N. \tag{4.2}$$

Here $G : \mathbb{R}^n \times \mathbb{R}^n \to \mathbb{R}^n$ describes the coupling between two oscillators, ϵ is referred to as the coupling strength, and $W = [w_{ij}]$ is the coupling matrix. Note that the ϵw_{ij} in the above equation correspond to $g_{syn,ij}$ (or $g_{gap,ij}$) in (2.4) (or (2.6)). Since the conductance is always greater than 0, we assume $w_{ij} \geq 0$.

We assume the model for the decoupled system, for a single oscillator,

$$\frac{dX}{dt} = F(X(t)), \tag{4.3}$$

admits an exponentially asymptotically stable periodic orbit, denoted by $\hat{X}(t)$, with period T. Further, we denote by $Z = \hat{Z}(t)$ the unique periodic solution of the system adjoint to the linearization of (4.3) about $\hat{X}(t)$ satisfying the normalization condition:

$$\frac{1}{T} \int_0^T \hat{Z}(t) \cdot F(\hat{X}(t)) dt = 1.$$

When ϵ is sufficiently small and the w_{ij} are of order 1 with respect to ϵ, we can apply the theory of weakly coupled oscillators, and reduce (4.2) to a phase model [41, 64, 70]. The appropriate phase model with respect to the coupling strength ϵ is

$$\frac{d\theta_i}{dt} = \Omega + \epsilon \sum_{j=1}^{N} w_{ij} H(\theta_j(t - \tau_{ij}) - \theta_i) + O(\epsilon^2), \ i = 1, 2, \cdots, N, \tag{4.4}$$

where the interaction function H is a 2π-periodic function which satisfies

$$H(\theta) = \frac{1}{T} \int_0^T \hat{Z}(s) \cdot G(\hat{X}(s), \hat{X}(s + \theta/\Omega)) \, ds.$$

with $\hat{X}, \hat{Z}$ as defined above.

As we discussed before, when the size of the time delays is small relative to other time constants in the model, it is appropriate to enter time delays as phase shift into the

corresponding phase model [70, 36, 65]. Let $\Omega = 2\pi/T$. If the delays satisfy $\Omega\tau_{ij} = O(1)$ with respect to the coupling strength ϵ, then the appropriate phase model can be written as

$$\frac{d\theta_i}{dt} = \Omega + \epsilon \sum_{j=1}^{N} W_{ij} H(\theta_j - \theta_i - \eta_{ij}) + O(\epsilon^2), \ i = 1, 2, \cdots, N, \tag{4.5}$$

where $\eta_{ij} = \Omega\tau_{ij}$. That is, the delays enter as phase lags.

To study cluster solutions we will make two simplifications. First, we assume that all the delays are equal:

$$\tau_{ij} = \tau, \text{ i.e., } \eta_{ij} = \eta. \tag{4.6}$$

Second, we will assume the network has some symmetry. In particular, we will consider the coupling matrix to be in circulant form:

$$W = circ(w_0, w_1, w_2, \cdots, w_{N-1}), \quad \text{equivalently,} \quad W_{ij} = w_{j-i \pmod N}. \tag{4.7}$$

Following [82], we will say the network has connectivity radius r, if $w_k > 0$ for all $k \leq r$, and $w_k = 0$ for all $k > r$. For example, a network with nearest neighbor coupling has connectivity radius $r = 1$. Our results will be derived with the coupling matrix (4.7), but can be applied to coupling with any connectivity radius by setting the appropriate $w_k = 0$.

We will also assume there is no self coupling, $w_0 = 0$, as this generally the case in applications. The results are essentially unchanged if we include it [115]. These simplifications will apply for the next two sections. In section 4.5, we will return to the general model (4.5).

4.3 Existence and stability of cluster solutions

Rewriting (4.5) using the simplifications (4.6)-(4.7) and dropping the higher order terms in ϵ we have

$$\frac{d\theta_i}{dt} = \Omega + \epsilon \sum_{j=1, j\neq i}^{N} w_{j-i \mod N} H(\theta_j - \theta_i - \eta), \ i = 1, 2, \cdots, N. \tag{4.8}$$

Now the right hand sides of equation (4.8) depend only on the difference of phases. Thus, introducing the phase difference variables:

$$\phi_i = \theta_{i+1} - \theta_i, \ i = 1, \ldots, N, \tag{4.9}$$

we can transform the phase equation (4.8), to the following system

$$\frac{d\phi_i}{dt} = \epsilon \sum_{k=1}^{N-1} w_k \left(H(\sum_{s=0}^{k-1} \phi_{i+s+1 \pmod N} - \eta) - H(\sum_{s=0}^{k-1} \phi_{i+s \pmod N} - \eta) \right) \tag{4.10}$$

for $i = 1, 2, \cdots, N$.

Note that the N phase difference variables are not independent but satisfy the relation

$$\sum_{i=1}^{N} \phi_i = 0 \mod 2\pi. \tag{4.11}$$

Thus, the $N-$dimensional system (4.10) could be reduced to system of dimension $N-1$. However, to take advantage of the symmetry, we choose instead to work with the full set of N equations and apply the constraint (4.11).

As discussed above, a cluster solution of the DDE model (4.2) is one where all the oscillators have the same waveform, but they separate into different groups or clusters. Oscillators within a cluster are synchronized, while oscillators in different clusters are phase-locked with some fixed phase difference. It follows that in a cluster solution the difference between the phases of any two oscillators are fixed. Using (4.8) we can show that, to order ϵ, these solutions correspond to the lines

$$\theta_i = (\Omega + \epsilon\omega)t + \theta_{i0}. \tag{4.12}$$

See [91] for details of this calculation in the case that $\eta = 0$ and $w_k = w$. The case we are considering is completely analogous. Further, from the definition (4.9), it is clear that cluster solutions correspond to equilibrium points of the phase difference equation (4.10). Therefore, by studying the existence of the equilibrium points of the phase difference model (4.10), we can obtain the existence of the corresponding cluster solutions of the original DDE model.

We can now state our first result.

Theorem 14 (Existence of cluster solutions)**.** *For any values of H and the w_k, the phase difference model (4.10) admits N equilibrium points of the form $\phi_i = \psi$, $i = 1, \ldots, N$:*

(i) $\psi = 0$ corresponds to the 1-cluster or fully synchronized solution.

(ii) $\psi = \frac{2p\pi}{N}$ where p, N are relatively prime corresponds to an N-cluster solution, also called a splay or rotating wave solution.

(iii) $\psi = \frac{2m\pi}{n}$ *where* $N = nk$ *for some positive integers* $n, k > 1$, $1 \leq m < n$, *and* m, n *are relatively prime corresponds to a symmetric* n*-cluster solution.*

If ψ *is a solution then so is* $2\pi - \psi$ *and they have the same number of clusters. The ordering of the clusters of the* $2\pi - \psi$ *solution is the reverse of the* ψ *solution. For generic weights, these are the only model independent equilibrium points.*

Proof. The proof of this result is similar to the proof of [82, Theorem 3.1], which considers the case of no delays ($\eta = 0$).

It is clear from Eq. (4.10) that, for any H and w_k, there are equilibrium points given by $\phi_i = \psi$, $i = 1, \ldots, N$, subject to the constraint

$$N\psi = 0 \bmod 2\pi. \tag{4.13}$$

The basic idea is that the above constraint determines the possible values for ψ. Using these values in the solution (4.12) determines the number and ordering of clusters in the solution. Notice that we only need consider the cases of $N\psi = 2k\pi, k = 1, 2, \cdots, N$ since other values of k give solutions which are equivalent to those which $k \leq N$. Let $\gcd(N, k) = p$.

If $p = 1$, then (N, k) are relatively prime. The corresponding solution is $\psi = \frac{2k\pi}{N}$, which corresponds to a splay solution where the oscillators are equally separated over k periods. Note that $2\pi - \psi = (N-k)\frac{2\pi}{N}$. If (N, k) are relatively prime, so are $(N, N-k)$. Therefore, $N - k < N$ also corresponds to a N-cluster solution.

If $p > 1$, let $N = np$. Therefore, we have $k = mp$ for some $m < n$, and $\gcd(m, n) = 1$. In this case, the corresponding solution is $\psi = \frac{2\pi m}{n}$. In terms of the original phase variables, we have

$$\theta_{i+1}(t) - \theta_i(t) = \frac{2\pi m}{n}, \ i = 1, 2, \cdots, N.$$

It follows that

$$\theta_{n+1} - \theta_1 = \phi_n + \phi_{n-1} + \cdots + \phi_1 = 2m\pi.$$

That is, the $(n+1)$-th oscillator is synchronized with the 1-st oscillator. Similarly, we have that oscillators with indices $1,\ n+1,\ 2n+1, (p-1)n+1$ form one cluster, oscillators with indices $2,\ n+2,\ 2n+2, (p-1)n+2$ form another cluster, and the rest of the oscillators separated into another $n-2$ clusters. Thus, we conclude that $\psi = \frac{2\pi m}{n}$ corresponds to an n-cluster solution. Note that in this case $2\pi - \psi = (n-m)\frac{2\pi}{n}$. Since (m, n) are relatively prime, so are $(n-m, n)$. Therefore, $(n-m)\frac{2\pi}{n}$ is another n-cluster solution.

In the case of generic weights, i.e., no further symmetry in the connection matrix, model-independent equilibrium points exist if and only if there are constant values of the ϕ_i satisfying

$$\phi_{i+k} - \phi_i = 0 \bmod 2\pi, \quad i = 1, \ldots, N, \quad k = 1, \ldots, N-i.$$

Analysis of these equations shows that the only possible solutions are in the form $\phi_i = \psi$, $i = 1, \ldots, N$.

□

Note that different values of ψ can have the same number of clusters with different oscillators in the clusters and/or a different ordering of the clusters in the solution. We shall see some examples of this in section 4.4.

We next analyze the stability of the equilibrium points $\phi_i = \psi$.

Theorem 15 (Stability of cluster solutions)**.** *Let $\epsilon > 0$ and define*

$$\mu_j = \sum_{k=1}^{N-1} w_k H'(k\psi - \eta)\left(1 - \cos\left(2\pi kj/N\right)\right). \tag{4.14}$$

The equilibrium point $\psi = \frac{2\pi k}{N}$, $k \in \{0, \cdots, N-1\}$, and the corresponding cluster solution is asymptotically stable when $\mu_j > 0$ for $j = 1, \ldots, \lfloor \frac{N}{2} \rfloor$, and unstable if at least one $\mu_j < 0$.

Proof. The Jacobian matrix of the linearization of (4.10) about the equilibrium point $\phi_i = \psi$, $i = 1, \ldots, N$, is the circulant matrix $\epsilon J = circ(c_0, c_1, \ldots, c_{N-1})$ with $c_0 = -\sum_{s=1}^{N-1} w_s H'(s\psi - \eta)$ and $c_k = w_k H'(k\psi - \eta), k = 1, \cdots, N-1$. A standard result for circulant matrices [51] shows that the eigenvalues of J are $\epsilon\lambda_j$, $j = 0, 1, \ldots, N$ where

$$\lambda_j = -\sum_{k=1}^{N-1} w_k H'(k\psi - \eta)(1 - e^{\frac{2\pi i}{N}kj}).$$

Thus there is always one zero eigenvalue, corresponding to λ_0. This is because the phase differences in (4.10) are not all independent. It can be verified that if the constraint (4.11) is used to reduce the phase difference model (4.10) to $N-1$ equations then the linearization yields only the eigenvalues $\epsilon\lambda_j$, $j = 1, \ldots, N-1$. A simple calculation shows that $\lambda_{N-j} = \overline{\lambda_j}$, $j = 1, \ldots, \lfloor \frac{N}{2} \rfloor$ and $\mathrm{Re}(\lambda_j) = -\mu_j$. The result follow. □

Recall that a cluster solution corresponds to a line in the phase model (4.8). The zero eigenvalue corresponds to the motion along this line.

Remark 2. *Due to the periodicity of H, the stability of the cluster solutions is $2\pi-$periodic in the parameter η. Recall that $\eta = 2\pi\tau/T$ where τ is the time delay in the coupling and T is the intrinsic period of the uncoupled oscillators. Thus the stability is $T-$periodic in τ. That is, if a given solution is asymptotically stable (unstable) for $\tau = \tau_0$ then it is asymptotically stable (unstable) for $\tau = \tau_0 + kT$, $k = 1, 2, \ldots$ This will carry over to the original delay differential equation model so long as τ is sufficiently small that the phase model is a valid approximation, i.e., $\frac{2\pi\tau}{T} = O(1)$ with respect to ϵ.*

From the two theorems above we can obtain some general results about certain common solutions.

Corollary 1 (Synchronized solution)**.** *The phase difference model (4.10) always admits the $1-$cluster solution, $\psi = 0$, corresponding to the solution where all the oscillators are synchronized. The stability of this solution is independent of the size of the network and coupling between oscillators (w_k). In particular, the synchronized solution is asymptotically stable when $H'(-\eta) > 0$, and unstable when $H'(-\eta) < 0$.*

Proof. Following from the proof of Theorem 15, it is clear that when $\psi = 0$, the circulant Jacobian matrix of the corresponding linearization system ϵJ satisfies $c_0 = -\sum_{s=1}^{N-1} w_s H'(-\eta)$ and $c_k = w_k H'(-\eta)$, $k = 1, 2, \cdots, N-1$. Therefore, the eigenvalues of ϵJ are $\epsilon\lambda_j$, $j = 0, 1, \cdots, N-1$, where

$$\lambda_j = -H'(-\eta) \sum_{k=1}^{N-1} w_k (1 - e^{\frac{i2\pi}{N} kj}).$$

Simple calculation follows that $\mathrm{Re}(\lambda_j) = -H'(-\eta) \sum_{k=1}^{N-1} w_k (1 - \cos(\frac{i2\pi}{N} kj))$. Therefore, the results follows.

□

Corollary 2 (Anti-phase solution)**.** *If N is even the phase difference model (4.10) admits $2-$cluster solution, $\psi = \pi$, which corresponds to the anti-phase solution where adjacent oscillators are out of phase by one half period. The stability of this solution is independent of the coupling. For $N = 2$ it is asymptotically stable (unstable) if $H'(\pi - \eta) > 0$ (< 0). For all $N > 2$ this solution is asymptotically stable if $H'(-\eta) > 0$ and $H'(\pi - \eta) > 0$ and unstable if $H'(\pi - \eta) < 0$.*

Proof. Following from the proof of Theorem 15, it is clear that when $\psi = \pi$, the circulant

Jacobian matrix of the corresponding linearization system ϵJ satisfies

$$\begin{aligned} c_0 &= -\sum_{k=1,\ k \text{ odd}}^{N-1} w_k H'(\pi-\eta) - \sum_{k=2,\ k \text{ even}}^{N-1} w_k H'(-\eta) \\ c_k &= w_k H'(-\eta), \text{ if } k \text{ is even, and} \\ &= w_k H'(\pi-\eta), \text{ if } k \text{ is odd.} \end{aligned}$$

Therefore, the real parts of the eigenvalues are $\epsilon\mu_j$, $j = 0, 1, \cdots, N-1$, with

$$\lambda_j = -H'(\pi-\eta) \sum_{k=1,k \text{ odd}}^{N-1} w_k(1-\cos(\frac{i2\pi}{N}kj)) - H'(-\eta) \sum_{k=1,k \text{ even}}^{N-1} w_k(1-\cos(\frac{i2\pi}{N}kj)).$$

Simple calculation follows that $\text{Re}(\lambda_j) = -H'(-\eta)\sum_{k=1}^{N-1} w_k(1-\cos(\frac{i2\pi}{N}kj))$. Therefore, the results follow. □

Remark 3. *In the above stability results, we assume $\epsilon > 0$. If $\epsilon < 0$, the stability of asymptotically stable solutions and totally unstable solutions will be reversed, and the saddle type solutions will remain of saddle type.*

4.3.1 Stability analysis for bi-directional, distance dependent coupling

In this section, we consider a special case where the coupling strength is distance-dependent and bi-directional. In real neural networks, coupling strength is not necessarily determined by the physical distance. However, the "distance" here can be generalized to include functional distance [76]: the degree of correlation in the activity of coupled neurons. Therefore, we consider a coupling matrix that satisfies

$$W = circ(0, w_1, w_2, \ldots, w_{N/2}, \ldots, w_2, w_1) \tag{4.15}$$

if N is even, and

$$W = circ(0, w_1, w_2, \ldots, w_{(N-1)/2}, w_{(N-1)/2}, \ldots, w_2, w_1) \tag{4.16}$$

if N is odd. Applying Theorem 15 to this system leads to the following.

Corollary 3. *Consider (4.10) with bi-directional, distance dependent coupling. Define*

$$\mu_j = \sum_{k=1}^{\frac{N-1}{2}} w_k \left[H'(k\psi-\eta) + H'(-k\psi-\eta)\right](1-\cos(2\pi kj/N))$$

for N odd and

$$\mu_j = w_m H'(m\psi - \eta)(1 - (-1)^j) + \sum_{k=1}^{m-1} w_k \left[H'(k\psi - \eta) + H'(-k\psi - \eta)\right](1 - \cos(2\pi kj/N))$$

for $N = 2m$, even. The equilibrium point $\psi = \frac{2\pi k}{N}$, $k \in \{0, \cdots, N-1\}$, and the corresponding cluster solution is asymptotically stable when $\mu_j > 0$ for $j = 1, \ldots, \lfloor \frac{N}{2} \rfloor$, and unstable if at least one $\mu_j < 0$.

Recall that ψ and $2\pi - \psi$ correspond to the same type of cluster solution. For a network with bi-directional coupling, these solutions have a stronger relationship.

Corollary 4. *For the phase model with coupling matrix given by (4.15) or (4.16), the solutions $\phi_i = \psi$ and $\phi_i = 2\pi - \psi$ have the same stability.*

Proof. This follows by replacing ψ by $2\pi - \psi$ in the expressions for μ_j in Corollary 3 and using the $2\pi-$periodicity of H. □

A special case of bi-directional coupling is when the only nonzero coupling coefficient is w_1. This is commonly called nearest-neighbour coupling. In this case the stability of any symmetric cluster solution is easily determined.

Corollary 5. *For the phase model with coupling matrix given by (4.15) or (4.16) with $w_1 \neq 0$ and $w_j = 0$, $j = 2, \ldots, N$, the symmetric cluster solution with $\phi_i = \psi$ is asymptotically stable if $H'(\psi - \eta) + H'(-\psi - \eta) > 0$ and unstable if $H'(\psi - \eta) + H'(-\psi - \eta) < 0$.*

Proof. In this case we have

$$\mu_j = -w_1 \left[H'(\psi - \eta) + H'(-\psi - \eta)\right](1 - \cos(2\pi j/N)).$$

The result follows. □

This extends the result in [82, Section 3.2] to systems with time delayed coupling.

4.3.2 Stability analysis for global homogeneous coupling

We next consider a special case: $W_h = circ(0, 1, \cdots, 1)$. That is, all the coupling weights are the same. A straightforward calculation shows that, in this case, for a symmetric n-cluster solution we have

$$\begin{aligned} \lambda_0 &= 0, \\ \lambda_0^{(n)} &= -\frac{N}{n}\sum_{k=0}^{n-1} H'(\frac{2\pi k}{n} - \eta), \text{ multiplicity } N-n, \\ \lambda_j^{(n)} &= -\frac{N}{n}\sum_{k=0}^{n-1} H'(\frac{2\pi k}{n} - \eta)(1 - e^{i2\pi kj/n}), \ j = 1, \cdots, n-1. \end{aligned} \tag{4.17}$$

where λ_j is as defined in the proof of Theorem 15.

This result is an extension to systems with time delayed coupling of results in [1, Section 6.1], [91, Section 2]. In [115] they made the following observation. The stability of an n-cluster solution (with $n < N$) depends on the number of clusters and the phase differences, not the size of the network. For example, any network with $N = 3m$ (m a positive integer) has a 3-cluster solution with $\psi = 2\pi/3$. The stability of this solution is the same for all networks with $m > 1$.

As discussed in [115, 1], since networks with global homogeneous coupling are unchanged by any rearrangement of the indices, there are many more cluster solutions. For example, consider a network where $N > 2$ is even. When the connection matrix is circulant with different w_k, there is one 2-cluster solution with oscillators $1, 3, 5, \ldots, N-1$ forming one cluster and oscillators $2, 4, \ldots N$ forming the second cluster. For a network with global homogeneous coupling, *any* division of the oscillators into two groups of $N/2$ oscillators is an admissible 2-cluster solution with stability described by (4.17) with $n = 2$.

4.3.3 Stability analysis for general synchronization

Recall that in section 3.6, (4.4) is further reduced to an ordinary differential equation (4.8) when the time delay satisfies $\Omega\tau = O(1)$ with respect to the coupling strength ϵ. Based on this condition, we discussed the stability for synchronization solutions and summarized the results in Corollary 1. It turns out that the stability of synchronization solutions depends on the sign of $\epsilon H'(-\eta)$.

In this section, we try to extend this analysis to be with respect to system (4.4), i.e. for any time delay. The analysis would involve studying eigenvalues of an infinite system.

Recall that when $\epsilon = 0$, the synchronization solution is $\theta_i(t) = \Omega t$. Therefore, we assume that a general inphase synchronization solution is described by

$$\theta_i(t) = \tilde{\Omega} t, \ i = 1, 2, \cdots, N. \tag{4.18}$$

Substituting (4.18) in to (4.4), we find that the collective frequency $\tilde{\Omega}$ is determined implicitly by the following equation

$$\tilde{\Omega} = \Omega + \epsilon \bar{w} H(-\tilde{\eta}), \tag{4.19}$$

where $\tilde{\eta} = \tilde{\Omega}\tau$, and $\bar{w} = \sum_{k=1}^{N-1} w_k$.

We then perform a linear stability analysis to determine the local stability of solution described in (4.18) by adding a small perturbation

$$\theta_i(t) = \tilde{\Omega} t + \varepsilon \tilde{\theta}_i(t), \ i = 1, 2, \cdots, N. \tag{4.20}$$

where ε is a sufficiently small positive parameter. Substituting (4.20) back into (4.4), and taking the first order with respect to ε, we have the following linear delay differential equation for $\tilde{\theta}_i(t)$:

$$\tilde{\theta}_i'(t) = \epsilon H'(-\tilde{\eta}) \sum_{j=1}^{N} W_{ij}(\tilde{\theta}_j(t-\tau) - \tilde{\theta}_i(t)), \tag{4.21}$$

Note that if $\epsilon H'(-\tilde{\eta}) = 0$, we have neural stability at linear order. In this case, higher order terms need to be considered for further details. From now on, we focus on the case that $\epsilon H'(-\tilde{\eta}) \neq 0$. To find a characteristic equation for (4.21), we substitute $\tilde{\theta}_i(t) = e^{\lambda t} e_i$ into (4.21), and obtain

$$(\lambda + \epsilon \bar{w} H'(-\tilde{\eta})) e^{\lambda \tau} e_i = \epsilon H'(-\tilde{\eta}) \sum_{j=1}^{N} w_{ij} e_j, \tag{4.22}$$

where $\bar{w} = w_1 + w_2 + \cdots + w_{N-1} = \sum_{j=1}^{N} w_{ij}$, for any $i = 1, 2, \cdots, N$. Define

$$\delta = \frac{(\lambda + \epsilon \bar{w} H'(-\tilde{\eta})) e^{\lambda \tau}}{\epsilon H'(-\tilde{\eta})}. \tag{4.23}$$

Thus we can rewrite equation (4.22) in the following matrix form

$$WE = \delta E. \tag{4.24}$$

It is clear that δ is an eigenvalue of the coupling matrix W. By the property of circulant matrices, the eigenvalues of W are

$$\delta_k = \sum_{j=1}^{N-1} w_j e^{\frac{2\pi i}{N} kj}, \ k = 0, 1, \cdots, N-1. \tag{4.25}$$

Note that $\delta_0 = \bar{w}$. Before introducing the stability results, we need the following properties.

Lemma 1. *The eigenvalues of W satisfies $|\delta_k| \leq \bar{w}$, $k = 1, \cdots, N-1$.*

Proof. The above result is a direct conclusion from the Gershgorin's circle theorem . The theorem [110] states that every eigenvalue of a matrix $B = (B_{ij})_{N\times N}$ lies in at least one of the circles $O_1, O_2, \cdots, O_N$, where O_i is has its center at the diagonal engry b_{ii} and radius equal to the absolute sum along the rest of the row, that is, the radius equal to $\sum_{j=1, j\neq i}^{N} |B_{ij}|$.

Applying Gerschgorin's theorem to the coupling matrix W, we find that all these circles are the same with center at the origin (since $W_{ii} = w_0 = 0$, for all $i = 1, 2, \cdots, N$), and with radius $\bar{w}$. Therefore, all the eigenvalues of W lie within this circle. Thus, we have $|\delta_k| \leq \bar{w}$. □

In conclusion, we have that $\delta \in \{\delta_0, \delta_1, \cdots, \delta_{N-1}\}$, and satisfies $|\delta| \leq \bar{w}$. Now we are ready to prove the stability theorem for solutions described in (4.18).

Theorem 16 (General synchronization solution)**.** *The phase model (4.4) admits the 1-cluster solution $\theta_i = \tilde{\Omega} t$ if there exists a solution of (4.19). The stability of this solution is independent of the size of the network and coupling between oscillators (W). In particular, the synchronization solution is asymptotically stable when $\epsilon H'(-\tilde{\eta}) > 0$ and unstable when $\epsilon H'(-\tilde{\eta}) < 0$.*

Proof. As we know, the stability of synchronization described in (4.23) depends on the sign of the real parts of the eigenvlaues λ in (4.24). That is, the synchronization solution is stable if and only if $\mathrm{Re}(\lambda) < 0$. Therefore, to proof the theorem, it is equivalent to prove that $\mathrm{Re}(\lambda) < 0$ if and only if $\epsilon H'(-\tilde{\eta}) > 0$.

Let $\lambda = x + iy$, and $\delta = \alpha + i\beta$, and separate the real and imaginary parts of equation (4.23):

$$\begin{aligned} \epsilon H'(-\tilde{\eta}) e^{-x\tau} (\alpha \cos(y\tau) + \beta \sin(y\tau)) &= x + \epsilon H'(-\tilde{\eta}) \bar{w}, \\ \epsilon H'(-\tilde{\eta}) e^{-x\tau} (-\alpha \sin(y\tau) + \beta \cos(y\tau)) &= y. \end{aligned} \tag{4.26}$$

Squaring and adding yields

$$(\epsilon H'(-\tilde{\eta}))^2 e^{-2x\tau}(\alpha^2+\beta^2) = x^2 + y^2 + 2\epsilon H'(-\tilde{\eta})\bar{w}x + (\epsilon H'(-\tilde{\eta}))^2\bar{w}^2. \tag{4.27}$$

We first prove that if $\epsilon H'(-\tilde{\eta}) > 0$, then $\mathrm{Re}(\lambda) < 0$ by contradiction. Suppose that there exists a λ satisfies (4.23) such that $x \geq 0$ and $\epsilon H'(-\tilde{\eta}) > 0$. In this case, (4.27) can be rewritten as

$$e^{-2x\tau}(\alpha^2+\beta^2) = \bar{w}^2 + \frac{x^2 + y^2 + 2\epsilon H'(-\tilde{\eta})\bar{w}x}{(\epsilon H'(-\tilde{\eta})^2)}. \tag{4.28}$$

Note that by Lemma 1, we have that $(\alpha^2+\beta^2) \leq \bar{w}$. Since $x \geq 0$, the left hand side of (4.28) must be between $[0, \bar{w}]$. The right hand side of (4.28) is greater than or equal to $\bar{w}$. Therefore, the equality is true only if $x = y = 0$, that is, $\lambda = 0$. This special case corresponds to $\delta = \bar{w} = \delta_0$ with corresponding eigenvector to be $(1, 1, \cdots, 1)^T$. This eigenvalue reflects the rotation symmetry of (4.4). The system is neurally stable to perturbations in which each phase is changed by the same constant amount. This is, however, the only neutral perturbation. Hence, for all other perturbation, $\lambda \neq 0$. Therefore, the right-hand side of (4.28) is strictly greater than $\bar{w}$, which contradicts the properties of the left hand side.

We next prove that if $\mathrm{Re}(\lambda) < 0$ then $\epsilon H'(-\tilde{\eta}) > 0$ by contradiction. Assume that $\epsilon H'(-\tilde{\eta}) < 0$. Therefore, we have

$$-|\epsilon H'(-\tilde{\eta})|e^{-x\tau}\sqrt{\alpha^2+\beta^2}\cos(y\tau - \arg(\delta)) = x - |\epsilon H'(-\tilde{\eta})|\bar{w}. \tag{4.29}$$

Note that $p = \sqrt{\alpha^2+\beta^2}\cos(y\tau - \arg(\delta))$ is between $[-\bar{w}, \bar{w}]$. First consider the case that p is between $[0, \bar{w}]$. Graphically, the plot of the right hand side of (4.29) is a line across the first, third and forth quadrants, while the left hand side goes through the third and fourth quadrants. By the property of the exponential function, the only intersection of the curves is in the fourth quadrant, i.e., $x > 0$. Next consider the case that $p \in [-\bar{w}, 0)$. Thus, (4.29) can be rewritten as

$$|\epsilon H'(-\tilde{\eta})||p|e^{-x\tau} + |\epsilon H'(-\tilde{\eta})| = x. \tag{4.30}$$

The left hand side of the above equation is always greater than 0. Therefore, we have $x > 0$. Thus, the proof is complete.

□

Remark 4. *The result of Theorem 16 can be extended to the cases that the coupling matrix W is not circulant but satisfies $W_{ii} = 0$ and $\sum_{j=1, j\leq i} W_{ij} = K$, $i = 1, \cdots, N$. That is,*

the signals that each oscillator receives from all the other oscillators are the same. By a similar proof as for Lemma 1, we obtain that the eigenvalues of W in this case are still within the circle centered at the origin with radius K. Therefore, we can get the same result by replacing $\bar{w}$ by K in the proof for Theorem 16.

4.3.4 Stability analysis for other types of cluster solutions

If more conditions are put on the coupling matrix then different cluster solutions may occur. For example, consider a 2-cluster solution where the phase differences between adjacent elements is not the same, but is described by

$$\phi_1 = \phi_3 = \cdots = \phi_{N-1} = 0, \text{ and } \phi_2 = \phi_4 = \cdots = \phi_N = \pi, \tag{4.31}$$

or

$$\phi_1 = \phi_3 = \cdots = \phi_{N-1} = \pi, \text{ and } \phi_2 = \phi_4 = \cdots = \phi_N = 0. \tag{4.32}$$

In this situation the elements group into pairs, so that each element is synchronized with one of its nearest neighbours and one-half period out of phase with its other nearest neighbour. As shown by the next result, these solutions exist under appropriate conditions on the connectivity matrix.

Theorem 17. *For a network with a circulant connectivity matrix, the system (4.10) admits solutions of the form (4.31) and (4.32) if $N = 4p$ for some integer p, and $\sum_{k=0}^{p-1} w_{4k+1} = \sum_{k=0}^{p-1} w_{4k+3}$. These two solutions have the same stability.*

Proof. Applying the constraint condition (4.11) to (4.31) or (4.32), we have that, for some integer p,

$$\frac{N}{2} \cdot \pi = 2p\pi.$$

Therefore, $N = 4p$, for some integer p.

Substituting solution (4.31) or (4.32) into the system (4.10), we have that

$$\sum_{k=0}^{p-1} w_{4k+1}\big(H(\pi-\eta) - H(-\eta)\big) = \sum_{k=0}^{p-1} w_{4k+3}\big(H(\pi-\eta) - H(-\eta)\big).$$

To satisfy this for any H, we must have $\sum_{k=0}^{p-1} w_{4k+1} = \sum_{k=0}^{p-1} w_{4k+3}$.

□

The Jacobian matrix of the linearization of system (4.10) at (4.31) is in the form

$$L = \begin{pmatrix} \alpha_0 & \alpha_1 & \alpha_2 & \alpha_3 & \cdots & \alpha_{N-1} \\ \beta_{N-1} & \beta_0 & \beta_1 & \beta_2 & \cdots & \beta_{N-2} \\ \alpha_{N-2} & \alpha_{N-1} & \alpha_0 & \alpha_1 & \cdots & \alpha_{N-3} \\ \beta_{N-3} & \beta_{N-2} & \beta_{N-1} & \beta_0 & \cdots & \beta_{N-4} \\ \vdots & \vdots & \vdots & \vdots & \ddots & \vdots \\ \alpha_2 & \alpha_3 & \alpha_4 & \alpha_5 & \cdots & \alpha_1 \\ \beta_1 & \beta_2 & \beta_3 & \beta_4 & \cdots & \beta_0 \end{pmatrix}, \tag{4.33}$$

with α_k, β_k as defined as follows

$$\alpha_0 = \beta_0 = -H'(-\eta)\big(\sum_{k=0}^{p-1} w_{4k+1} + \sum_{k=1}^{p-1} w_{4k}\big) - H'(\pi-\eta)\sum_{k=0}^{p-1}(w_{4k+2} + w_{4k+3}),$$

and, for $k = 1, \cdots, N-1$ and appropriate s values

$$\alpha_k = \begin{cases} w_k H'(\pi-\eta) + B_1(s)\big(H'(\pi-\eta) - H'(-\eta)\big), & k = 4s+1, 4s+2 \\ w_k H'(-\eta) + B_2(s)\big(H'(\pi-\eta) - H'(-\eta)\big), & k = 4s+3, 4s \end{cases}$$

$$\beta_k = \begin{cases} w_k H'(-\eta) - B_2(s)\big(H'(\pi-\eta) - H'(-\eta)\big), & k = 4s+1, \\ w_k H'(\pi-\eta) - B_2(s)\big(H'(\pi-\eta) - H'(-\eta)\big), & k = 4s+2, \\ w_k H'(\pi-\eta) - B_1(s)\big(H'(\pi-\eta) - H'(-\eta)\big), & k = 4s+3 \\ w_k H'(-\eta) - B_1(s)\big(H'(\pi-\eta) - H'(-\eta)\big), & k = 4s \end{cases}$$

where

$$B_1(s) = \big(\sum_{j=s+1}^{p-1} w_{4j+1} - \sum_{j=s+1}^{p-1} w_{4j+3}\big), \quad B_2(s) = \big(\sum_{j=s+1}^{p-1} w_{4j+1} - \sum_{j=s}^{p-1} w_{4j+3}\big).$$

For $k = 0, 1, \cdots, p-1$, define

$$L_k = \begin{pmatrix} \alpha_{4k} & \alpha_{4k+1} & \alpha_{4k+2} & \alpha_{4k+3} \\ \beta_{4k+3} & \beta_{4k} & \beta_{4k+1} & \beta_{4k+1} \\ \alpha_{4k+2} & \alpha_{4k+3} & \alpha_{4k} & \alpha_{4k+1} \\ \beta_{4k+1} & \beta_{4k+2} & \beta_{4k+3} & \beta_{4k} \end{pmatrix}$$

Therefore, L can be rewritten as a block circulant matrix

$$L = \begin{pmatrix} L_0 & L_1 & \cdots & L_{p-1} \\ L_{p-1} & L_0 & \cdots & L_{p-2} \\ \vdots & \vdots & \ddots & \vdots \\ L_1 & L_2 & \cdots & L_0 \end{pmatrix}$$

Based on the block circulant structure, we calculate the eigenvalues of L based on the method introduced on [107, 113]. Recall that λ is an eigenvalue of L if and only if there is a non-zero vector E such that

$$LE = \lambda E. \tag{4.34}$$

Let ρ be any N-th root of unity, that is

$$\rho \in \{\rho_0, \rho_1, \cdots, \rho_{N-1}\}, \text{ with } \rho_k = e^{i\frac{2\pi}{N}k}, \ k = 0, 1, \cdots, N-1.$$

Let $\xi \in \mathbb{R}^4$. Then the compound vector

$$E = \begin{pmatrix} \xi \\ \xi\rho^4 \\ \vdots \\ \xi\rho^{4(p-1)} \end{pmatrix}$$

satisfies (4.34) if and only if ξ satisfies $\mathcal{H}\xi = 0$ where

$$\mathcal{H} = \lambda I_p - (L_0 + \rho^4 L_1 + \rho^8 L_2 + \cdots + \rho^{4(p-1)} L_{p-1}) = \begin{pmatrix} M_0 & M_1 & M_2 & M_3 \\ \rho N_3 & N_0 & N_1 & N_2 \\ \rho M_2 & \rho M_3 & M_0 & M_1 \\ \rho N_1 & \rho N_2 & \rho N_3 & N_0 \end{pmatrix}$$

with I_p to be the $p \times p$ identity matrix, and for $s = 0, 1, 2, 3$, $M_s = \sum_{k=0}^{p-1} \alpha_{4k+s}\rho^{4k}$, $N_s = \sum_{k=0}^{p-1} \beta_{4k+s}\rho^{4k}$. Therefore, the N eigenvalues of L are, for $k = 0, 1, \cdots, p-1$,

$$\begin{aligned} \lambda_{1,k}^{\pm} &= \frac{\sqrt{2}}{2}\Big((M_0 + \rho_k^2 M_2 + N_0 + rho_k^2 N_2) \\ &\quad \pm \sqrt{(M_0 + \rho_k^2 M_2 - N_0 - \rho_k^2 N_2)^2 + 4\rho_k^2 (M_1 + \rho_k^2 M_3)(N_1 + \rho_k^2 N_3)}\Big), \\ \lambda_{2,k}^{\pm} &= \frac{\sqrt{2}}{2}\Big((M_0 - \rho_k^2 M_2 + N_0 - rho_k^2 N_2) \\ &\quad \pm \sqrt{(M_0 - \rho_k^2 M_2 - N_0 + \rho_k^2 N_2)^2 - 4\rho_k^2 (M_1 - \rho_k^2 M_3)(N_1 - \rho_k^2 N_3)}\Big). \end{aligned} \tag{4.35}$$

Thus, we have the following results.

Theorem 18. *Let $\epsilon > 0$. The 2-cluster solutions described by (4.31) and (4.32) are stable when all the $\lambda_{1,k}^{\pm}$ and $\lambda_{2,k}^{\pm}$ ($k = 0, 1, \cdots, p-1$) defined in (4.35) have negative real parts.*

Remark 5. *The Jacobian matrix of the linearization of system (4.10) at (4.32) is in the form*

$$\hat{L} = \begin{pmatrix} \beta_0 & \beta_1 & \beta_2 & \beta_3 & \cdots & \beta_{N-1} \\ \alpha_{N-1} & \alpha_0 & \alpha_1 & \alpha_2 & \cdots & \alpha_{N-2} \\ \beta_{N-2} & \beta_{N-1} & \beta_0 & \beta_1 & \cdots & \beta_{N-3} \\ \alpha_{N-3} & \alpha_{N-2} & \alpha_{N-1} & \alpha_0 & \cdots & \alpha_{N-4} \\ \vdots & \vdots & \vdots & \vdots & \ddots & \vdots \\ \beta_2 & \beta_3 & \beta_4 & \beta_5 & \cdots & \beta_1 \\ \alpha_1 & \alpha_2 & \alpha_3 & \alpha_4 & \cdots & \alpha_0 \end{pmatrix}, \tag{4.36}$$

which is equivalent to L. Therefore, The 2-cluster solutions described by (4.31) and (4.32) have the same stability.

Remark 6. *Note that, for networks with bi-directional coupling or global homogeneous coupling, the second condition, $\sum_{k=0}^{p-1} w_{4k+1} = \sum_{k=0}^{p-1} w_{4k+3}$, is automatically satisfied if $N = 4p$.*

We were not able to obtain more general results about the eigenvalues of L and $\hat{L}$. Thus, we are not able to make any conclusions about the stability of solutions (4.31) and (4.32) directly with respect to the coupling matrix W. However, we can use the expressions for $\lambda_{1,k}^{\pm}$ and $\lambda_{2,k}^{\pm}$ in the next section.

4.4 Application to networks of Morris-Lecar oscillators with global synaptic coupling

In this section, we apply our results to a specific network: globally coupled Morris-Lecar oscillators. Since the nondimensional form of Morris-Lecar equation is more convenient to work with, we adopt the dimensionless Morris-Lecar model which is formulated by Rinzel and Ermentrout in [99]. We briefly introduce the idea of non-dimensionalization here. Please see [68] for details of the non-dimensionalization procedure. From (2.2), we first introduce the dimensionless parameters $v = V_m/V_{ca}$, and $m = M$. Then define $v_n = V_n/V_{Ca}$ where $n \in \{\text{Ca, K, L}\}$, $g_n = \bar{g}_n/\bar{g}_{ref}$, $I_{app} = \bar{I}_{app}/(V_{Ca}\bar{g}_{ref})$. V_{Ca} is chosen to normalize the calcium ionic channel so that we will have $v_{Ca} = 1$. The conductance parameters are normalized towards a reference value $\bar{g}_{ref} = 4ms/cm^2$. Then introduce $\bar{g}_{ref}t/C_m \to t$ as the dimensionless time variable. Thus, we have a dimensionless Morris-Lecar oscillators

with the form

$$\begin{aligned} v' &= I_{app} - g_{Ca}C_\infty(v)(v - v_{Ca}) - g_K m_i(v - v_K) \\ m' &= \varphi\lambda(v)(m_\infty(v) - m), \end{aligned}$$

where

$$\begin{aligned} C_\infty(v) &= \frac{1}{2}(1 + \tanh((v - \nu_1)/\nu_2)), \\ \lambda(v) &= \cosh((v - \nu_3)/2\nu_4), \\ m_\infty(v) &= \frac{1}{2}(1 + \tanh((v - \nu_3)/\nu_4)). \end{aligned}$$

Considering N identical Morris-Lecar oscillators with delayed synaptic coupling, we have the following model

$$\begin{aligned} v_i' &= I_{app} - g_{Ca}C_\infty(v_i)(v_i - v_{Ca}) - g_K m_i(v_i - v_K) \\ &\quad -g_L(v_i - v_L) - \epsilon \sum_{j=1, j\neq i}^{N} w_{ij} s(v_j(t - \tau))(v_i(t) - E_{syn}), \\ m_i' &= \varphi\lambda(v_i)(m_\infty(v_i) - m_i), \end{aligned} \tag{4.37}$$

where $i = 1, \ldots, N$ and

$$s(v) = \frac{1}{2}(1 + \tanh(10v)).$$

Using the parameter set I from [18, Table 1], when there is no coupling in the network each oscillator has a unique exponentially asymptotically stable limit cycle with period $T \approx 23.87$ corresponding to $\Omega = 0.2632$.

4.4.1 Phase model analysis

The calculation of the phase model interaction function, H, described in sections 3.6 and 4.2 , may be carried out numerically. We used the numerical simulation package XPPAUT [38] to do this for model (4.37) with $\tau = 0$, and to calculate a finite number of terms in the Fourier series approximation for H. This gives an explicit approximation for H:

$$H(\phi) \approx a_0 + \sum_{k=1}^{K}(a_k \cos(k\phi) + b_k \sin(k\phi)). \tag{4.38}$$

Parameter	Name	value
v_{Ca}	Calcium equilibrium potential	1
v_K	Potassium equilibrium potential	-0.7
v_L	Leak equilibrium potential	-0.5
g_K	Potassium ionic conductance	2
g_L	Leak ionic conductance	0.5
φ	Potassium rate constant	$\frac{1}{3}$
ν_1	Calcium activation potential	-0.01
ν_2	Calcium reciprocal slope	0.15
ν_3	Potassium activation potential	0.1
ν_4	Potassium reciprocal slope	0.145
g_{Ca}	Calcium potential conductance	1
I_{app}	Applied current	0.09

Table 4.1: Parameters used in system (4.37) [18, Table 1]

The first nine terms of Fourier coefficients are shown in Table 4.2. Figure 4.1 shows the plot of the interaction function (red solid), H, together with the approximations using one (black solid) and 20 terms (green dashed) of Fourier Series. Obviously, the one term approximation is not enough to explain the behavior of H. However, the 20-term approximation is indistinguishable with the numerically calculated H. Therefore, we adopt the 20-term approximation for subsequent calculations.

k	a_k	b_k	k	a_k	b_k
0	-2.0214064	0	5	-0.01054942	0.010251001
1	1.994447	-0.93897837	6	-0.002131111	0.0046384884
2	0.010604496	0.27575842	7	9.9814584e-05	0.0013808256
3	-0.051657807	0.042355601	8	0.00015646126	7.391713e-05
4	-0.029127343	0.01801952	9	-8.1846403e-05	-0.00024995379

Table 4.2: Fourier coefficients of the interaction function for model (4.37).

With the explicit approximation for H (4.38) and the value of the coefficients a_j, b_j, we can determine the asymptotic stability of any possible symmetric cluster states for any N using the eigenvalues calculated in the last section. In this section, we consider two

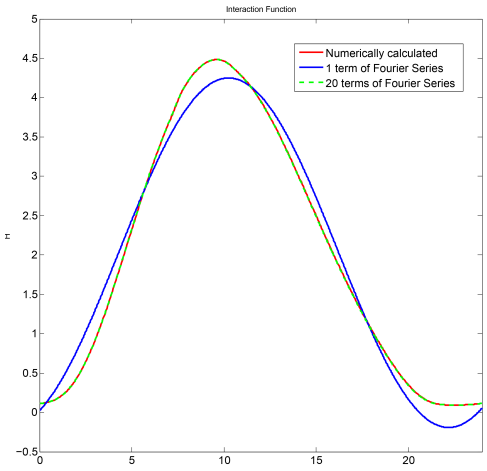

Figure 4.1: Interaction function for model (4.37) and the approximations using 1 and 20 terms of Fourier Series

coupling matrices

$$W_b = circ(0, 1, \frac{1}{2}, \frac{1}{3}, \cdots, \frac{1}{2}, 1), \text{ bi-directional, distance dependent} \quad (4.39)$$

$$W_h = circ(0, 1, 1, \cdots, 1), \text{ global homogeneous.} \quad (4.40)$$

With the coupling matrices W_b and W_h, various values of ϵ and the time delay τ, we used our phase model results above to predict the stability of all possible symmetric cluster solutions for $N = 2, \cdots, 10$. The results are shown in Tables 4.3 and 4.4. Comparing the phase model prediction and DDE-BIFTOOL continuation for the full model, we observe that the agreement gets better as ϵ gets smaller. The disagreements appear usually on the endpoints of intervals. For the full model, some extra intervals of stability appear as ϵ varies. For example for networks with b-directional coupling, the 3-cluster solutions with $N = 6$, the 7-cluster solutions corresponds to $\psi = \frac{2\pi}{7}$ and $\psi = \frac{12\pi}{7}$, and the 8-cluster solutions correspond to $\psi = \frac{\pi}{4}$ and $\psi = \frac{7\pi}{4}$ have extra intervals of stability comparing to the phase model prediction. Note that, in all cases, for $\tau = 0$ only the synchronous ($1-$cluster) solution is asymptotically stable. However, increasing τ may destabilize this solution and/or stabilize other cluster solutions. In particular, for some values of τ multi-stability between different cluster solutions occurs. Further, changing the coupling matrix from W_b (bi-directional, distance dependent coupling) to W_h (global homogeneous coupling) can cause significant changes in stability. For example, when N is a prime number, the only clustered states are splay states (rotating waves). With W_h all the splay states for

a given N have the same stability (Table 4.4), while with W_b splay states corresponding to different ψ can have quite different stabilities (Table 4.3).

4.4.2 Numerical studies

In this section, we perform numerical continuation studies of the full model (4.37) for two cases. When τ is not to large, i.e. $\Omega\tau_{ij} = O(1)$ with respect to the coupling strength ϵ, we use DDE-BIFTOOL [35] in MATLAB to numerically compute branches of periodic orbits and their stability as parameters are varied. Furthermore, we carry out numerical simulations to determine the stability of general synchronization solutions as defined in section 4.3.3 for any time delay τ values.

Numerical simulation and continuation when τ is not too large

Taking the time delay as a continuation parameter, we use this package DDE-BIFTOOL to compute the stability of all possible symmetric cluster solutions for $N = 2, 3, \cdots, 10$ with the two different coupling matrices W_b, W_h and four different values of ϵ, $\epsilon = 0.001, 0.01, 0.05, 0.1$. These results indicated that the phase model prediction is accurate up to $\epsilon = 0.01$. The results for $\epsilon = 0.01, 0.05$ are summarized in Tables 4.3 and 4.4. Some of the plots are shown in Figures 4.2 4.3, and 4.4. The red circles denote a stable cluster solutions while the green circles denote unstable ones. The x-axis of each diagram corresponds to the value of τ, while the y-axis shows the maximum amplitude of $v_1(t)$ for each cluster solution. In the simulation, we can see that for $\epsilon = 0.001$ and $\epsilon = 0.01$, the profiles of the cluster solutions are relatively unaffected by time delay τ, while for $\epsilon = 0.05, 0.1$ the solution profiles varies with τ (see Figure 4.2 for example). In particular we observe that the synchronous solution is stable for approximately the same $\tau-$interval in all networks (cf. Figure 4.3) and the $2-$cluster solution is stable for approximately the same $\tau-$interval in all networks with $N > 2$ and even (cf. Figure 4.4), which agrees with Corollaries 1 and 2.

Using dde23 in MATLAB, we are able to numerically simulate the solution for larger sizes of networks. In the following, we use dde23 in MATLAB, and numerically simulate the solutions for networks with larger sizes. we show several numerical simulations that verify the predictions of the phase model for the case of a network with $N = 140$ oscillators. This network admits 1-cluster, 2-cluster, 5-cluster, 7-cluster, 10-cluster, 14-cluster, 35-cluster, 70-cluster, and 140-cluster solutions. The initial conditions that we use for n-cluster

N	n	ψ	Phase model prediction	Full model	
				$\epsilon = 0.01$	$\epsilon = 0.05$
4	1	0	$(0, 1.53) \cup (14.28, 23.87)$	$(0, 1.44) \cup (12.75, 23.87)$	$(0, 1.62) \cup (8.83, 23.87)$
	2	π	$(2.47, 10.46)$	$(2.20, 10.21)$	$(1.68, 9.32) \cup (17.47, 23.87)$
	4	$\frac{\pi}{2}, \frac{3\pi}{2}$	(0.57,3.22)∪(8.69,14.69)	(0,2.96)∪(8.36,14.16)	(0,2.26)∪(6.86,12.36)
5	1	0	$(0, 1.53) \cup (14.28, 23.87)$	$(0, 1.41) \cup (12.51, 23.87)$	$(0, 1.67) \cup (8.19, 23.87)$
	5	$\frac{2\pi}{5}, \frac{8\pi}{5}$	(1.26,2.48)∪(10.84,13.46)	(0,2.21)∪(10.31,12.71)	(0,1.51)∪(8.71,10.81)
	5	$\frac{4\pi}{5}, \frac{6\pi}{5}$	(1.66,3.66)∪(4.26,13.09)	(1.513,12.61)	(0.70,11.49)
6	1	0	$(0, 1.53) \cup (14.28, 23.87)$	$(0, 1.41) \cup (12.31, 23.87)$	$(0, 1.70) \cup (7.82, 23.87)$
	2	π	$(2.64, 9.45)$	$(2.30, 9.10)$	$(1.58, 7.79) \cup (16.59, 27.31)$
	3	$\frac{2\pi}{3}, \frac{4\pi}{3}$	$(0.41, 12.91)$	$(0.31, 13.01) \cup (23.11, 23.87)$	$(0, 4.19) \cup (5.30, 11.40) \cup (17.41, 20.9) \cup (22.31, 23.87)$
	6	$\frac{\pi}{3}, \frac{5\pi}{3}$	(0.58,0.87)∪(12.32,14.10)	(0,1.51)∪(12.01,13.11)	(0,1.11)∪(9.21,10.31)
7	1	0	$(0, 1.53) \cup (14.28, 23.87)$	$(0, 1.49) \cup (12.19, 23.87)$	$(0, 1.68) \cup (7.52, 23.87)$
	7	$\frac{2\pi}{7}, \frac{12\pi}{7}$	(12.82,13.86)	(0,1.21)∪(12.11,12.81)	(0,1.10)∪(8.82,9.82)
	7	$\frac{4\pi}{7}, \frac{10\pi}{7}$	(2.33,4.37)∪(7.59,13.83)	(0.51,3.91)∪(7.21,13.11)	(0,2.71)∪(5.81,11.11)
	7	$\frac{6\pi}{7}, \frac{8\pi}{7}$	(2.51,3.45)∪(4.04,4.93)∪(5.48,5.96)∪(7.47,13.13)	(2.51,4.91)∪(6.91,12.11)	(1.70,3.81)∪(5.70,10.82)
8	1	0	$(0, 1.53) \cup (14.28, 23.87)$	$(0, 1.44) \cup (12.04, 23.87)$	$(0, 1.74) \cup (7.27, 23.87)$
	2	π	$(2.63, 9.53)$	$(2.25, 9.05)$	$(1.55, 7.45) \cup (15.73, 23.87)$
	4	$\frac{\pi}{2}, \frac{3\pi}{2}$	$(1.71, 3.22) \cup (8.69, 14.57)$	$(0.31, 2.81) \cup (8.11, 13.71)$	$(0, 1.80) \cup (6.21, 11.20)$
	8	$\frac{\pi}{4}, \frac{7\pi}{4}$	(13.34,13.95)	(0,1.01)∪(12.31,12.71)	(0,1.00)∪(8.52,9.42)
	8	$\frac{3\pi}{4}, \frac{5\pi}{4}$	(3.96,13.13)	(3.41,12.41)	(0.11,0.71)∪(2.61,10.82)
9	1	0	$(0, 1.53) \cup (14.28, 23.87)$	$(0, 1.66) \cup (11.93, 23.87)$	$(0, 1.73) \cup (7.06, 23.87)$
	3	$\frac{2\pi}{3}, \frac{4\pi}{3}$	$(0.41, 5.04) \cup (8.08, 12.93)$	$(0.41, 4.61) \cup (7.71, 12.41)$	$(0, 3.30) \cup (5.80, 10.60) \cup (16.61, 19.31)$
	9	$\frac{2\pi}{9}, \frac{16\pi}{9}$	(13.46,14.01)	—	—
	9	$\frac{4\pi}{9}, \frac{14\pi}{9}$	(2.50,2.57)∪(9.81,13.94)	(0.41,2.61)∪(9.11,13.01)	(0,1.71)∪(6.51,10.41)
	9	$\frac{8\pi}{9}, \frac{10\pi}{9}$	(2.90,3.77)∪(8.08,11.38)	(2.61, 4.01)∪(7.51,11.01)	(1.60,3.12)∪(5.92,8.81)

Table 4.3: Comparison of phase model prediction of τ-intervals of asymptotic stability for n-cluster solution with numerical of the full model. The coupling matrix is W_b. Other parameter values are given in Table 4.1.

N	n	Phase model prediction	Full model	
			$\epsilon = 0.01$	$\epsilon = 0.05$
2	1	$(0, 1.53) \cup (14.28, 23.87)$	$(0, 1.46) \cup (13.56, 23.87)$	$(0, 1.43) \cup (11.53, 23.87)$
	2	(2.35,13.46)	(2.23,13.43)	(1.92,13.32)
3	1	$(0, 1.53) \cup (14.28, 23.87)$	$(0, 1.48) \cup (13.09, 23.87)$	$(0, 1.52) \cup (9.53, 23.87)$
	3	(0.41,13.74)	(0.50,13.40)	(0,12.6)
4	1	$(0, 1.53) \cup (14.28, 23.87)$	$(0, 1.47) \cup (12.57, 23.87)$	$(0, 1.70) \cup (8.11, 23.87)$
	2	$(2.73, 9.19)$	$(2.41, 8.91)$	$(1.71, 7.71) \cup (17.53, 23.87)$
	4	(1.93,3.22) $\cup$ (8.69,14.47)	(0.97,2.87)$\cup$(8.47,13.97)	(0,1.96)$\cup$(6.97,12.27)
5	1	$(0, 1.53) \cup (14.28, 23.87)$	$(0, 1.49) \cup (11.99, 23.87)$	$(0, 1.79) \cup (7.22, 23.87)$
	5	(1.57,2.69)$\cup$(9.76,13.20)	(0.93,2.23)$\cup$(9.13,12.43)	(0,1.32)$\cup$(6.13,10.42)
6	1	$(0, 1.53) \cup (14.28, 23.87)$	$(0, 1.46) \cup (11.56, 23.87)$	
	2	$(2.73, 9.19)$	$(2.30, 8.51)$	$(1.48, 6.29) \cup (15.0, 23.19)$
	3	$(0.41, 4.83) \cup (8.29, 12.79)$	$(0.28, 4.18) \cup (7.98, 11.98)$	$(0, 3.03) \cup (5.54, 9.83) \cup (15.94, 18.44)$
	6	(12.26,13.86)	(11.96,12.72)	(0,0.91)$\cup$(9.21,9.91)
7	1	$(0, 1.53) \cup (14.28, 23.87)$	$(0, 1.49) \cup (11.01, 23.87)$	$(0, 1.94) \cup (6.10, 23.87)$
	7	(12.47,13.54)	(11.92,12.32)	(0,0.92)$\cup$(8.52,9.32)
8	1	$(0, 1.53) \cup (14.28, 23.87)$	$(0, 1.50) \cup (10.70, 23.87)$	$(0, 2.00) \cup (5.70, 23.87)$
	2	$(2.73, 9.19)$	$(2.22, 8.22)$	$(1.34, 5.44) \cup (13.24, 20.34)$
	4	$(1.94, 3.22) \cup (8.69, 9.35) \cup (12.37, 14.47)$	$(0.53, 2.63) \cup (7.53, 8.43) \cup (11.13, 13.03) \cup (22.63, 23.23)$	$(0, 1.33) \cup (5.13, 6.03) \cup (7.33, 9.14) \cup (19.04, 20.34) \cup (20.94, 21.64)$
	8	All unstable	(0,1.35)$\cup$(6.15,6.95)$\cup$(16.36,17.56)	(0,0.95)$\cup$(7.95,8.75)
9	1	$(0, 1.53) \cup (14.28, 23.87)$	$(0, 1.48) \cup (10.22, 23.87)$	$(0, 2.08) \cup (5.40, 23.87)$
	3	$(0.41, 4.83) \cup (8.29, 12.79)$	$(0.19, 4.00) \cup (7.49, 11.29) \cup (21.39, 23.87)$	$(0, 2.78) \cup (5.00, 8.29) \cup (14.39, 15.80) \cup (17.50, 22.40)$
	9	(13.30,13.65)	(0.56,1.16)$\cup$(11.36,11.96)	(0,0.96)$\cup$(7.56,8.37)

Table 4.4: Comparison of phase model prediction of τ-intervals of asymptotic stability for n-cluster solution with numerical of the full model. The coupling matrix is W_h. Other parameter values are given in Table 4.1.

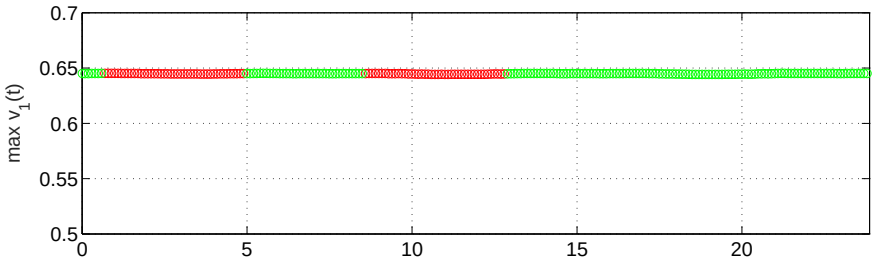

(a) $\epsilon = 0.001$, 3-cluster

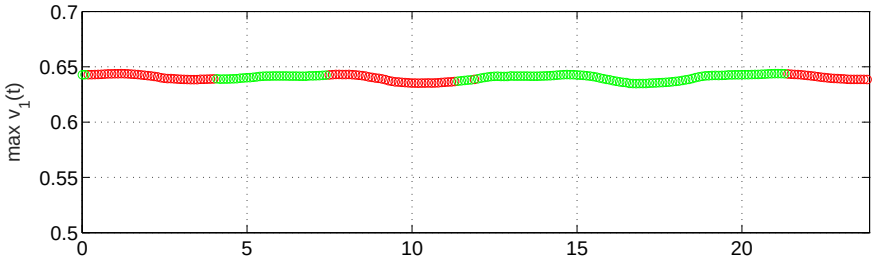

(b) $\epsilon = 0.01$, 3-cluster

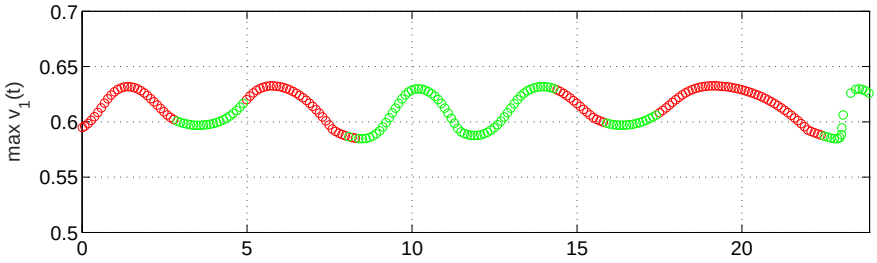

(c) $\epsilon = 0.05$, 3-cluster

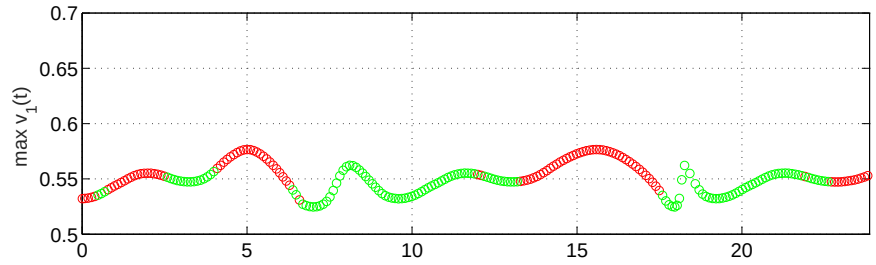

(d) $\epsilon = 0.1$, 3-cluster

Figure 4.2: Branches of 3-cluster solutions with respect to τ for system (4.37) with $N = 9$ and homogeneous coupling. (a) 3-cluster solution with $\epsilon = 0.001$, (b) 3-cluster solution with $\epsilon = 0.01$, (c) 3-cluster solution with $\epsilon = 0.05$ (d) 3-cluster solution with $\epsilon = 0.1$

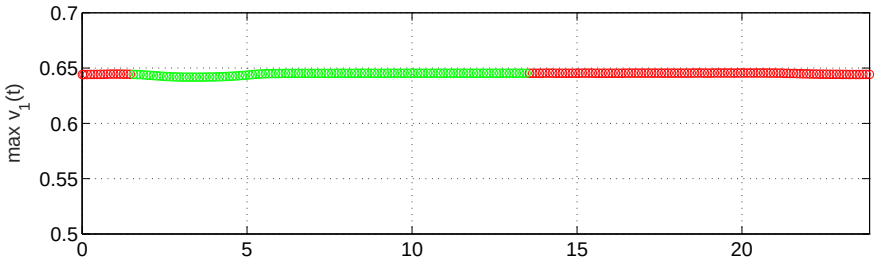

(a) $\epsilon = 0.01,\ N = 2$

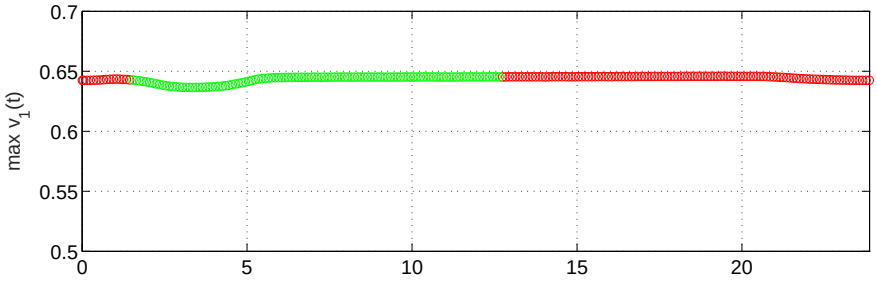

(b) $\epsilon = 0.01,\ N = 4$

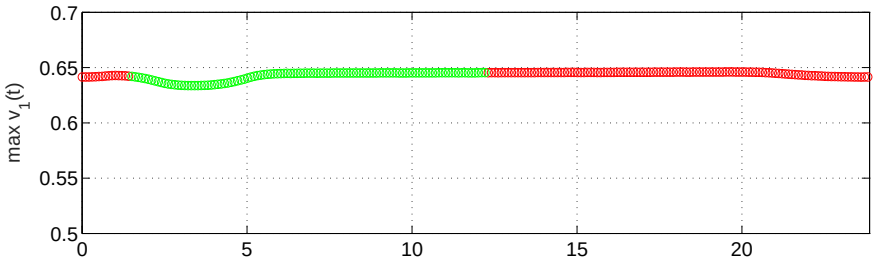

(c) $\epsilon = 0.01,\ N = 6$

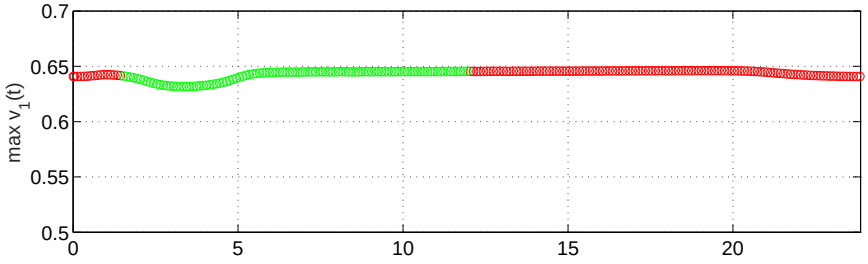

(d) $\epsilon = 0.01,\ N = 8$

Figure 4.3: Branches of the synchronization solutions with respect to τ for system (4.37) with $N = 2, 4, 6, 8$, bidirectional coupling and $\epsilon = 0.01$. (a) $N = 2$, (b) $N = 4$, (c) $N = 6$, (d) $N = 8$.

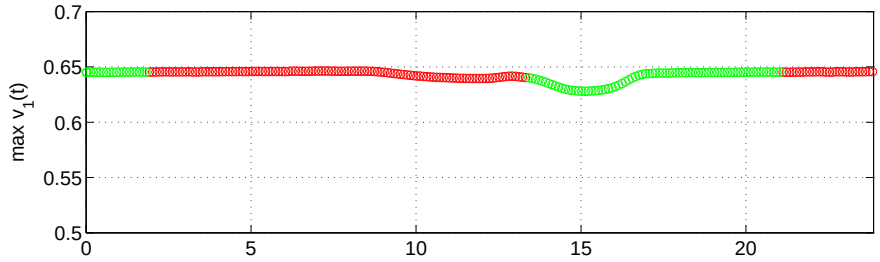

(a) $\epsilon = 0.05,\ N = 2$

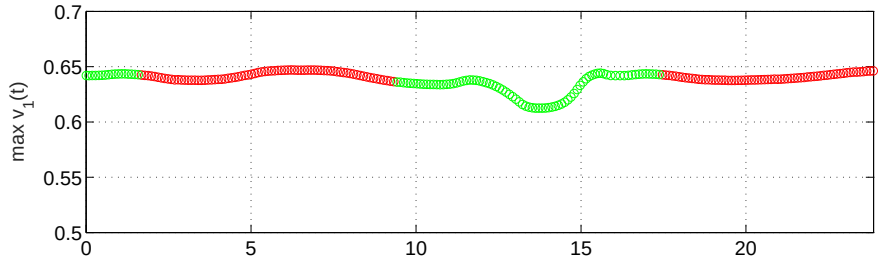

(b) $\epsilon = 0.05,\ N = 4$

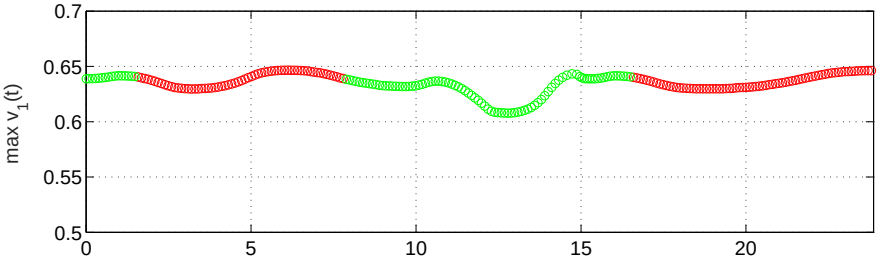

(c) $\epsilon = 0.05,\ N = 6$

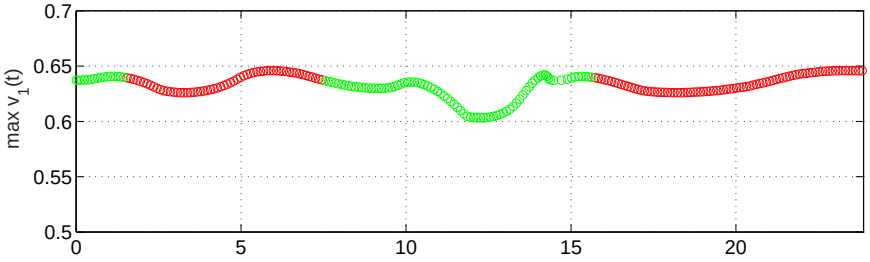

(d) $\epsilon = 0.05,\ N = 8$

Figure 4.4: Branches of 2-cluster and 3-cluster solutions with respect to τ for system (4.37) with $N = 6$, bidirectional coupling. (a) $N = 2$, (b) $N = 4$, (c) $N = 6$, (d) $N = 8$.

n	ψ	Stability w.r.t. τ	
		W_b	W_h
1	0	(0, 1.52) $\cup$ (14.28,23.87)	(0, 1.52) $\cup$ (14.28,23.87)
2	π	(2.73, 9.19)	(2.73, 9.19)
5	$\frac{2\pi}{5}, \frac{8\pi}{5}$ $\frac{4\pi}{5}, \frac{6\pi}{5}$	(1.52, 2.61) $\cup$ (10.78, 12.55) (1.61, 2.81) $\cup$ (6.21, 7.77) $\cup$ (10.03, 12.55)	(1.57, 2.69) $\cup$ (10.03, 12.54)
7	$\frac{2\pi}{7}, \frac{12\pi}{7}$ $\frac{4\pi}{7}, \frac{10\pi}{7}$ $\frac{6\pi}{7}, \frac{8\pi}{7}$	(12.77, 13.29) (8.13, 9.81) $\cup$ (11.12, 13.28) (8.45, 9.88) $\cup$ (11.11, 13.13)	(12.47, 13.28)
10	$\frac{\pi}{5}, \frac{9\pi}{5}$ $\frac{3\pi}{5}, \frac{7\pi}{5}$	All unstable (7.85, 7.86) $\cup$ (11.80, 12.62)	All unstable

Table 4.5: Phase model prediction of intervals of τ where stable 1-, 2-, 5-, 7-, and 10-cluster solutions exist. The network has 140 oscillators and the coupling matrix W_b or W_h.

solutions are in the following form

$$\begin{aligned} v_{\frac{N}{n}l+k}(t) &= -0.5 + \frac{n}{N} + 0.1RD,\ k = 1, \cdots, \frac{N}{n},\ l = 0, \cdots, n-1. \\ m_i(t) &= 0,\ i = 1, \cdots, N. \end{aligned} \tag{4.41}$$

for $t \in [-\tau, 0]$. Here RD is a random number between $[0, 1]$.

From the phase model analysis, we are able to predict the stability regions for all the cluster states. Table 4.5 summarize the stability intervals with respect to τ for the first five cluster types.

The phase model predicts that, for bidirectional coupling, there should be four stable 5-cluster solutions when $\tau = 12$ corresponding to $\psi = \frac{k\pi}{5}$, $k = 1, 2, 3, 4$. In these 5-cluster solutions, the clusters are the same and given by

$$\begin{aligned} C_1 &= \{1, 6, 11, \ldots, 136\}, \\ C_2 &= \{2, 7, 12, \ldots, 137\}, \\ &\vdots \\ C_5 &= \{5, 10, 15, \ldots, 140\}. \end{aligned}$$

but each solution has a different cluster ordering. The ordering is $C_1 - C_2 - C_3 - C_4 - C_5$ with $\psi = 2\pi/5$ (see Figure 4.5 (a)), $C_1 - C_4 - C_2 - C_5 - C_3$ with $\psi = 4\pi/5$ (see Figure 4.5 (b)), $C_1 - C_3 - C_5 - C_2 - C_4$ with $\psi = 6\pi/5$(see Figure 4.5 (c)) and $C_1 - C_5 - C_4 - C_3 - C_2$

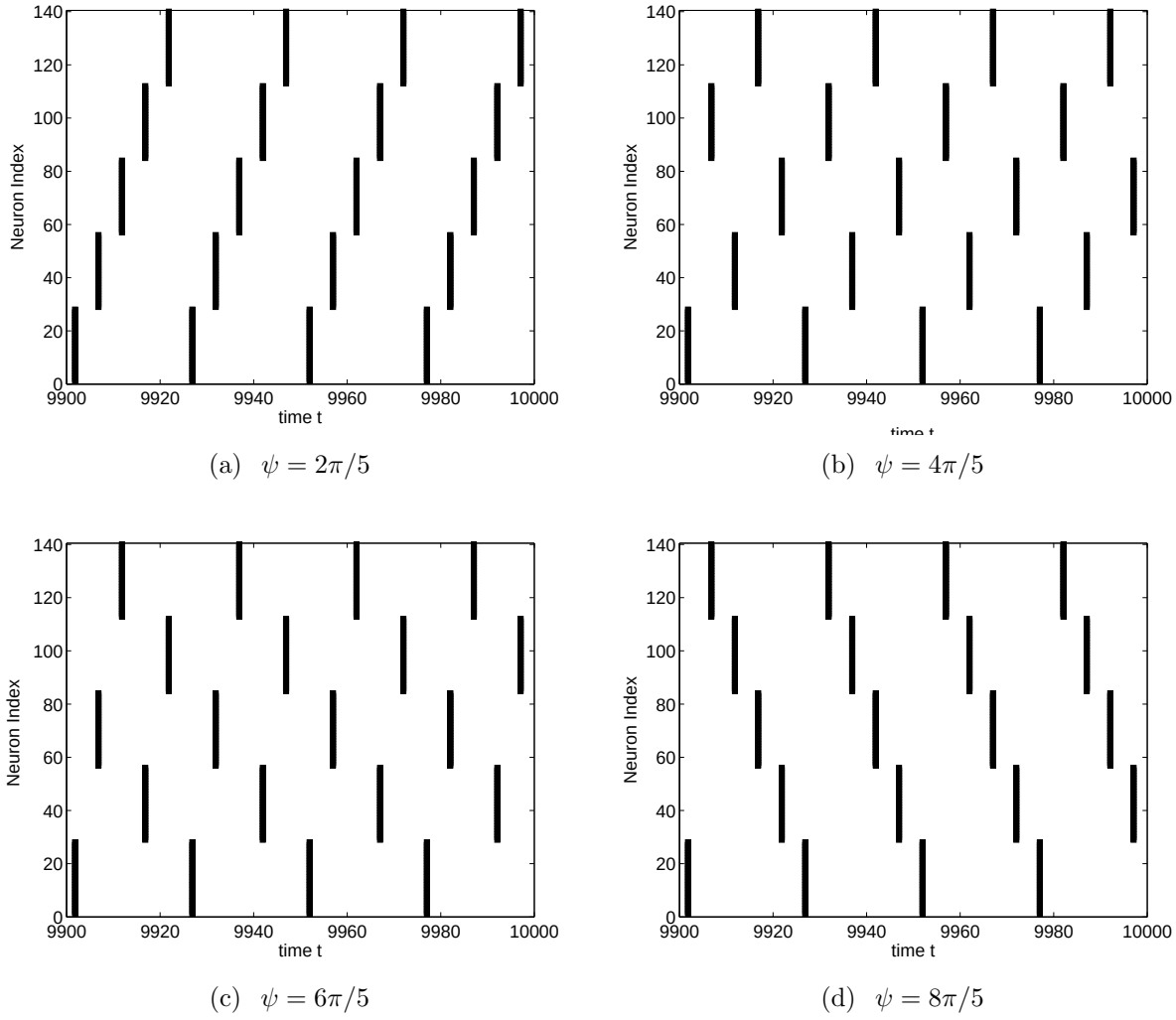

(a) $\psi = 2\pi/5$ (b) $\psi = 4\pi/5$

(c) $\psi = 6\pi/5$ (d) $\psi = 8\pi/5$

Figure 4.5: Raster plots showing a stable 5-cluster solutions in a network with $N = 140$ neurons and bi-directional coupling (connectivity matrix W_b). $\tau = 12$ and $\epsilon = 0.001$ all other parameters values are given in Table 4.1. (a) $\psi = 2\pi/5$, cluster ordering $C_1 - C_2 - C_3 - C_4 - C_5$ (b) $\psi = 4\pi/5$, cluster ordering $C_1 - C_4 - C_2 - C_5 - C_3$ (c) $\psi = 6\pi/5$, cluster ordering $C_1 - C_3 - C_5 - C_2 - C_4$ (d) $\psi = 8\pi/5$, cluster ordering $C_1 - C_5 - C_4 - C_3 - C_2$

with $\psi = 8\pi/5$ (see Figure 4.5 (d)). Note that in Figure 4.5 we reorder the indices so that oscillators that belong to the same cluster are plotted together.

Now consider the 7-cluster solution with connection matrix W_b. The phase model predicts that when $\tau = 13$ there exist six stable 7-cluster solutions with clusters:

$$\begin{aligned} C_1 &= \{1, 8, 15, \ldots, 134\}, \\ C_2 &= \{2, 9, 16, \ldots, 135\}, \\ &\vdots \\ C_7 &= \{7, 14, 21, \ldots, 140\}. \end{aligned}$$

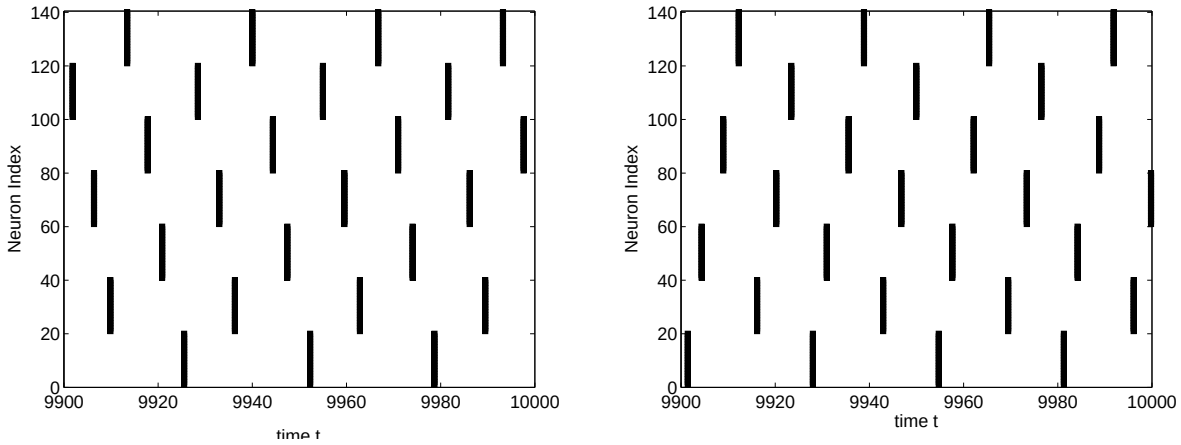

(a) $\psi = 8\pi/7$ (b) $\psi = 6\pi/7$

Figure 4.6: Raster plots showing stable 7-cluster solutions with $\tau = 13$, $\epsilon = 0.01$ in a network with $N = 140$ neurons and bi-directional coupling (connectivity matrix W_b). (a) $\psi = \frac{6\pi}{7}$, cluster ordering $C_1 - C_6 - C_4 - C_7 - C_5 - C_3$. (b) $\psi = \frac{8\pi}{7}$, cluster ordering $C_1 - C_3 - C_5 - C_7 - C_2 - C_4 - C_6$.

For $\psi = \frac{6\pi}{7}$, the cluster ordering is $C_1 - C_6 - C_4 - C_2 - C_7 - C_5 - C_3$ (see Figure 4.6(a)), while for $\psi = \frac{8\pi}{7}$, the cluster ordering is $C_1 - C_3 - C_5 - C_7 - C_2 - C_4 - C_6$ (see Figure 4.6(b)). In Figure 4.6, we reorder the oscillator indices so that oscillators that belong to the same cluster are plotted together. We were unable to find the other 7-cluster solutions numerically. There may be two reasons. First, it is caused by the multistability, and the basin of attraction for the other 7-cluster solutions are smaller that some other cluster solutions. The other reason is that we choose the initial conditions in the numer-

ically studies to be constants for $t \in [-\tau, 0]$. Modifying the initial conditions to be other functions may help on finding the other 7-cluster solutions.

Remark 7. *We have observed other types of stable cluster solutions. For example, Figure 4.7 shows solutions of the type (4.31) and (4.32) which appear to be stable. With $N = 8$ and bidirectional coupling in (4.39), the phase model predicts that the solutions of the type (4.31) and (4.32) are unstable for all τ when $\epsilon > 0$, and stable for $\tau \in (1.5, 2.0] \cup (13.8, 14.1)$ when $\epsilon < 0$. This prediction is consistent the numerically observed solution which occurs for $\epsilon = -0.01$, and $\tau = 2$.*

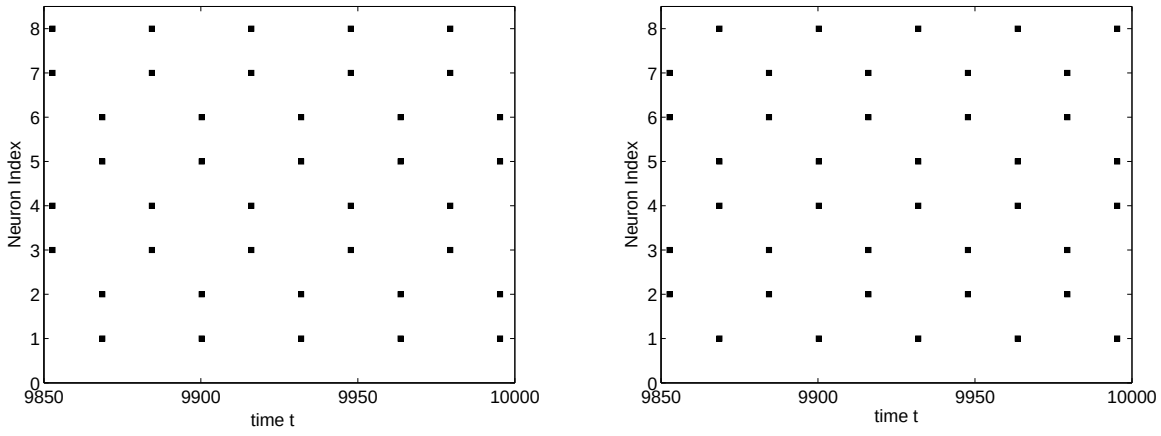

(a) (b)

Figure 4.7: 2-cluster solutions of the form (4.31) (a) and (4.32) (b) for $N = 8$, $\epsilon = -0.01$, $\tau = 2$ and connectivity matrix W_b.

From Tables 4.3 and 4.4 it is clear that the system exhibits multistability for a large of range of τ values. To further investigate the multistability, we carried out numerical simulations of the model (4.37) with $N = 6$ and coupling matrix W_b using XPPAUT [38]. We start with constant initial conditions ($v_i(t) = v_{i0}$, $w_i(t) = w_{i0}$, $-\tau \le t \le 0$), and apply a small perturbation to the input current of one or more neurons during the simulation. The perturbations could cause switching between two different cluster types or between different realizations of the same cluster type. Figure 4.8 show two examples, where the dark bars indicate when a particular neuron spikes. When $\tau = 8$, both the 2-cluster solutions and 3-cluster solutions are stable. Figure 4.8 (a) shows that when $\tau = 8$, a perturbation to neurons 1, 2, 3, 4 and 6 for $600 \le t \le 650$ switches the networks from a 3-cluster solution (with clusters (1, 4), (2, 5) and (3, 6)) to a 2-cluster solution (with clusters (1, 3, 5), and

(2, 4, 6)). Figure 4.8 (b) shows when $\tau = 8$, a perturbation to neuron 2, 4, 5, and 6 for $600 \leq t \leq 650$ switches the network from a 3-cluster solution with clusters ordering (1, 4)-(3, 6)-(2, 5) to a 3-cluster solution with clusters ordering (1, 4)-(2, 5)-(3, 6).

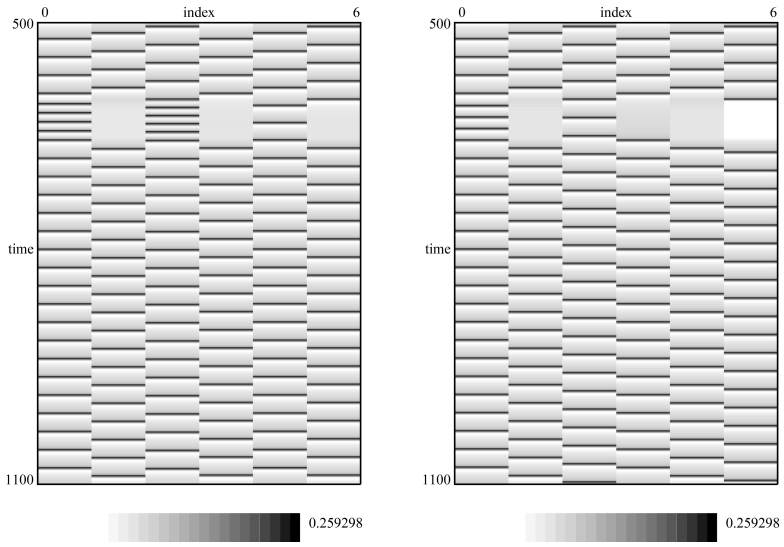

(a) $\tau = 8$ (b) $\tau = 8$

Figure 4.8: Numerical simulations showing multi-stability in a 6 neuron network with bidirectional coupling. (a) Switching from a 3-cluster solution to a 2-cluster solution. (b) Switching from a 3-cluster solution to a 3-cluster solution. $\tau = 8$ and $\epsilon = 0.001$. All other parameters are given in Table 4.1.

We further investigate the model (4.37) with $N = 6$ and coupling matrix W_h. The initial conditions are same as above, and a small perturbation. Table 4.4 show that when $\tau = 3$ both the 2-cluster solutions and 3-cluster solutions are stable. When $\tau = 8$ the 2-cluster solutions are the only stable solutions. Figure 4.9 shows theses two examples. Figure 4.9(a) shows that when $\tau = 3$, a small perturbation to neurons 3 and 4 for $600 \leq t \leq 620$ switches the network from a 3-cluster solution to a 2-cluster solution. Figure 4.9(b) shows that when $\tau = 8$, a small perturbation to neurons 2 and 5 for $600 \leq t \leq 620$ switches the network from a 2-cluster solution with cluters 1, 3, 5 and 2, 4, 6 to a 2-cluster solution with clusters 1,2, 3 and 4, 5, 6.

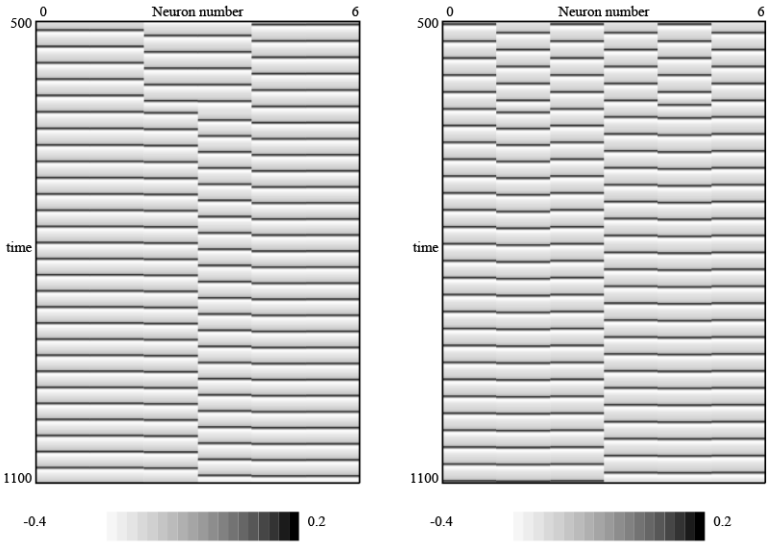

(a) $\tau = 3$ (b) $\tau = 8$

Figure 4.9: Numerical simulations showing multistability in a 6 neuron network with homogeneous coupling. (a) Switching from a 3-cluster solution to a 2-cluster solution when $\tau = 3$. (b) Switching from a 2-cluster solution to a 2-cluster solution when $\tau = 8$. $\epsilon = 0.001$ and all other parameters are given in Table 4.1.

Numerical simulation for any time delay τ

In the above, we have an approximate expression for the interaction function H. The collective frequency $\tilde{\Omega}$ of the 1-cluster solution (4.18) is determined by (4.19) which can be rewritten as

$$\frac{\tilde{\Omega}\tau}{\epsilon\bar{w}\tau} - \frac{\Omega}{\epsilon\bar{w}} = H(-\tilde{\Omega}\tau). \tag{4.42}$$

The solution can be graphically seen in Figure 4.10. The left hand side of (4.42) is a line with slope $1/\epsilon\bar{w}\tau$ and horizontal intercept $\Omega\tau$. Applying the stability theorem (Theorem 16) for positive ϵ values, we see that if the line intersects the positive slope of the $H(-\tilde{\Omega}\tau)$ curve (displayed by solid circles in Figure 4.10), the synchronization solution at that particular $\tilde{\Omega}$ is stable. The synchronization solution is unstable if the line intersects the negative slope of the curve which is denoted by empty circles. Figure 4.11 plots $\tilde{\Omega}$ as a function of the time delay for two ϵ values. Branches with stable and unstable synchronous frequencies alternate with each other. For small coupling strength $\epsilon = 0.001$, it is only possible to have one stable synchronous solutions for $\tau \in [0, 100]$. However, for $\epsilon = 0.01$, it is possible to have two, or three synchronous solutions for larger τ values. Increasing coupling strength induces multistability.

From equation (4.42) we can get more insight about how the coupling strength ϵ and time delay τ affect stability of the synchronization solutions. Fixing Ω, τ and increasing ϵ corresponds to rotating the line counterclockwise about its horizontal intercept. For very small and positive ϵ, the line is approximately vertical, and intersects the periodic $H(-\tilde{\Omega}\tau)$ curve only once (see Figure 4.10 (a) for example). That means that there is only one synchronous frequency $\tilde{\Omega}$ whose stability depends on the horizontal intercept $\Omega\tau$. In particular, as $\Omega\tau$ is varied, the stability of the synchronization solution changes periodically as the line alternates from an intersection at a negative slope to an intersection at a positive slope. As ϵ increases, the line is approximately horizontal and there are more intersections with the $H(-\tilde{\Omega}\tau)$ curve (see Figure 4.10 (b) for example). In this case, there exists at least one stable synchronous solution. From Theorem 16, it is clear that only the local extreme points of H are needed in determine the stability analysis. Thus, we plot the stability diagram in the (τ, ϵ)-plane in Figure 4.4.2. It is interesting to note that the stability regions of instability becomes thiner as increasing of τ.

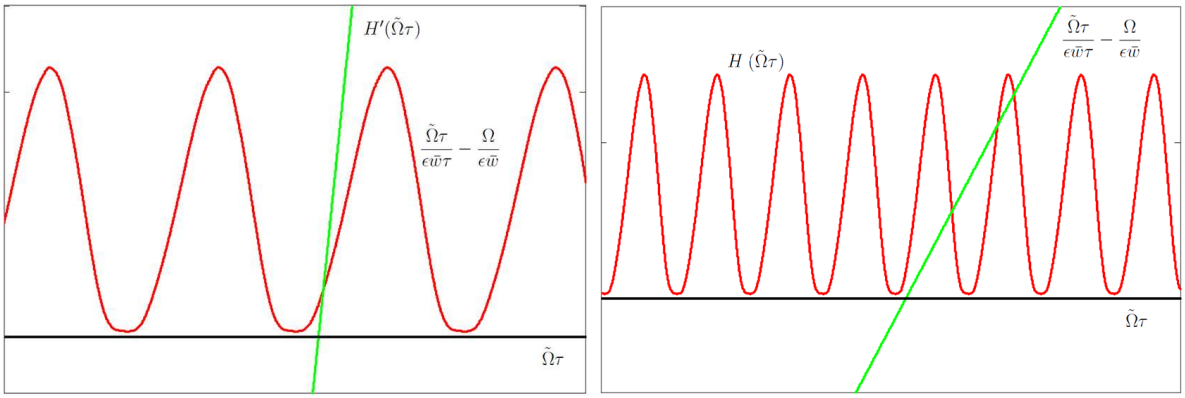

(a) $\epsilon = 0.001$ (b) $\epsilon = 0.01$

Figure 4.10: Graphical determination of (4.42) for $\tau = 100$, and (a) $\epsilon = 0.001$; (b) $\epsilon = 0.01$. The intersections with solid circles denote stable states, and those with empty circles denote unstable states.

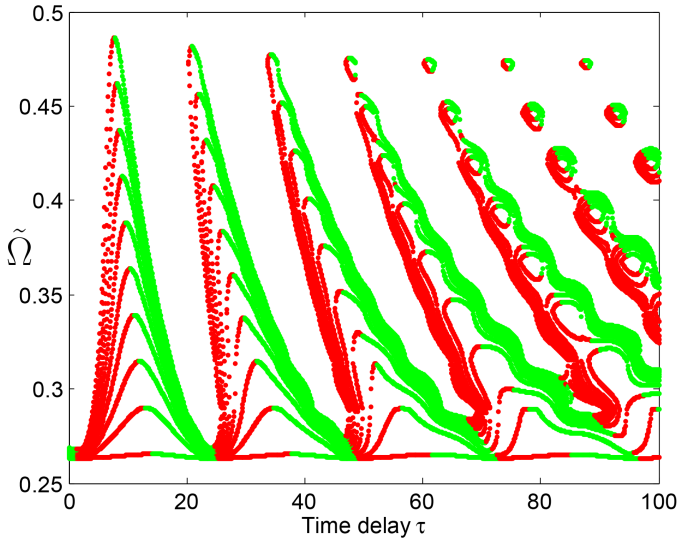

Figure 4.11: The frequences $\tilde{\Omega}$ as a function of τ for $\epsilon \in (0, 0.01]$. The green curves corresponds to stable in-phase solutions, the red curves correspond to unstable in-phase solutions.

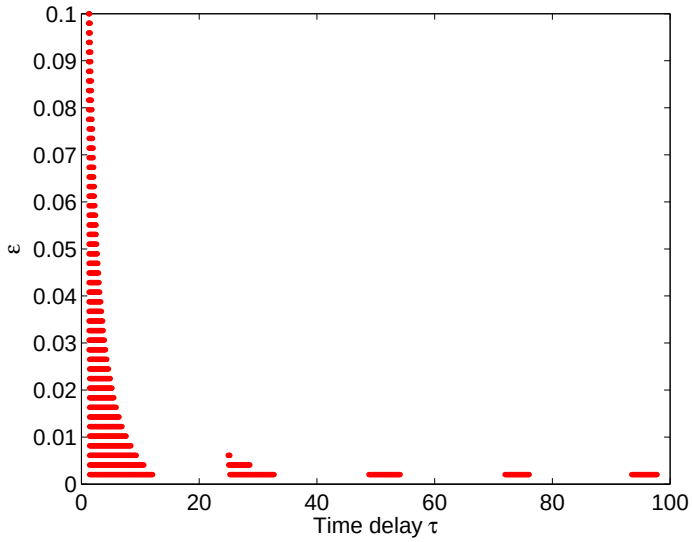

Figure 4.12: Stability diagram in the (τ, ϵ)-plane. In the white region, at least one stable synchronous solution exists. In the red regions, no stable synchronous states exist.

4.5 Persistence under symmetry breaking.

By the weakly connected theory [64], the phase model analysis should persist under ϵ-perturbation of the original model. From the steps of phase model reduction, we can see that if we perturb the connectivity matrix $W = (w_{ij})$ as $\tilde{W} = w_{ij}\,(1 + \epsilon\, m_{ij})$, the ϵ-perturbation term will finally add to $O(\epsilon^2)$ term in the phase model (4.8). A similar conclusion is obtained if we perturb the time delay τ as $\tau_{ij} = \tau\,(1+\epsilon\,\sigma_{ij})$. Here $M = (M_{ij})$, and $S = (\sigma_{ij})$ are $N \times N$ matrices with elements which are $O(1)$ with respect to ϵ. τ_{ij} represents transmission time from the jth oscillator to the ith oscillator. Note that, after the perturbation, system (4.2) no longer possesses any symmetry. To $O(\epsilon)$ the symmetry persists, however. We thus expect that, for ϵ sufficiently small, the analysis of section 4.3 should still predict the behaviour of the system.

In order to investigate the effect of the ϵ-perturbation on the connectivity matrix and time delay, we carried out sets of numerical simulations. For each set, we compare the original model with W and τ, to a model with $\tilde{W}$ and τ, and a model with W and τ_{ij}. Take $N = 6$, $W = circ\{0, 1, 1/2, 1/3, 1/2, 1\}$, and M_{ij}, σ_{ij} to be random numbers between 0 and 1. We simulate the original model and two perturbed models with $\tau = 1, \cdots, 15$, and $\epsilon = 0.001, 0.01, 0.05, 0.1$, respectively. From the simulation results, we see that for

τ	PMP	$\epsilon = 0.001$			$\epsilon = 0.01$			$\epsilon = 0.05$			$\epsilon = 0.1$		
		original	$\tilde{W}$	$\tilde{\tau}$	original	$\tilde{W}$	$\tilde{\tau}$	original	$\tilde{W}$	$\tilde{\tau}$	original	$\tilde{W}$	$\tilde{\tau}$
1	1C/3C	1C	1C	1C	NC	NC	NC	NC	NC	NC	6C	NC	NC
2	3C	6C	6C	6C	3C	3C	3C	2C	2C	2C	2C	2C	2C
3	2C/3C	2C	2C	2C	3C	3C	3C	2C	2C	2C	2C	2C	2C
4	2C/3C	2C	2C	2C	2C	2C	2C	2C	2C	2C	2C	2C	2C
5	2C/3C	3C	3C	3C	2C	2C	2C	2C	2C	2C	2C	2C	2C
6	2C/3C	2C	2C	2C	2C	2C	2C	2C	2C	2C	2C	2C	NC
7	2C/3C	2C	2C	2C	2C	2C	2C	2C	2C	2C	1C	1C	1C
8	2C/3C	2C	2C	2C	2C	2C	2C	3C	3C	NC	1C	1C	1C
9	2C/3C	3C	3C	3C	2C	2C	2C	NC	1C	1C	1C	1C	1C
10	3C	3C	3C	3C	1C	1C	1C	1C	1C	1C	1C	1C	1C
11	3C	NC	NC	NC	NC	NC	NC	1C	1C	1C	1C	1C	1C
12	3C	NC	NC	NC	NC	NC	NC	1C	1C	1C	1C	1C	1C
13	3C/6C	6C	6C	6C	1C	1C	1C	1C	1C	1C	1C	1C	1C
14	6C	6C	6C	6C	1C	1C	1C	1C	1C	1C	1C	1C	1C
15	1C	1C	1C	1C	1C	1C	1C	1C	1C	1C	1C	2C	NC

Table 4.6: Comparison of the original model and the two perturbed models for $\tau = 1, 2, \cdots, 15$ with $N = 6$. The first column shows the stable cluster solutions predicted by the phase model for each τ.

$\epsilon = 0.001, 0.01, 0.05$ the behavior of the perturbed models are the same as the unperturbed one for large time t. More accurately, the perturbed models take longer to settle at steady states than the original model. For $\epsilon = 0.1$, the behavior of unperturbed model almost captures the behavior of the perturbed ones. However, the system is sensitive to the τ values where steady states switch stability. Therefore, we conclude that for a network with 6 oscillators, the analysis of the original model is valid under perturbation with ϵ up to 0.05. Furthermore, for a network with N oscillators, the analysis of the system (4.2) should persist under sufficiently small ϵ-perturbation.

4.6 Conclusions and future work

In this chapter, we studied a general system of identical oscillators with global circulant, time-delayed coupling and showed that clustering behavior is a quite prevalent pattern of solution. We classified different clusters by the phase differences between neighboring oscillators, and investigated the existence and linear stability of clustering solutions. We focussed on symmetric cluster solutions, where the same number of oscillators belong to each cluster. In particular, we showed that certain symmetric cluster solutions exist for any

type of oscillator and any value of the delay – their existence depends only on the presence of circulant coupling. We gave a complete analysis of the linear stability of these cluster solutions. In the case of global bidirectional coupling and global homogeneous coupling, more details about how the stability changes with parameters could be obtained using the symmetry. Our results extend some previous work [1, Section 6.1], [91, Section 2], [82, Section 3.2] to the case with time delayed and more general circulant coupling.

Further exploration was done through numerical continuation and numerical simulation studies of a specific example: circulantly coupled Morris-Lecar oscillators. We considered both small ($N = 6, 8$) and large ($N = 140$) networks and two types of coupling: homogeneous and bi-directional, distance dependent. As expected, the numerical studies agree with the theoretical predictions of the phase model, so long as the strength of the coupling (ϵ) was sufficiently small. For the parameters we explored this was $\epsilon \lesssim 0.05$. In all cases we explored, the $1-$cluster (synchronous) solution was the only asymptotically stable solution when there was no delay in the system. For non-zero delay, this solution could become unstable and other cluster solutions became stable. We found ranges of the delay for which the system exhibits a high degree of multistability. The multistability persisted even under in perturbations of the coupling matrix (W), and time delay (τ) which break the symmetry of the model. The perturbed model agreed with the phase model prediction for $\epsilon \lesssim 0.01$.

Delay-induced multistability has been observed in Hopfield neural networks (e.g., [80, 127]), in networks of spiking neurons [79, 44, 46], and even in experimental systems [45], where it has been postulated as a potential mechanism for memory storage. The multistability we observe has similar potential. It also provides the network with a simple way to respond differently to different inputs, without changing synaptic weights. Switching between solutions with a different number of clusters changes the network average frequency, which could then change how the network affects downstream neurons.

Multistability between different cluster solutions also has potential connections with the concept of neural assemblies. A neural assembly is a group of neurons which transiently act together to achieve a particular purpose [32, 61, 97]. A network with multiple stable cluster solutions provides a basic model for such behaviour. As the system switches between different cluster solutions different neurons become synchronized with each other. As we have shown, it possible for network to possess multiple stable solutions with the same number of clusters but with different groupings of the neurons.

In the future, it would be interesting to pursue a variety of the directions suggested by our results. The switching of stability of the cluster solutions as the delay is varied should be associated with bifurcations in the model. In the case of system with two neurons it has been shown that delay induced stability changes of the $1-$ and $2-$ cluster solutions are

associated with pitchfork and saddle-node bifurcations in the phase model and sometimes involve other phase-locked solutions [18]. It would be interesting to explore the delay induced bifurcations that occur in our network model. Preliminary numerical investigations of the phase model (not shown) indicate a quite complex bifurcation structure. It would also be interesting to compute the bifurcation structure of the cluster solutions in the (τ, ϵ) parameter plane to get a better understanding of the limits of the validity of the phase model.

Chapter 5

Symmetry, Hopf bifurcation and Emergence of Cluster Solutions in Time Delayed Neural Networks

5.1 Introduction

In recent years, there has been considerable research studying clustering in systems with time delays using a variety of techniques. Among all the clustering solutions, synchronization, where the phase difference between any two oscillators is zero, (see, e.g., the review paper of Dörfler and Bullo[27] and references therein) is of great interest. However, synchronization is just one of many possible phase-locked solutions that can occur in coupled oscillator systems. Further, synchronization is not always a desirable state [96].

Phase model analysis can be used in the case where the uncoupled elements are intrinsically oscillating and the coupling is weak [8, 9, 115, 20, 26]. Alternatively, the stability of cluster solutions can be analyzed directly using Floquet theory and the properties of the connection matrix [22, 24, 28, 92, 93, 94]. When the uncoupled elements are not oscillatory, the emergence of in-phase and anti-phase (1-cluster and 2-cluster) solutions in two cell networks has been studied by bifurcation analysis [14, 13, 17, 107].

In many cases, cluster solutions occur in networks of coupled oscillators with symmetry. Symmetric bifurcation theory was first developed by Golubitsky et al. [50] for systems of ordinary differential equations and later extended by Wu [120] to systems with time delays. The key point in such symmetric bifurcation theories is that the patterns of bifurcated equilibria and typical oscillators can be predicted in terms of their symmetry. There has been

great interest in applying these results to artificial neural network models with D_N symmetry (especially nearest neighbour coupling)[19, 53, 54, 89, 11, 55, 122, 123]. However, little has been done on more general neural oscillator models or on systems with other symmetries. A notable exception is the work of Song and Xu [107] who use symmetric bifurcation theory to study the existence of 1-cluster and 2-cluster solutions in a two cell network of FitzHugh-Nagumo neurons. Further, Buono et al. [12] studied rings of delay-coupled lasers with unidirectional and bidirectional coupling. They use group-theoretic techniques to classify symmetric compound laser modes (CLMs) according to isotropy subgroups, and further study the symmetry-breaking bifurcations from maximally symmetric solutions. We note also the related work of Blyuss et al. [7, 5, 6] which uses symmetric bifurcation theory to study the cluster solutions arising in various disease models. In this chapter, we extend [107] to networks with arbitrary N identical neurons with circulant coupling.

In order to determine the properties of bifurcating periodic solutions, normal form calculation is important. As we know, center manifold reduction [23, 117, 74] and multiple time scales [86, 87, 88, 124] are two useful techniques for computing the normal forms. To apply the center manifold reduction to a delay differential equation, one needs to first rewrite the delay differential equation in an operator form, and then decompose the solution space of the corresponding linear equation into stable and center manifolds, finally compute the normal form on the center manifold by the adjoint operator equation. The calculation is complex, while the method of multiple time scales can be applied directly to delay differential equations. Yu et al. [125] proved the equivalence of the multiple time scales method and the center manifold reduction method for delay differential equation, i.e. the normal forms, derived using the multiple time scales and center manifold reduction methods, are identical up to third order.

In this chapter we investigate how symmetric bifurcation theory can help predict the cluster periodic solutions occurring in time delayed neural oscillator systems. We consider a network of arbitrary size with arbitrary oscillators and time delayed, global circulant coupling. The general model is as follows

$$X_i'(t) = F(X_i(t), X_i(t-\tau_s)) + \sum_{j=1}^{N} w_{ij} G(X_i(t), X_j(t-\tau)),\ i = 1, \cdots, N, \tag{5.1}$$

where X_i denotes the variables of a m-dimensional subsystems, τ_s is the self-feedback delay, and τ is the coupling time delay between different nodes. F and G are smooth functions that describe the internal and coupling behavior of the subsystems, respectively. We will focus on models which are relevant to neural networks. Denote $W = (w_{ij}) = circ(w_0, w_1, \cdots, w_{N-1})$. In particular, we take $w_0 = 0$, all w_i to be positive and $w_i \neq w_j$, if $i \neq j$. As we show below, the structure of W means that the system has $\mathbb{Z}_N$ symmetry.

The rest of this chapter is organized as follows. In section 5.2, we determine the critical values of the delay in (5.1) which lead to Hopf bifurcation. In section 5.3, we investigate the synchronization patterns of the periodic solutions generated by the Hopf bifurcation using the symmetric local Hopf bifurcation theory for delay differential equations. In sections 5.4 and 5.5, we apply the results obtained in previous sections to two particular examples: a FitzHugh-Nagumo network with diffusive coupling and a Morris-Lecar network with synaptic coupling. We use the method of multiple time scales to determine the stability of bifurcating periodic solutions and compare the theoretical results with numerical simulations for specific parameter values.

5.2 Hopf bifurcations induced by the coupling time delay

Let $E^* = (X_1^*, \cdots, X_N^*)$ be a symmetric equilibrium point of (5.1). That is, $X_1^* = \cdots = X_N^* = X^*$ where X^* satisfies $F(X^*, X^*) + \bar{w}G(X^*, X^*) = 0$ with $\bar{w} = \sum_{k=0}^{N-1} w_k$. The linearization of (5.1) about E^* is given by

$$X_i' = A_1 X_i(t) + A_2 X_i(t-\tau_s) + \sum_{j=1}^{N} w_{ij} B X_j(t-\tau), \ i = 1, \cdots, N. \tag{5.2}$$

Here A_1, A_2 are the Jacobian matrix of $F(X_i, X_i(t-\tau_s)) + \sum_{j=1}^{N} w_{ij} G(X_i(t), X_j(t-\tau))$ with respect to X_i, $X_i(t-\tau_s)$, evaluated at E^*, respectively. B is the Jacobian matrix of $G(X_i(t), X_j(t-\tau))$ with respect to $X_j(t-\tau)$, evaluated at E^*. Therefore, the characteristic matrix of the linearization (5.2) is given by

$$\mathcal{M}(\lambda, \tau) = \begin{pmatrix} \lambda I - A_1 - A_2 e^{-\lambda\tau_s} & -e^{-\lambda\tau} w_1 B & \cdots & -e^{-\lambda\tau} w_{N-1} B \\ -e^{-\lambda\tau} w_{N-1} B & \lambda I - A_1 - A_2 e^{-\lambda\tau_s} & \cdots & -e^{-\lambda\tau} w_{N-2} B \\ \vdots & \vdots & \ddots & \vdots \\ -e^{-\lambda\tau} w_1 B & -e^{-\lambda\tau} w_2 B & \cdots & \lambda I - A_1 - A_2 e^{-\lambda\tau_s} \end{pmatrix}$$

where I is the $m \times m$ identity matrix. Note that $\mathcal{M}(\lambda, \tau)$ is a block circulant matrix. We use this structure, inspired by the work of [107, 113], to simplify the characteristic equation.

Recall that λ is a root of the characteristic equation if and only if Ker $\mathcal{M}(\lambda, \tau)$ is nontrivial, i.e., there is a non-zero vector E such that

$$\mathcal{M}(\lambda, \tau) E = 0. \tag{5.3}$$

Let ρ be any N-th root of unity, that is

$$\rho \in \{\rho_0, \rho_1, \cdots, \rho_{N-1}\}, \text{ and } \rho_k = e^{i\frac{2\pi}{N}k}, \ k = 0, 1, \cdots, N-1.$$

Let $\xi \in \mathbb{R}^m$. Then the compound vector

$$E = \begin{pmatrix} \xi \\ \rho\xi \\ \vdots \\ \rho^{N-1}\xi \end{pmatrix}$$

satisfies (5.3) if and only if ξ satisfies $\mathcal{H}\xi = 0$ where

$$\mathcal{H} = \lambda I - A_1 - A_2 e^{-\lambda\tau_s} - e^{\lambda\tau}(w_1\rho + w_2\rho^2 + \cdots + w_{N-1}\rho^{N-1})B.$$

Using the form of the vectors E with $\rho = \rho_k, \ k = 0, \ldots, N-1$, then shows that the characteristic equation of the linearization (5.2) is

$$\Delta(\lambda, \tau) = \det(\mathcal{M}(\lambda, \tau)) = \prod_{k=0}^{N-1} \Delta_k(\lambda, \tau) = 0, \tag{5.4}$$

where

$$\Delta_k(\lambda, \tau) = \det(\lambda I - A_1 - A_2 e^{-\lambda\tau_s} - e^{-\lambda\tau}\delta_k B). \tag{5.5}$$

Here $\delta_k = \sum_{j=1}^{N-1} w_j \rho_k^j$, $k = 0, 1, \cdots, N-1$, are eigenvalues of the connectivity matrix W. Define $\delta_k = \alpha_k + i\beta_k$ and note that $\delta_{N-k} = \overline{\delta_k}$.

For the rest of the paper we will focus on the case of neural oscillators which can be written in the form:

$$\begin{aligned} V_i' &= F_V(V_i, V_i(t-\tau_s), U_i(t)) + \sum_{j=1}^{N} w_{ij} G(V_i(t), V_j(t-\tau)) \\ U_i' &= F_U(V_i, U_i(t)) \end{aligned}$$

where the variable $V_i \in \mathbb{R}$ corresponds to the voltage and the variables $U_i \in \mathbb{R}^{m-1}$ correspond to gating and other variables (such as intracellular ionic concentrations). This includes artificial neural networks with delayed self feedback as considered in [19, 21] and networks of conductance based models such as those we consider in sections 5.4 and 5.5. Since the connectivity is always through the first variable in these models, the matrix B

in (5.2) has all components 0 except the $B_{1,1}$. In this situation we can describe explicitly how coupling delay gives rise to Hopf bifurcations.

Suppose that the characteristic equation has a pair of pure imaginary eigenvalues. Specifically, for some value of τ, let $i\omega_k$ be a root of $\Delta_k(\lambda,\tau)$ for some $k \in \{0,1,\cdots,N-1\}$. In this situation we have

$$\Delta_k(i\omega_k,\tau) = L(i\omega_k) + H(i\omega_k)\delta_k e^{-i\omega_k\tau}$$

Separating into real and imaginary parts we have

$$\begin{aligned}(H_R\alpha_k - H_I\beta_k)\cos(\omega_k\tau) + (H_I\alpha_k + H_R\beta_k)\sin(\omega_k\tau) = \quad -L_R\\ (H_I\alpha_k + H_R\beta_k)\cos(\omega_k\tau) - (H_R\alpha_k - H_I\beta_k)\sin(\omega_k\tau) = \quad -L_I\end{aligned} \tag{5.6}$$

where L_R, L_I, H_R, H_I denote the real and imaginary parts of $L(i\omega_k)$, and $H(i\omega_k)$, respectively. Note that L_R, H_R are even functions of ω while L_I, H_I are odd. Squaring and adding the above two equations yields

$$L_R^2 + L_I^2 - (H_R^2 + H_I^2)(\alpha_k^2 + \beta_k^2) = 0. \tag{5.7}$$

There are several possibilities. If δ_k is complex, then $\Delta_k(\lambda,\tau)$ has a root $i\omega_k$ and $\Delta_{N-k}(\lambda,\tau)$ has a root $-i\omega_k$, corresponding to the roots $\pm\omega_k$ of (5.7). If δ_k is real, then $\Delta_k(\lambda,\tau)$ has a pair of pure imaginary roots $(\pm i\omega_k)$ corresponding to the roots $\pm\omega_k$ of (5.7). This is the case for $k = 0$ and $k = \frac{N}{2}$ (for N even). If δ_k is real and $k \neq 0, \frac{N}{2}$ then $\Delta_k(\lambda,\tau) = \Delta_{N-k}(\lambda,\tau)$ and both have a pair of purely imaginary roots $(\pm i\omega_k)$, thus $\Delta(\lambda,\tau)$ has a repeated pair of pure imaginary roots. This will occur, for example, if the connection matrix W is symmetric as well as circulant. In all cases, it is enough to consider $\Delta_k(\lambda,\tau)$, $k = 0,1,\ldots,\lfloor\frac{N}{2}\rfloor$ to determine all the roots of $\Delta(\lambda,\tau)$ with pure imaginary real parts.

Provided that ω_k exists, (5.6) may be solved for the corresponding value of τ

$$\begin{aligned}\tau_{k,j} &= \frac{1}{\omega_k}\left(2\pi j - \psi_k + \arccos\left(\frac{-L_R}{\sqrt{(H_R^2+H_I^2)(\alpha_k^2+\beta_k^2)}}\right)\right), \text{ if } L_I > 0\\ &= \frac{1}{\omega_k}\left((2\pi(j+1) - \psi_k - \arccos\left(\frac{-L_R}{\sqrt{(H_R^2+H_I^2)(\alpha_k^2+\beta_k^2)}}\right)\right), \text{ if } L_I < 0.\end{aligned} \tag{5.8}$$

with

$$\psi_k = \arg(H(i\omega)\delta_k).$$

We now have the following result.

Theorem 19. *Assume that the characteristic equation (5.4) has a simple pair of pure imaginary roots $\pm i\omega_k$ when $\tau = \tau_{k,j}$ as defined in (5.8), and all other roots λ satisfy $\lambda \neq li\omega_k$ for any integer l. Assume*

$$|L(i\omega)|^2[H_R(\omega)H_R'(\omega) + H_I(\omega)H_I'(\omega)] - |H(i\omega)|^2[L_R(\omega)L_R'(\omega) + L_I(\omega)L_I'(\omega)] \neq 0.$$

Then, (5.1) undergoes a Hopf bifurcation near the equilibrium point E^* at each critical value $\tau_{k,j}$.

Proof. Straightforward calculations show that

$$\mathrm{Re}\left[\frac{d\lambda(\tau)}{d\tau}\bigg|_{\tau=\tau_{k,j}}\right] \neq 0$$

if and only if

$$|L(i\omega)|^2[H_R(\omega)H_R'(\omega) + H_I(\omega)H_I'(\omega)] - |H(i\omega)|^2[L_R(\omega)L_R'(\omega) + L_I(\omega)L_I'(\omega)] \neq 0.$$

The result then follows from the standard Hopf bifurcation theorem for delay differential equations [58]. □

5.3 Patterns of bifurcating periodic solutions

In this section, we investigate the patterns of periodic solutions arising in the Hopf bifurcation described above. To do this, we must reformulate (5.1) and study its symmetry. Set $u(t) = (X_1(t), \cdots, X_N(t))^T$ and define $u_t(\vartheta) = u(t+\vartheta)$, for $\vartheta \in [-\tau, 0]$. Let $u_t \in \mathcal{C} = C([-\tau, 0], \mathbb{R}^{mN})$, the Banach space of continuous mapping from $[-\tau, 0]$ to $\mathbb{R}^{mN}$ equipped with supremum norm. Then (5.1) can be rewritten

$$u'(t) = h(u_t) \tag{5.9}$$

where

$$h_i(\phi) = F_k(\phi_l(0), \phi_l(-\tau_s)) + \sum_{j=1}^{N} w_{lj} G_k(\phi_l(0), \phi_j(-\tau)) \tag{5.10}$$

with $i = lm + k,\ l = 0, \ldots, N-1,\ k = 0, \ldots, m-1$. Similarly, the linearization (5.2) may be rewritten

$$u'(t) = \mathcal{L}(\tau)u_t \tag{5.11}$$

where

$$\mathcal{L}(\tau)\phi = (A_1 \otimes I_m)\phi(0) + (A_2 \otimes I_m)\phi(-\tau_s) + \epsilon(W \otimes B)\phi(-\tau) \tag{5.12}$$

where I_m is the $m \times m$ identity matrix, and "$\otimes$ " represents the Kronecker product of matrices. From standard theory [58], this linear system generates a strongly continuous semi-group of linear operators on $\mathcal{C}$ with infinitesimal generator, $\mathcal{A}$, defined by

$$\begin{aligned} \mathcal{A}(\tau)\phi &= \dot{\phi},\ \phi \in \mathrm{Dom}(A) \\ \mathrm{Dom}(\mathcal{A}(\tau)) &= \{\phi \in \mathcal{C} : \dot{\phi} \in \mathcal{C}, \dot{\phi}(0) = \mathcal{L}(\tau)\phi\}. \end{aligned}$$

Let Γ be a group acting on $\mathbb{R}^{mN}$. It follows from [50, 120] that (5.9) is Γ-equivariant if $h(\gamma u_t) = \gamma h(u_t)$ for all $\gamma \in \Gamma$. From (5.10), the symmetry of (5.9) is determined by the symmetry of the connection matrix W. We will focus on the case where W is circulant but does not possess any other symmetry. Thus we consider $\Gamma = \mathbb{Z}_N$, the cyclic group of order N, with generator γ, where the action of $\mathbb{Z}_N$ on $\mathbb{R}^{mN}$ is given by

$$(\gamma u)_i = u_{i-m},\ \text{for } i, i-m \bmod Nm,$$

where u_i is the ith component of u. Then it is easy to verify that both (5.9) and (5.11) are $\mathbb{Z}_N$ equivariant.

Suppose that when $\tau = \tau_{k,j}$ the characteristic equation (5.4) has a pair of pure imaginary roots, $\pm i\omega_k$, with corresponding vectors, $\xi_k, \bar{\xi}_k \in \mathrm{Ker}\ \mathcal{M}(i\omega, \tau_{k,j})$, as described in the previous section. Then $\mathcal{A}(\tau_{k,j})$ has eigenvalues $\pm i\omega_k$ and the corresponding generalized eigenspace, $U_{i\omega_k}$, is spanned by the eigenfunctions $\mathrm{Re}(e^{i\omega_k\theta}\xi_k)$, $\mathrm{Im}(e^{i\omega_k\theta}\xi_k)$ [58, 120].

Lemma 2. *Assume that for one and only one* $k \in 0, 2, \ldots, \lfloor \frac{N}{2} \rfloor$ *and some* $j \in \mathbb{Z}_0^+$, $\tau = \tau_{k,j} > 0$ *as defined in (5.8), i.e., the characteristic equation* (5.4) *has a simple pair of pure imaginary roots* $\pm i\omega_k$. *Then*

$$\dim \mathrm{Ker}\ \mathcal{M}(\pm i\omega_k, \tau_{k,j}) = 2,$$

and the restricted action of $\mathbb{Z}_N$ *on* $\mathrm{Ker}\ \mathcal{M}(i\omega_k, \tau_{k,j})$ *is isomorphic to the action of* $\mathbb{Z}_N$ *on* $\mathbb{R}^2$.

Proof. It follows from the discussion of the previous section that

$$\mathrm{Ker}\ \mathcal{M}(i\omega_k, \tau_{k,j}) = \{(y_1 + iy_2)\xi_k;\ y_1, y_2 \in \mathbb{R}\}.$$

From [50], $\mathbb{R}$ is an absolutely irreducible representation of $\mathbb{Z}_N$. Define $J : \mathrm{Ker}\ \mathcal{M}(i\omega_k, \tau_{k,j}) \cong \mathbb{R}^2$ as

$$J((y_1 + iy_2)\xi_k) = (y_1, y_2)^T.$$

Clearly, J is a linear isomorphism. Note that

$$\gamma((y_1+iy_2)\xi_k) = (y_1+iy_2)\gamma(\xi_k) = \rho_k^{N-1}(y_1+iy_2)\xi_k.$$

Consequently

$$J[\gamma((y_1+iy_2)\xi_k)] = \gamma[J((y_1+iy_2)\xi_k)].$$

This completes the proof. □

Let $\mathcal{T} = \frac{2\pi}{\omega_k}$, and denote by $P_{\mathcal{T}}$ the Banach space of continuous $\mathcal{T}$-periodic mappings, $u : \mathbb{R} \to \mathbb{R}^{mN}$, and by $SP_{\mathcal{T}}$ the subspace of $P_{\mathcal{T}}$ consisting of all $\mathcal{T}$-periodic solutions of (5.11) when $\tau = \tau_{k,j}$. Specifically,

$$SP_{\mathcal{T}} = \big\{x_1\epsilon_1(t) + x_2\epsilon_2(t),\ x_1, x_2 \in \mathbb{R}\big\}, \tag{5.13}$$

where

$$\begin{aligned}\epsilon_1(t) &= \cos(\omega_k t)\mathrm{Re}(\xi_k) - \sin(\omega_k t)\mathrm{Im}(\xi_k),\\ \epsilon_2(t) &= \sin(\omega_k t)\mathrm{Re}(\xi_k) + \cos(\omega_k t)\mathrm{Im}(\xi_k).\end{aligned}$$

Let S^1 be the circle group. Then $\mathbb{Z}_N \times S^1$ acts on $P_{\mathcal{T}}$ (and hence, $SP_{\mathcal{T}}$) as follows

$$(\gamma,\theta)u(t) = \gamma u(t+\theta),\ \gamma \in \mathbb{Z}_N, \theta \in [0,\mathcal{T}). \tag{5.14}$$

For any $\theta \in (0,\mathcal{T})$, let Σ^θ be the subgroup of $\mathbb{Z}_N \times S^1$ generated by (γ,θ). Its fixed point set is given by

$$\mathrm{Fix}(\Sigma^\theta, SP_{\mathcal{T}}) = \big\{u \in SP_{\mathcal{T}}, (\gamma,\theta)u(t) = u(t)\big\}. \tag{5.15}$$

Lemma 3. *Assume that the characteristic equation (5.4) has a simple pair of pure imaginary roots $\pm i\omega_k$. If $\theta = \frac{k}{N}\mathcal{T}$, then $Fix(\Sigma^\theta, SP_{\mathcal{T}}) = SP_{\mathcal{T}}$, otherwise $Fix(\Sigma^\theta, SP_{\mathcal{T}}) = 0$. Moreover,*

$$dim(Fix(\Sigma^\theta, SP_{\mathcal{T}})) = \begin{cases} 2, & \text{if } \theta = \frac{k}{N}\mathcal{T},\\ 0, & \text{otherwise.}\end{cases}$$

Proof. To begin, note that

$$\begin{aligned}\gamma(\mathrm{Re}(\xi_k)) &= \cos\frac{2\pi k}{N}\mathrm{Re}(\xi_k) + \sin\frac{2\pi k}{N}\mathrm{Im}(\xi_k),\\ \gamma(\mathrm{Im}(\xi_k)) &= -\sin\frac{2\pi k}{N}\mathrm{Re}(\xi_k) + \cos\frac{2\pi k}{N}\mathrm{Im}(\xi_k).\end{aligned}$$

Therefore,

$$\begin{aligned}\gamma(x_1\epsilon_1(t)+x_2\epsilon_2(t)) &= x_1\cos(\omega_k t)\gamma(\mathrm{Re}(\xi_k)) - \sin(\omega_k t)\gamma(\mathrm{Im}(\xi_k))\\ &\quad + x_2\sin(\omega_k t)\gamma(\mathrm{Re}(\xi_k)) + \cos(\omega_k t)\gamma(\mathrm{Im}(\xi_k))\\ &= (x_1\cos\frac{2\pi k}{N} - x_2\sin\frac{2\pi k}{N})\epsilon_1(t) + (x_1\sin\frac{2\pi k}{N} + x_2\cos\frac{2\pi k}{N})\epsilon_2(t).\end{aligned}$$

Further, straightforward calculations show that

$$(x_1\epsilon_1 + x_2\epsilon_2)(t+\theta) \;=\; (x_1\cos(\omega_k\theta) + x_2\sin(\omega_k\theta))\epsilon_1(t) + (-x_1\sin(\omega_k\theta) + x_2\cos(\omega_k\theta))\epsilon_2(t).$$

Now consider

$$\gamma(x_1\epsilon_1(t)+x_2\epsilon_2(t)) = (x_1\epsilon_1 + x_2\epsilon_2)(t+\theta). \tag{5.16}$$

In order for this to hold we must have

$$\begin{aligned}x_1\cos\frac{2\pi k}{N} - x_2\sin\frac{2\pi k}{N} &= x_1\cos(\omega_k\theta) + x_2\sin(\omega_k\theta),\\ x_1\sin\frac{2\pi k}{N} + x_2\cos\frac{2\pi k}{N} &= -x_1\sin(\omega_k\theta) + x_2\cos(\omega_k\theta).\end{aligned}$$

Solving the above two equations, we obtain

$$\begin{aligned}\theta &= \frac{(N-k)\mathcal{T}}{N} \text{ and } x_1, x_2 \in \mathbb{R}, \text{or}\\ \theta &\neq \frac{(N-k)\mathcal{T}}{N} \text{ and } x_1 = x_2 = 0.\end{aligned}$$

Note that $\gamma u(t) = u(t+\frac{(N-k)\mathcal{T}}{N})$ if and only if $\gamma u(t+\frac{k\mathcal{T}}{N}) = u(t)$. The conclusion follows. □

From Lemma 2, and 3, we can apply the symmetric local Hopf bifurcation theorem for delay differential equation in [120, Theorem 2.1] to obtain the following results.

Theorem 20. *Assume the conditions of Theorem 19 are satisfied. The spatio-temporal symmetry of the periodic solution of (5.1) arising in the Hopf bifurcation at $\tau = \tau_{k,j}$ is determined by $Fix(\Sigma^\theta, SP_{\mathcal{T}})$ as described in Lemma 3. Specifically, we have the following*

(1) For $\tau = \tau_{0,j} > 0$, there exists a bifurcation of periodic solutions of (5.1) with period near $\frac{2\pi}{\omega_k}$, and satisfying

$$u_{i-pm}(t) = u_i(t),\ i = 1, 2, \ldots, m,\ p = 1, \ldots, N-1,$$

which is the in-phase (1-cluster) periodic solution.

(2) *For $\tau = \tau_{k,j} > 0$ such that k and N are relatively prime, there exists a bifurcation of N-cluster periodic solutions of (5.1). These solutions satisfy*

$$u_{i-pm}(t) = u_i(t - p\tfrac{k\mathcal{T}}{N}),\ i = 1, 2, \ldots, m,\ p = 1, \ldots, N-1.$$

where $\mathcal{T}$ is near $\frac{2\pi}{\omega_k}$.

(3) *For $\tau_{k,j}$ such that k and N have greatest common factor $b > 1$, there exists a bifurcation of n-cluster periodic solutions of (5.1). These solutions satisfy*

$$u_{i-pm}(t) = u_i(t - p\tfrac{l\mathcal{T}}{n}),\ i = 1, 2, \ldots, m,\ p = 1, \ldots, N-1.$$

where $n = N/b$, $l = k/b$ and $\mathcal{T}$ is near $\frac{2\pi}{\omega_k}$.

Remark 8. *We have focussed on the case of minimal symmetry in W. The case that W has more symmetry can be dealt with analogously. For example, when W is symmetric and circulant the system (5.1) has D_n symmetry. In this case, the additional symmetry leads to multiple pairs of pure imaginary eigenvalues and the standard Hopf bifurcation theorem does not apply. However, analysis similar to that carried out in this section can be done and the symmetric local Hopf bifurcation theorem [120, Theorem 2.1] may be applied. See [120, 54, 21] for examples of this in the case of artificial neural network models with delay.*

5.4 Application to a FitzHugh-Nagumo network

In this section, we apply the theory of the previous sections to the following network of FitzHugh-Nagumo neurons:

$$\begin{aligned} \mu x_i' &= x_i - \frac{x_i^3}{3} - y_i + \epsilon \sum_{j=1}^{N} w_{ij}(x_j(t-\tau) - x_i(t)) \\ y_i' &= x_i + a, \quad i = 1, 2, \cdots, N. \end{aligned} \tag{5.17}$$

where x_i, y_i correspond to single neurons which are linearly coupled with coupling strength ϵ and coupling matrix W. Here a is an excitability parameter whose value defines whether the system is excitable ($|a| > 1$), or exhibits self-sustained periodic firing ($|a| < 1$), and $\mu > 0$ is the time-scale parameter, which is usually chosen to be much smaller than unity, corresponding to fast activator variables, x_i, and slow inhibitor variables, y_i [43, 85]. The coupling between two different neurons is modeled as a diffusive or electrical coupling. The time delay τ in the coupling is motivated by the propagation delay of action potentials

between different neurons. The connectivity matrix $W = (w_{ij})$ describes how information is distributed between neurons. Notice that in the simplification from the four dimensional Hodkgin-Huxley equation to the two dimensional FitzHugh-Nagumo model, the activation variable x is taken to represent the effect of the membrane potential V_m and sodium activation variable m, and y is "recovery" variable that represents the combined effect of sodium channel deinactivation $(1-h)$ and potassium channel deactivation (n). Therefore, y_i depends on x_i. Thus there is no time delay on y_i variables.

Each neuron is described by a simplified FitzHugh-Nagumo system [43, 85]. In [27, 102], the authors numerically studied the networks with two neurons, i.e. $N = 2$. They took the time delay τ as parameter, and found when $a > 1$, the existence of bistability between the stable fixed point and periodic solutions for sufficiently large delay τ and coupling strength ϵ. In addition, [102] found the antiphase (2-cluster) solutions. Song et.al [107] further investigated the problem theoretically. They studied the existence of a Hopf bifurcation induced by τ, and then investigated the influence of τ on different patterns of Hopf bifurcating periodic solutions.

In this section, we systematically study the stability and Hopf bifurcation of the delay-coupled FitzHugh-Nagumo system (5.17), and theoretically investigate the oscillation patterns induced by coupling delay. In particular, we specify the relation between oscillation patterns and coupling delay, and further study how the critical time delays depends on the coupling strength ϵ. Finally, we investigate the stability of Hopf bifurcating periodic solutions explicitly in terms of τ and ϵ

5.4.1 Stability and Hopf bifurcations induced by the coupling time delay

In the model (5.17) there is a unique symmetric equilibrium point given by $E^* = (x^*, y^*, \cdots, x^*, y^*)^T$ with $x^* = -a$, $y^* = -a + \frac{a^3}{3}$. The linearization of (5.17) at this equilibrium point is given by (5.2) with

$$A_1 = \begin{pmatrix} \frac{1}{\mu}(1 - a^2 - \epsilon\bar{w}) & -\frac{1}{\mu} \\ 1 & 0 \end{pmatrix}, \; A_2 = 0, \; B = \begin{pmatrix} \frac{\epsilon}{\mu} & 0 \\ 0 & 0 \end{pmatrix}.$$

Hence the characteristic equation is given by (5.4) with

$$\Delta_k = \lambda^2 + pr\lambda + r - \epsilon r \delta_k \lambda e^{-\lambda\tau} \tag{5.18}$$

where $p = a^2 - 1 + \epsilon\bar{w}$, $r = \frac{1}{\mu} > 0$, $\bar{w} = \sum_{j=1}^{N-1} w_{ij} = \sum_{k=1}^{N-1} w_k$, and δ_k is as defined in section 5.2.

It is well-known that the number of roots (counting their multiplicity) of equation (5.4) in the open right half plane $\{\lambda \in \mathbb{C}, Re\lambda \geq 0\}$ can change only if a root appears on, or crosses the imaginary axis. Thus, the condition guaranteeing that (5.4) has a root with zero real part will play a key role in the analysis of the distribution of roots.

Straightforward calculations lead to the following

Lemma 4. *Assume that $\tau = 0$ and let $\mathcal{I}_N = \{0, 1, \ldots, \lfloor \frac{N}{2} \rfloor\}$. Then we have*

1. *All $2N$ roots of (5.4) have negative real parts if $\epsilon(\alpha_k - \bar{w}) < a^2 - 1$, for all $k \in \mathcal{I}_N$.*
2. *At least one root of (5.4) has positive real part if $\epsilon(\alpha_k - \bar{w}) > a^2 - 1$ for some $k \in \mathcal{I}_N$.*
3. *If $\epsilon(\alpha_k - \bar{w}) = a^2 - 1$, for $k = 0$ or $k = N/2$ (N even), (5.4) has a pair of purely imaginary roots $\pm i\sqrt{r}$.*
4. *If $\epsilon(\alpha_k - \bar{w}) = a^2 - 1$, for some $k = 1, \cdots, \lfloor \frac{N-1}{2} \rfloor$, then (5.4) has two pairs of purely imaginary roots $\pm i\frac{\epsilon\beta_k \pm \sqrt{\epsilon^2\beta_k^2 + 4\mu}}{2\mu}$*

In the following, we seek the condition such that (5.4) has purely imaginary roots when $\tau > 0$. That is, for some $k \in \mathcal{I}_N$, Δ_k has purely imaginary roots. Noting that

$$L(i\omega) = \frac{1}{\mu} - \omega^2 + i\frac{\omega p}{\mu}, \quad H(i\omega) = -i\frac{\omega\epsilon}{\mu}$$

we define $\omega_k^{\pm}$ and $\tau_{k,j}^{\pm}$, as follows:

$$\omega_k^{\pm} = \frac{\sqrt{2}}{2\mu}\sqrt{(2\mu - p^2 + \epsilon^2|\delta_k|^2) \pm \sqrt{(2\mu - p^2 + \epsilon^2|\delta_k|^2)^2 - 4\mu^2}} \tag{5.19}$$

and

$$\begin{aligned} \tau_{k,j}^{+} &= \frac{1}{\omega_k^{+}}\left[2\pi(j+1) - \psi_k - \arccos\left(\frac{a^2 - 1 + \epsilon\bar{w}}{\epsilon|\delta_k|}\right)\right], \\ \tau_{k,j}^{-} &= \frac{1}{\omega_k^{-}}\left[2\pi j - \psi_k + \arccos\left(\frac{a^2 - 1 + \epsilon\bar{w}}{\epsilon|\delta_k|}\right)\right], \end{aligned} \tag{5.20}$$

and $\hat{\tau}_{k,j}^{\pm} = \tau_{k,j}^{\pm} - \frac{2\psi_k}{\omega_k^{\pm}}$, where

$$\psi_k = \arg(\delta_k).$$

Then, Lemma 4 and the results of section 5.2 give the following.

Lemma 5. *for $k \in \mathcal{I}_N$ and $j \in \mathbb{Z}_0^+ = \{0, 1, \ldots\}$,*

1. *If $|\epsilon||\delta_k| < \mu|p|$, the equation $\Delta_k = 0$ has no purely imaginary roots for all $\tau \geq 0$.*
2. *If $|\epsilon||\delta_k| > \mu|p|$, the equation $\Delta_k = 0$ has purely imaginary roots $i\omega_k^{\pm}$ $(-i\omega_k^{\pm})$ at $\tau = \tau_{k,j}^{\pm}$ $(\hat{\tau}_{k,j}^{\pm})$ and the equation $\Delta_{N-k} = 0$ has purely imaginary roots $-i\omega_k^{\pm}$ $(i\omega_k^{\pm})$ at $\tau = \tau_{k,j}^{\pm}$ $(\hat{\tau}_{k,j}^{\pm})$.*
3. *If $\epsilon|\delta_k| = -\mu p$ then $\omega_k^+ = \omega_k^- = \sqrt{r}$ and $\tau_{k,j}^+ = \tau_{k,j}^-$. If $\epsilon|\delta_k| = \mu p$ then $\omega_k^+ = \omega_k^- = \sqrt{r}$ and $\tau_{k,j}^+ = \tau_{k,j+1}^-$.*
4. *Let $\lambda(\tau) = \eta(\tau) + i\omega(\tau)$ be a solution of the equation $\Delta_k = 0$ satisfying $\eta(\tau_{k,j}^{\pm}) = 0$ and $\omega(\tau_{k,j}^{\pm}) = \omega_k^{\pm}$, then we have*

$$Re\left(\left.\frac{d\lambda}{d\tau}\right|_{\tau=\tau_{k,j}^+,\hat{\tau}_{k,j}^+}\right) \geq 0, \quad Re\left(\left.\frac{d\lambda}{d\tau}\right|_{\tau=\tau_{k,j}^-,\hat{\tau}_{k,j}^-}\right) \leq 0,$$

with equality occurring only when $|\epsilon||\delta_k| = \mu|p|$.

Remark 9. *When $\epsilon < 0$, the above statements remain true with*

$$\tau_{k,j}^+ = \frac{1}{\omega_k^+}\left[2\pi j + \psi_k + \arccos\left(\frac{a^2 - 1 + \epsilon\bar{w}}{\epsilon|\delta_k|}\right)\right],$$
$$\tau_{k,j}^- = \frac{1}{\omega_k^-}\left[(2j+2)\pi + \psi_k - \arccos\left(\frac{a^2 - 1 + \epsilon\bar{w}}{\epsilon|\delta_k|}\right)\right],$$

If $\epsilon|\delta_k| = \mu p$ then $\omega_k^+ = \omega_k^- = \sqrt{r}$ and $\tau_{k,j+1}^+ = \tau_{k,j}^-$.

We can now completely describe the stability of E^* and the Hopf bifurcations.

Theorem 21. *Assume that $\omega_k^{\pm}$ and $\tau_{k,j}^{\pm}$ are defined as in (5.19) and (5.20), respectively.*

1. *If $|a| > 1$ and $\epsilon > \frac{1-a^2}{2\bar{w}}$, then the equilibrium point E^* is asymptotically stable for all $\tau \in [0, \infty)$.*
2. *If either $|a| > 1$ and $\epsilon < \frac{1-a^2}{\bar{w}-|\delta_k|}$ for some $k \in \mathcal{I}_N \setminus \{0\}$, or $|a| < 1$ and $\epsilon < \frac{1-a^2}{\bar{w}+|\delta_k|}$ for some $k \in \mathcal{I}_N$, then the equilibrium point E^* is unstable for all $\tau \in [0, \infty)$.*
3. *If either $|a| > 1$ and $\epsilon < \frac{1-a^2}{2\bar{w}}$ or $|a| < 1$ and $\epsilon > \frac{1-a^2}{2\bar{w}}$ then the system undergoes Hopf bifurcation at the equilibrium point E^* for $\tau = \tau_{0,j}^+$ and $\tau = \tau_{0,m}^-$, for all $j, m \in \mathbb{Z}_0^+$ such that $\tau_{0,j}^+ \neq \tau_{p,s}^{\pm}$ for any $p \in \mathcal{I}_N, s \in \mathbb{Z}_0^+$ and $\tau_{0,m}^- \neq \tau_{q,t}^{\pm}$ for any $q \in \mathcal{I}_N, t \in \mathbb{Z}_0^+$.*

4. *If either* $|a| > 1$ *and* $\frac{1-a^2}{\bar{w}-|\delta_k|} < \epsilon < \frac{1-a^2}{\bar{w}+|\delta_k|}$ *for some* $k \in \mathcal{I}_N \setminus \{0\}$, *or* $|a| < 1$ *and* $\epsilon > \frac{1-a^2}{\bar{w}+|\delta_k|}$ *for some* $k \in \mathcal{I}_N \setminus \{0\}$, *then system (5.17) undergoes Hopf bifurcation near the equilibrium point* E^* *at* $\tau = \tau^+_{k,j}$ *and* $\tau = \tau^-_{k,m}$, *for all* $j, m \in \mathbb{Z}^+_0$ *such that* $\tau^+_{k,j} \neq \tau^\pm_{p,s}$ *for any* $p \in \mathcal{I}_N, s \in \mathbb{Z}^+_0$ *and* $\tau^-_{k,m} \neq \tau^\pm_{q,t}$ *for any* $q \in \mathcal{I}_N, t \in \mathbb{Z}^+_0$.

Proof. The proof follows from Lemma 5 and consideration of the distribution of roots of the characteristic equation. □

We now use a Lyapunov functional to establish a global stability result for the equilibrium point E^*. First, letting $x_i + a \mapsto \tilde{x}_i$, $y_i + a - \frac{a^3}{3} \mapsto \tilde{y}_i$, and dropping the $\tilde{}$ for simplicity, we transform E^* to a zero equilibrium point for the following system

$$\begin{aligned} x_i' &= \frac{1}{\mu}\Big[(1 - a^2 - \epsilon\bar{w})x_i - y_i + \epsilon \sum_{j=1}^{N} w_{ij} x_j(t-\tau) + a x_i^2 - \frac{x_i^3}{3}\Big] \\ y_i' &= x_i. \end{aligned} \tag{5.21}$$

Theorem 22. *If* $|a| > 2$ *and* $\epsilon > \frac{4-a^2}{8\bar{w}}$, *the equilibrium point* E^* *of (5.17) is globally asymptotically stable.*

Proof. Consider system (5.21), and define

$$V(x,y)(t) = \mu \sum_{i=1}^{N} x_i^2(t) + \sum_{i=1}^{N} y_i^2(t) + |\epsilon| \sum_{i=1}^{N} \Big(\sum_{j=1}^{N} w_{ij} \int_{t-\tau}^{t} x_j^2(v) dv \Big).$$

Thus

$$\begin{aligned}
\frac{dV}{dt} &= 2\mu\sum_{i=1}^{N} x_i(t)x'(t) + 2\sum_{i=1}^{N} y_i(t)y'(t) + |\epsilon|\sum_{i=1}^{N}\left(\sum_{j=1}^{N} w_{ij}(x_j^2(t) - x_j^2(t-\tau))\right) \\
&= 2\sum_{i=1}^{N}(1-a^2-\epsilon\bar{w})x_i^2 - 2\sum_{i=1}^{N} x_i y_i + \epsilon\sum_{i=1}^{N}\sum_{j=1}^{N} 2w_{ij}x_i x_j(t-\tau) + 2a\sum_{i=1}^{N} x_i^3 \\
&\quad - 2/3\sum_{i=1}^{N} x_i^4 + 2\sum_{i=1}^{N} y_i x_i + |\epsilon|\sum_{i=1}^{N}\left(\sum_{j=1}^{N} w_{ij}(x_j^2(t) - x_j^2(t-\tau))\right) \\
&\leq \sum_{i=1}^{N} 2(1-a^2-\epsilon\bar{w})x_i^2 + |\epsilon|\sum_{i=1}^{N}\left(\sum_{j=1}^{N} w_{ij}(x_i^2(t) + x_j^2(t-\tau))\right) - 2/3\sum_{i=1}^{N} x_i^4 \\
&\quad + \sum_{i=1}^{N}(3a^2/2x_i^2 + 2/3x_i^4) + |\epsilon|\sum_{i=1}^{N}\left(\sum_{j=1}^{N} w_{ij}(x_j^2(t) - x_j^2(t-\tau))\right) \\
&= \sum_{i=1}^{N}(2 - 1/2a^2 - 2\epsilon\bar{w} + 2|\epsilon|\bar{w})x_i^2(t).
\end{aligned}$$

If $\epsilon \geq 0$, the zero equilibrium point of (5.21) is globally asymptotically stable if $2 - 1/2a^2 < 0$; and if $\epsilon < 0$, the zero equilibrium point is globally asymptotically stable if $2 - 1/2a^2 - 4\epsilon\bar{w} < 0$. Since the zero equilibrium point has the same stability as E^* of (5.17), we have the conclusion of the theorem.

□

The Hopf bifurcations described by Theorem 21 create cluster periodic solutions, as described by Theorem 20. To understand how this effects the dynamics of the system, we need to determine the stability of these solutions, which we do in the next section.

5.4.2 Direction and stability of Hopf bifurcations

In this section, we first derive the normal form of Hopf bifurcation by using the multiple time scales method taking the time delay or the coupling strength ϵ as the bifurcation parameter, and then give a bifurcation analysis based on the normal form.

As discussed above, system (5.17) undergoes Hopf bifurcation at $\tau_{k,j}^{\pm}$. Here we denote $\tau_{k,j}^{\pm} = \tau_k$ for simplicity. In this section, we assume that the characteristic equation (5.4)

has a pair of pure imaginary roots $\pm\omega_k^{\pm}$ at τ_k, and all the other eigenvalues have negative real parts.

Defining $u(t) = (u_1(t), \cdots, u_{2N}(t))^T = (x_1(t), y_1(t), \cdots, x_N(t), y_N(t))^T$, system (5.21) can be rewritten as

$$u' = N_0 u(t) + N_1 u(t-\tau) + f(u(t)), \tag{5.22}$$

where

$$N_0 = \begin{Bmatrix} M & 0 & \cdots & 0 \\ 0 & M & \cdots & 0 \\ \vdots & \vdots & \ddots & \vdots \\ 0 & 0 & \cdots & M \end{Bmatrix}, N_1 = \frac{\epsilon}{\mu} \begin{Bmatrix} 0 & \bar{w_1} & \bar{w_2} & \cdots & \bar{w_{N-1}} \\ \bar{w_{N-1}} & 0 & \bar{w_1} & \cdots & \bar{w_{N-2}} \\ \vdots & \vdots & \vdots & \ddots & \vdots \\ \bar{w_1} & \bar{w_2} & \bar{w_3} & \cdots & 0 \end{Bmatrix}, \text{ and}$$

$$f(u(t)) = \frac{1}{\mu} \begin{bmatrix} au_1^2 - \frac{u_1^3}{3} \\ 0 \\ \vdots \\ au_{2N-1}^2 - \frac{u_{2N-1}^3}{3} \\ 0 \end{bmatrix}$$

with

$$M = \begin{bmatrix} \frac{1-a^2-\epsilon\bar{w}}{\mu} & -\frac{1}{\mu} \\ 1 & 0 \end{bmatrix}, \text{and } \bar{w_i} = \begin{bmatrix} w_i & 0 \\ 0 & 0 \end{bmatrix}, \ i = 1, \cdots, N-1.$$

Defining

$$\tau = \tau_k + \zeta^2 \tau_2, \tag{5.23}$$

we seek a second-order uniform expansion of the solution of equation (5.22) in the neighborhood of $\tau = \tau_k$ in the form

$$u(t, \zeta) = \zeta u_1(T_0, T_2) + \zeta^2 u_2(T_0, T_2) + \zeta^3 u_3(T_0, T_2). \tag{5.24}$$

Here $T_0 = t$, $T_1 = \zeta t$, $T_2 = \zeta^2 t$, and ζ is a dimensional bookkeeping parameter. Note that, the solution does not depend on the slow scale T_1 because secular terms first appear at $\mathcal{O}(\zeta^3)$. In this case, the derivative with respect to t is transformed into

$$\frac{d}{dt} = \frac{\partial}{\partial T_0} + \zeta^2 \frac{\partial}{\partial T_2} = D_0 + \zeta^2 D_2,$$

with $D_i = \frac{\partial}{T_i}$, $i = 0, 2$. Substituting (5.24) into $f(u(t,\zeta))$ yields

$$f(u(t,\zeta)) = \sum_{k\geq 2} \zeta^k f_k(u_1(T_0,T_2), u_2(T_0,T_2), u_3(T_0,T_2)). \tag{5.25}$$

Moreover, we express $u(t-\tau)$ in terms of the scales T_0 and T_2 as

$$u(t-\tau,\zeta) = \zeta u_1(T_0-\tau, T_2-\zeta^2\tau) + \zeta^2 u_2(T_0-\tau, T_2-\zeta^2\tau) + \zeta^3 u_3(T_0-\tau, T_2-\zeta^2\tau)$$

which upon expansion for small ζ becomes

$$u(t-\tau,\zeta) = \zeta u_{1\tau} + \zeta^2 u_{2\tau} + \zeta^3(u_{3\tau} - \tau_2 D_0 u_{1\tau} - \tau_k D_2 u_{1\tau}) \tag{5.26}$$

with $u_{i\tau} = u_i(T_0-\tau_k, T_2)$, $i = 1, 2, 3$. Substituting equations (5.24) - (5.26) into equation (5.22), and equating coefficients of like powers of ζ yields

$$\begin{aligned}
D_0u_1 - N_0u_1 - N_1u_{1\tau} &= 0, &(5.27)\\
D_0u_2 - N_0u_2 - N_1u_{2\tau} &= f_2, &(5.28)\\
D_0u_3 - N_0u_3 - N_1u_{3\tau} &= -D_2u_1 - \tau_2 N_1 D_0 u_{1\tau} - \tau_k N_1 D_2 u_{1\tau} + f_3, &(5.29)
\end{aligned}$$

The general solution of equation (5.27) is

$$u_1 = A_k(T_2)\mathbf{p_k} e^{i\omega_k T_0} + \bar{A}_k(T_2)\bar{\mathbf{p}}_\mathbf{k} e^{-i\omega_k T_0}, \tag{5.30}$$

where $\mathbf{p_k}$ is given by

$$\mathbf{p_k} = (i\omega_k, 1, i\omega_k\rho_k, \rho_k, \cdots, i\omega_k\rho_k^{N-1}, \rho_k^{N-1})^T, \tag{5.31}$$

with $\rho_k = e^{\frac{i2\pi}{N}k}$. Substituting equation (5.30) into equation (5.28) yields

$$D_0u_2 - N_0u_2 - N_1u_{2\tau} = \frac{a\omega_k^2}{\mu}\big[-A^2 e^{2i\omega_k T_0}\boldsymbol{\alpha} + A\bar{A}\boldsymbol{\beta}\big] + c.c, \tag{5.32}$$

where $c.c$ stands for the complex conjugate of the preceding terms and

$$\begin{aligned}
\boldsymbol{\alpha} &= (1, 0, \rho_k^2, 0, \cdots, \rho_k^{2(N-1)}, 0)^T,\\
\boldsymbol{\beta} &= (1, 0, 1, 0, \cdots, 1, 0)^T.
\end{aligned}$$

A particular solution of (5.32) has the form

$$u_2 = \alpha_1 e^{2i\omega_k T_0} + \beta_1 + c.c. \tag{5.33}$$

Substituting (5.33) into (5.32), and balancing similar terms, we have

$$u_2 = \gamma e^{2i\omega_k T_0} \begin{bmatrix} 1 \\ \frac{1}{2i\omega_k} \\ \rho_k^2 \\ \frac{1}{2i\omega_k}\rho_k^2 \\ \vdots \\ \rho_k^{2(N-1)} \\ \frac{1}{2i\omega_k}\rho_k^{2(N-1)} \end{bmatrix} + a\omega_k^2 A\bar{A} \begin{bmatrix} 0 \\ 1 \\ 0 \\ 1 \\ \vdots \\ 0 \\ 1 \end{bmatrix} + c.c, \tag{5.34}$$

where

$$\gamma = \frac{-a\omega_k^2}{\mu[2i\omega_k - \frac{1-a^2+\epsilon\bar{w}}{\mu} + \frac{1}{2i\omega_k\mu} - \frac{\epsilon}{\mu}e^{-2i\omega_k\tau_k}(w_1\rho_k^2 + \cdots + w_{N-1}\rho_k^{2(N-1)})}. \tag{5.35}$$

Substituting (5.30) and (5.34) into (5.29), we have that

$$\begin{aligned} D_0 u_3 - N_0 u_3 - N_1 u_{3\tau} = -\big[&(\mathbf{p_k} - \tau_k N_1 \mathbf{p_k} e^{-i\omega_k\tau_k})A_k' - i\omega_k\tau_2 N_1 \mathbf{p_k} e^{-i\omega_k\tau_k} A_k \\ &- (\frac{i\omega_k^3}{\mu} + \frac{2i\omega_k a\gamma}{\mu}\boldsymbol{\eta})A_k^2\bar{A}_k\big]e^{i\omega_k T_0} + c.c + NRT \end{aligned} \tag{5.36}$$

Here $\boldsymbol{\eta} = (1, 0, \rho_k, 0, \cdots, \rho_k^{N-1}, 0)^T$, and NRT stands for non-secular terms that do not contribute the normal form. Because the homogeneous part of (5.36) has nontrivial solutions, the nonhomogeneous equation has a solution only if a solvability condition is satisfied. To determine this solvability condition, we seek a particular solution of (5.36) in the form

$$u_3(T_0, T_2) = \boldsymbol{\phi}(T_2)e^{i\omega_k T_0} + c.c. \tag{5.37}$$

and obtain

$$\begin{aligned} &(-i\omega_k I + N_0 + N_1 e^{-i\omega_k\tau_k})\boldsymbol{\phi} = \\ &\qquad (\mathbf{p_k} - \tau_k N_1 \mathbf{p_k} e^{-i\omega_k\tau_k})A_k' - i\omega_k\tau_2 N_1 \mathbf{p_k} e^{-i\omega_k\tau_k} A_k - (\frac{i\omega_k^3}{\mu} + \frac{2i\omega_k a\gamma}{\mu}\boldsymbol{\eta})A_k^2\bar{A}_k) \end{aligned} \tag{5.38}$$

Note that the problem of finding solvability condition for the system of different equations (5.36) has been transformed into finding the solvability condition for the system of algebraic equation (5.38). Again, because $i\omega_k$ is an eigenvalue of the homogeneous part, (5.38) has

solutions if and only if a solvability condition is satisfied. The condition is that the right-hand side of (5.38) be orthogonal to every solution of the adjoint homogeneous problem. In this case, the adjoint problem is

$$(N_0^T + N_1^T e^{i\omega_k \tau_k} + i\omega_k I)\mathbf{q_k} = 0. \tag{5.39}$$

Note that $\mathbf{q_k}$ is not unique. To make it unique, we impose the condition

$$\langle \mathbf{q_k}, \mathbf{p_k} \rangle = \bar{\mathbf{q}_\mathbf{k}}^T \mathbf{p_k} = 1. \tag{5.40}$$

Thus, we have

$$\mathbf{q_k} = \frac{1}{N(w_k^2 + \frac{1}{\mu})}(i\omega_k, \frac{1}{\mu}, i\omega_k\rho_k, \frac{\rho_k}{\mu}, \cdots, i\omega_k\rho_k^{N-1}, \frac{\rho_k^{N-1}}{\mu}))^T. \tag{5.41}$$

Taking inner product of the right-hand side of (5.38) with $\mathbf{q_k}$ yields the solvability condition, normal form

$$A_k' = D_1\tau_2 A_k + D_2 A_k^2 \bar{A}_k, \tag{5.42}$$

where

$$D_1 = -\frac{i\omega_k^3 \epsilon\delta_k e^{-i\omega_k\tau_k}}{\omega_k^2(\mu + \epsilon\delta_k\tau_k e^{-i\omega_k\tau_k}) + 1}, D_2 \quad = -\frac{\omega_k^4 + 2\omega_k^2 a\gamma}{\omega_k^2(\mu + \epsilon\delta_k\tau_k e^{-i\omega_k\tau_k}) + 1}.$$

Let $A_k = r_k e^{i\theta_k}$, substituting these expressions into (5.42), we have

$$\begin{aligned} r_k' &= d_1\tau_2 r_k + d_2 r_k^3 \\ \theta_k' &= d_3\tau_2 + d_4 r_k^2, \end{aligned} \tag{5.43}$$

where $d_1 = \mathrm{Re}(D_1), d_2 = \mathbb{R}(D_2), d_3 = \mathrm{Im}(D_1), d_4 = \mathrm{Im}(D_2)$.

This normal form determines both the direction of the Hopf bifurcation (supercritical when $d_1 d_2 < 0$, and subcritical when $d_1 d_2 > 0$), and the stability of bifurcating periodic solutions (stable if $d_2 < 0$, and unstable if $d_2 > 0$).

Normal form calculation taking ϵ as bifurcation parameter

Similarly, by the multiple time scale method, and taking the coupling strength ϵ as bifurcation parameter, we seek a second order uniform expansion of the solution of (5.17) in

the neighborhood of ϵ_c. Assume $\epsilon = \epsilon_c + \zeta^2\epsilon_2$. The normal form with ϵ as the bifurcation parameter is as follows:

$$\begin{aligned} r_k' &= d_{\epsilon,1}\epsilon_2 r_k + d_{\epsilon,2} r_k^3 \\ \theta_k' &= d_{\epsilon,3}\epsilon_2 + d_{\epsilon,4} r_k^2, \end{aligned} \tag{5.44}$$

with where $\gamma_1 = \mathrm{Re}(\Gamma_1), \gamma_2 = \mathrm{Re}(\Gamma_2), \gamma_3 = \mathrm{Im}(\Gamma_1), \gamma_4 = \mathrm{Im}(\Gamma_2)$. Here

$$\begin{aligned} \Gamma_1 &= -\frac{\omega_k^2(\delta_k e^{-i\omega_k\tau_k} - \bar{w})}{\omega_k^2(\mu + \epsilon_c\delta_k\tau e^{-i\omega_k\tau}) + 1}, \\ \Gamma_2 &= -\frac{\omega_k^4 + 2\omega_k^2 a\bar{\gamma}}{\omega_k^2(\mu + \epsilon_c\delta_k\tau e^{-i\omega_k\tau}) + 1}. \end{aligned}$$

and $\bar{\gamma}$ is defined as in (5.35) with $\epsilon \mapsto \epsilon_c$, and $\tau_k \mapsto \tau$, that is,

$$\bar{\gamma} = \frac{-a\omega_k^2}{\mu(2i\omega_k - \frac{1-a^2-\epsilon_c\bar{w}}{mu} + \frac{1}{2i\omega_k\mu} - \frac{\epsilon_c}{\mu}e^{-2i\omega_k\tau}(w_1\rho^2 + \cdots w_{N-1}\rho^{2(N-1)}))}.$$

Similarly, we have that system undergoes supercritical Hopf bifurcation at $\epsilon = \epsilon_c$ when $d_{\epsilon,1}d_{\epsilon,2} < 0$, and subcritical Hopf bifurcation when $d_{\epsilon,1}d_{\epsilon,2} > 0$). Furthermore, the stability of bifurcating periodic solutions are stable if $d_{\epsilon,2} < 0$, and unstable if $d_{\epsilon,2} > 0$.

5.4.3 Example: FitzHugh Nagumo network with 6 neurons

In this section, we illustrate our results by considering specific parameter values: $\mu = 0.1$, $N = 6$ neurons and coupling matrix $W = \mathrm{circ}(0, 1, \frac{1}{2}, \frac{1}{3}, \frac{1}{4}, \frac{1}{5})$.

From Theorems 21 and 22, for a fixed μ value, the delay independent stability regions can be plotted in the plane of parameters a and ϵ. This is done in Figure 5.1. In the region marked by GAS, the equilibrium point E^* is globally asymptotically stable for all $\tau \geq 0$. In the region marked by AS, E^* is asymptotically stable. In the region marked by US, E^* is unstable and there is no Hopf bifurcation for any $\tau \geq 0$. In the white region, E^* may be unstable, or experience stability switching when Hopf bifurcation occurs at $\tau = \tau_k$.

From Theorem 21, the characteristic equation has at least one root with positive real part for all $\tau \geq 0$ when (a, ϵ) is located on the region marked by US. It follows that periodic orbits created in Hopf bifurcations from E^* in this region are always unstable. Thus, Hopf bifurcations creating stable periodic orbits can occur only in the white region. To investigate in further detail, we fix the μ and a values, and plot the Hopf bifurcation

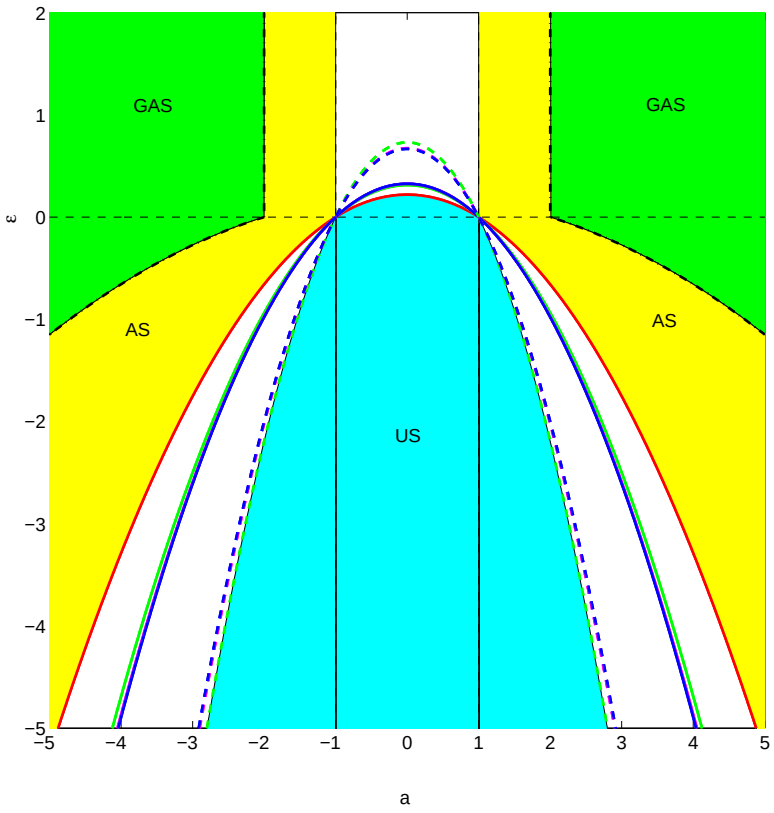

Figure 5.1: Delay independent stability of E^* and Hopf bifurcation regions in the $a-\epsilon$ plane for a network of 6 FitzHugh-Nagumo oscillators with $\mu = 0.1$ and connectivity matrix $W = \text{circ}(0, 1, \frac{1}{2}, \frac{1}{3}, \frac{1}{4}, \frac{1}{5})$. GAS stands for globally asymptotically stable, AS stands for asymptotically stable and US is unstable. In the white regions stability depends on the delay.

curves and stability region in the plane of the coupling strength ϵ and time delay τ. See Figures 5.2 and 5.3. Then, using Theorem 21, we can determine how many pairs of positive eigenvalues there are in each region of the $\epsilon - \tau$ plane. Hence we can determine the region of stability of E^*; shown by the shaded region in Figures 5.2 and 5.3. For $a > 1$ ($a < 0$), region of stability looks similar but as a increases/decreases the Hopf bifurcation curves move to the left/right (right/left). Note that the Hopf bifurcation is only possible when $\epsilon > 0$ ($\epsilon < 0$) when $a < 1$ ($a > 1$). When $a < 1$ equilibrium point is unstable for all ϵ when $\tau = 0$, but the delay induced Hopf bifurcation stabilizes the equilibrium point in the region shown. As a decreases the curves reorganize and this region of stability is completely lost for $a < 0.82$.

Numerical study taking τ as bifurcation parameter

From the expressions derived in the previous section, we can calculate the sign of the coefficients d_1, d_2 of the normal form (5.42), at each critical τ value along the Hopf bifurcation curves of Figure 5.3. Note that the sign of d_1 is the same as that of $d\mathrm{Re}(\lambda)/d\tau$ thus it is positive at the $\tau^+_{k,j}$ bifurcations (solid curves in Figure 5.3) and negative at the $\tau^-_{k,j}$ bifurcations (dashed curves in Figure 5.3). The sign of d_2 varies. For $a = 0.98$, all the $\tau^-_{k,j}$ bifurcations have $d_2 < 0$. However, d_2 changes sign along the $\tau^+_{k,j}$ bifurcation curves. For the 1-cluster Hopf (red, dashed curve) $d_2 > 0$ for most of the curve, while for the other Hopfs generally $d_2 < 0$ on the portions of the curves which formed the boundary of the stability region. This indicates that the 2, 3 and 6-cluster Hopf bifurcations that lie next to the region of stability give rise to stable periodic orbits while the 1-cluster Hopf bifurcations gives rise to stable periodic orbits along the solid curves and unstable periodic orbits along the dashed curves. See Figure 5.4 for an example.

In the following, we illustrate how the coupling time delay affects the stability of the equilibrium point E^* and the cluster periodic solutions arising in the Hopf bifurcations by considering $a = 0.98$ and four values of ϵ. We compare predictions of the theory with numerical simulations for $\tau = 0.1, 0.2, \cdots, 5.0$ with initial conditions

$$\begin{aligned} x_i(t) &= x^* + 0.5RD - 0.5RD, \\ y_i(t) &= y^* + 0.5RD - 0.5RD, \ t \in [-\tau, 0], \end{aligned} \tag{5.45}$$

where RD is any random number between $[0, 1]$.

For $\epsilon = 0.04$, the sequence of τ bifurcation values (rounded to two decimal places) is

$$0 < \tau^-_{0,1}(0.35) < \tau^+_{0,1}(1.49) < \tau^-_{0,2}(2.58) < \tau^+_{0,2}(3.26) < \tau^-_{0,3}(4.82) < \tau^+_{0,3}(5.02).$$

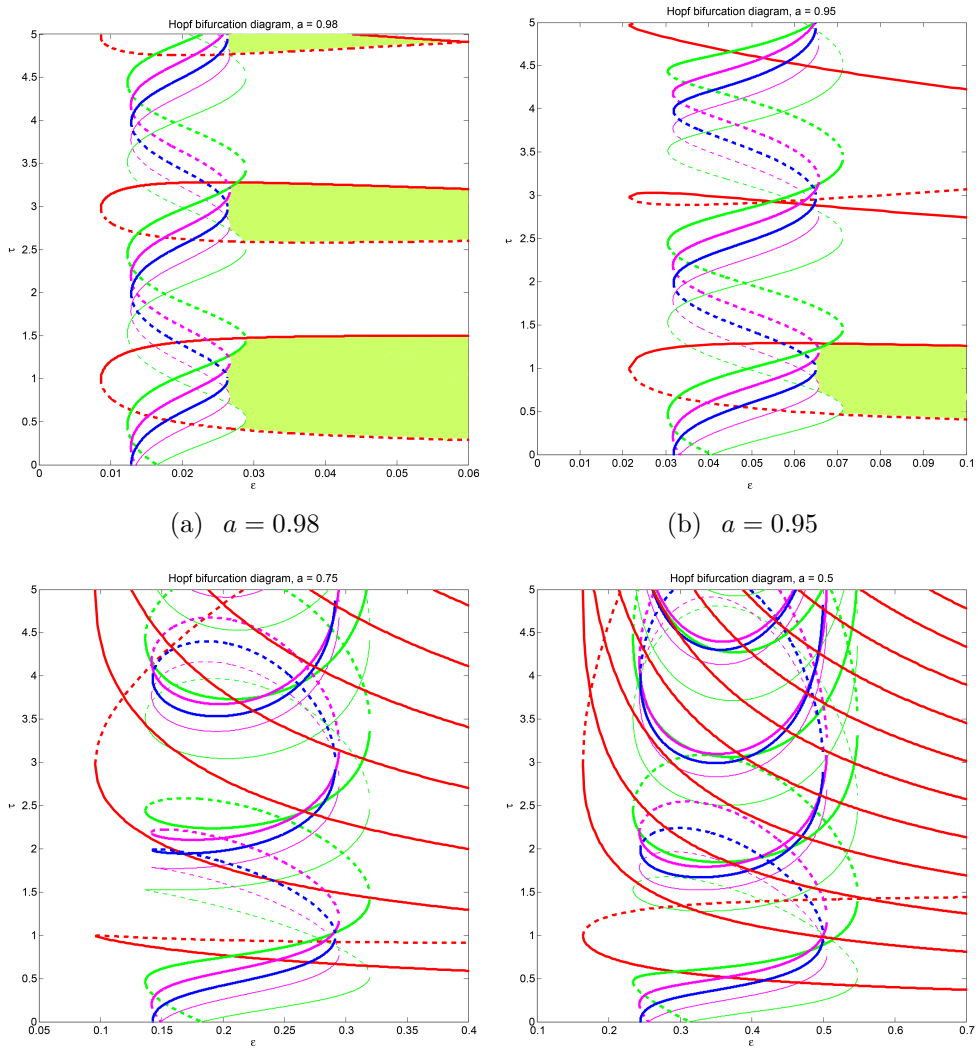

(a) $a = 0.98$ (b) $a = 0.95$

(c) $a = 0.75$ (d) $a = 0.5$

Figure 5.2: Hopf bifurcation curves for the system (5.17) with $N = 6$ neurons for $a < 1$. Red, green, magenta, blue curves are Hopf bifurcation curves for $k = 0, 1, \cdots, 3$, (corresponding to 1-cluster, 6-cluster, 3-cluster and 2-cluster periodic solutions), respectively. Thin (thick) dashed curves correspond to $\tau^-_{k,j}(\hat{\tau}^-_{k,j})$. Thin (thick) solid curves correspond to $\tau^+_{k,j}(\hat{\tau}^+_{k,j})$. Parameter values are $\mu = 0.1$, $W = \text{circ}(0, 1, \frac{1}{2}, \frac{1}{3}, \frac{1}{4}, \frac{1}{5})$ and a values as shown. The shaded regions correspond to the equilibrium point being asymptotically stable.

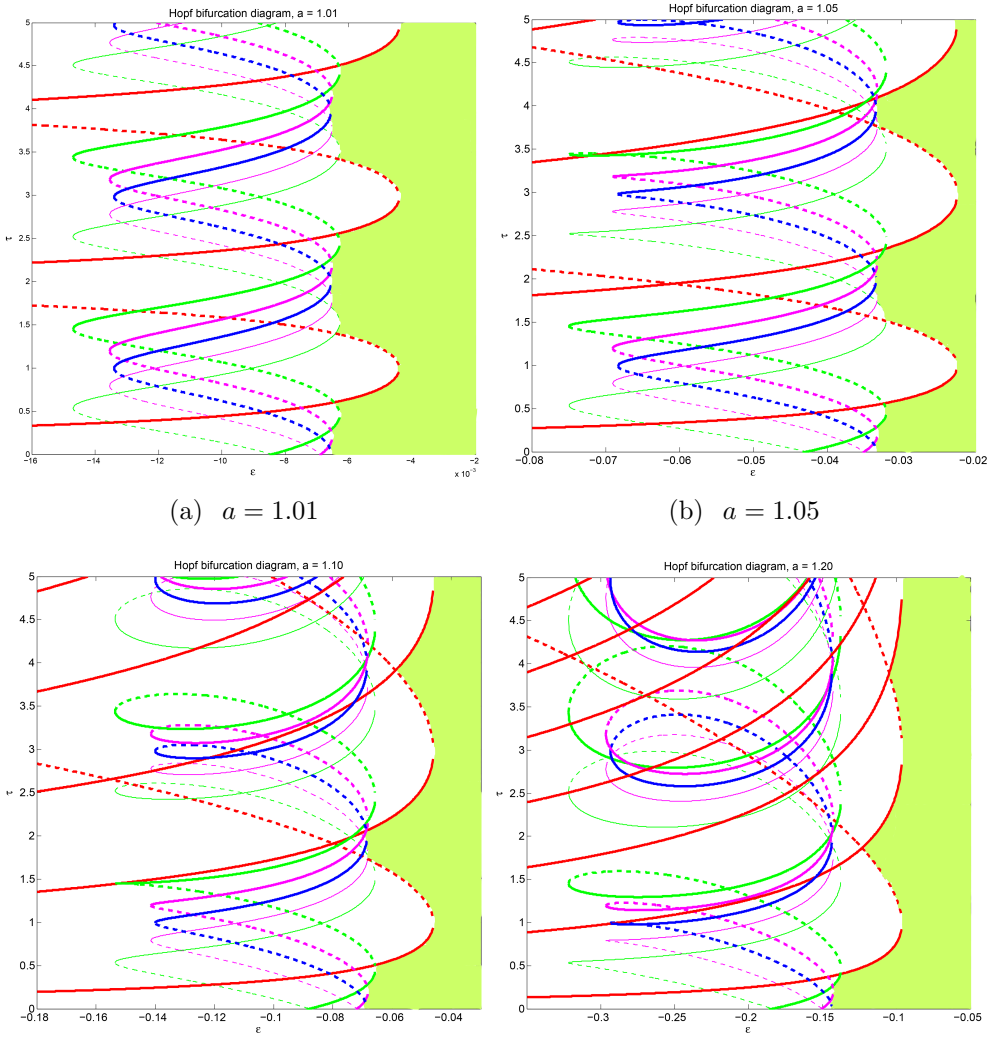

(a) $a = 1.01$ (b) $a = 1.05$

(c) $a = 1.10$ (d) $a = 1.20$

Figure 5.3: Hopf bifurcation curves for the system (5.17) with $N = 6$ neurons for $a > 1$. Red, green, magenta, blue curves are Hopf bifurcation curves for $k = 0, 1, \cdots, 3$, (corresponding to 1-cluster, 6-cluster, 3-cluster and 2-cluster periodic solutions), respectively. Thin (thick) dashed curves correspond to $\tau^-_{k,j}(\hat{\tau}^-_{k,j})$. Thin (thick) solid curves correspond to $\tau^+_{k,j}(\hat{\tau}^+_{k,j})$. The shaded regions correspond to the equilibrium point being asymptotically stable.

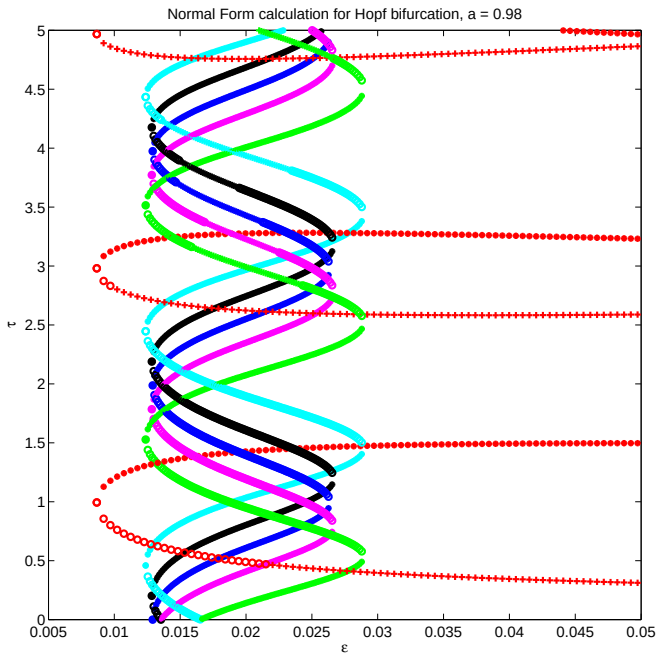

Figure 5.4: Normal form calculation for the Hopf bifurcation of (5.17) with $N = 6$ neurons for $a = 0.98$ considering τ as the bifurcation parameter. The stars and empty circles indicate supercritical and subcritical, respectively, Hopf bifurcations which produce a stable periodic solution. The plus sign indicates that an unstable periodic solution is bifurcating from the critical Hopf bifurcation value.

The theory predicts that the equilibrium point E^* is stable for $\tau \in (0.35, 1.49) \cup (2.58, 3.26) \cup (4.82, 5.02)$ and unstable elsewhere. Further, stable 1-cluster periodic orbits are predicted for τ greater than but sufficiently close to $\tau^+_{0,1}, \tau^+_{0,2}, \tau^+_{0,3}$ and unstable 1-cluster periodic orbits for τ greater than but sufficiently close to $\tau^-_{0,1}, \tau^-_{0,2}, \tau^-_{0,3}$. These predictions are confirmed by the numerical simulations. See Table 5.1. The simulations also show that a stable 1-cluster solution or other, nonsymmetric cluster solutions exist for $\tau \in (0, \tau^-_{0,1}) \cup (\tau^+_{0,1}, \tau^-_{0,2}) \cup (\tau^+_{0,2}, \tau^-_{0,3})$. We conjecture the stable 1-cluster solution is created by a saddle node of limit cycles associated with the Hopf bifurcation creating the periodic orbit.

For $\epsilon = 0.0285$, we focus on $\tau < 1.7$. The sequence of τ critical values is

$$0 < \tau^-_{0,1}(0.41) < \tau^+_{1,0}(0.46) < \tau^-_{1,0}(0.61) < \hat{\tau}^+_{1,1}(1.37) < \tau^-_{0,2}(1.47).$$

The theory predicts a stable equilibrium for $\tau \in (0.61, 1.37)$, and stable 6-cluster periodic orbit bifurcating for $\tau \gtrapprox 0.41$, $\tau \lessapprox 0.46$, and $\tau \gtrapprox 1.37$, and stable 1-cluster periodic orbits bifurcating for $\tau \gtrapprox 1.47$. This is confirmed by the numerical simulations. See Table 5.1 and Figure 5.5.

When $\epsilon = 0.0266$, the bifurcation values are

$$\tau^-_{1,0}(0.71) < \tau^+_{2,0}(0.76) < \tau^-_{2,0}(0.83) < \hat{\tau}^+_{2,1}(1.15) < \hat{\tau}^-_{2,1}(1.24) < \hat{\tau}^+_{1,1}(1.263).$$

the theory predicts stable 6-cluster solutions for $\tau \lessapprox 0.71$, $\tau \gtrapprox 1.263$ and stable 3-cluster solutions for $\tau \gtrapprox 0.76$, $\tau \lessapprox 0.83$, $\tau \gtrapprox 1.15$, $\tau \lessapprox 1.24$. For $\epsilon = 0.0263$, the theory predicts stable 3-cluster solutions for $\tau \gtrapprox 0.94$ and $\tau \lessapprox 1.04$, and stable 6-cluster solutions for $\tau \gtrapprox 1.11$ and $\tau \lessapprox 0.87$. Taking $\tau = 0.825, 0.850, \cdots, 1.200$, we summarize the simulation results in Table 5.1 and Figure 5.6.

Numerical study by taking ϵ as bifurcation parameter

We then similarly calculate the sign of the coefficients $d_{\epsilon,1}$ and $d_{\epsilon,2}$ in the normal form (5.44) at each critical ϵ_c value along the Hopf bifurcation curves of Figures 5.2 and 5.3. Take $a = 0.98$ for example (see figure 5.7). For the τ ranges shown in Figure 5.7, $d_{\epsilon,1} < 0$ and $d_{\epsilon,2} < 0$, that is, the 2, 3, 6-cluster Hopf bifurcations lie on the left side next the region of stability give rise to stable periodic orbits along the Hopf bifurcation curves.

We next investigate how the coupling strength ϵ affects the stability od the equilibrium points E^* and the cluster periodic solutions arising in the Hopf bifurcation by considering two values of τ. The initial conditions for simulation are taken as in (5.45).

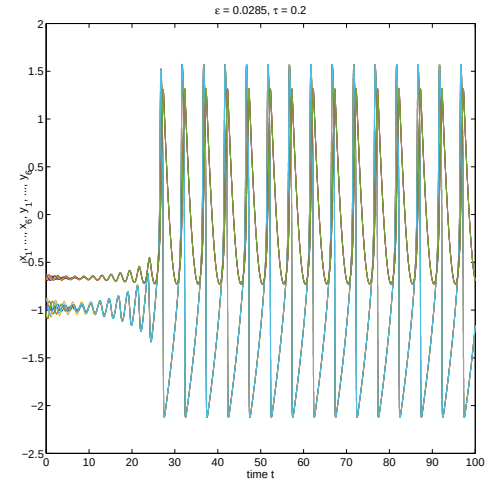

(a) $\tau = 0.2$

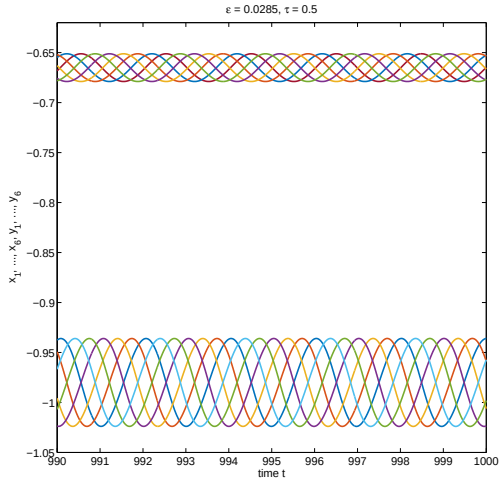

(b) $\tau = 0.5$

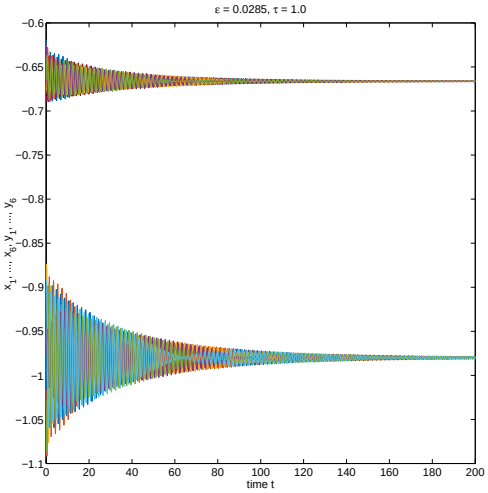

(c) $\tau = 1.0$

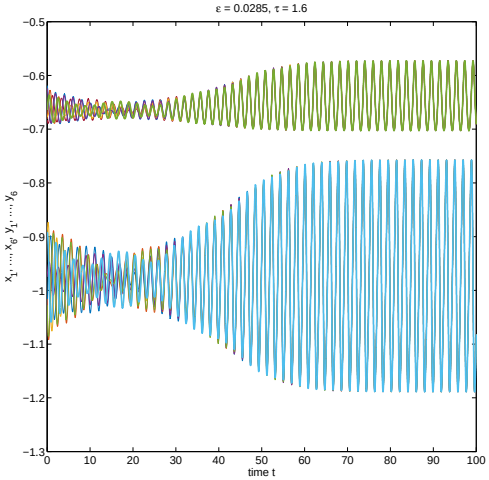

(d) $\tau = 1.6$

Figure 5.5: Numerical simulations showing stable behaviour for $\epsilon = 0.0285$ and τ values as shown. (a) In-phase (1-cluster) periodic orbit. (b) 6-cluster periodic orbit. (c) Equilibrium point, E^*. (c) In-phase periodic orbit.

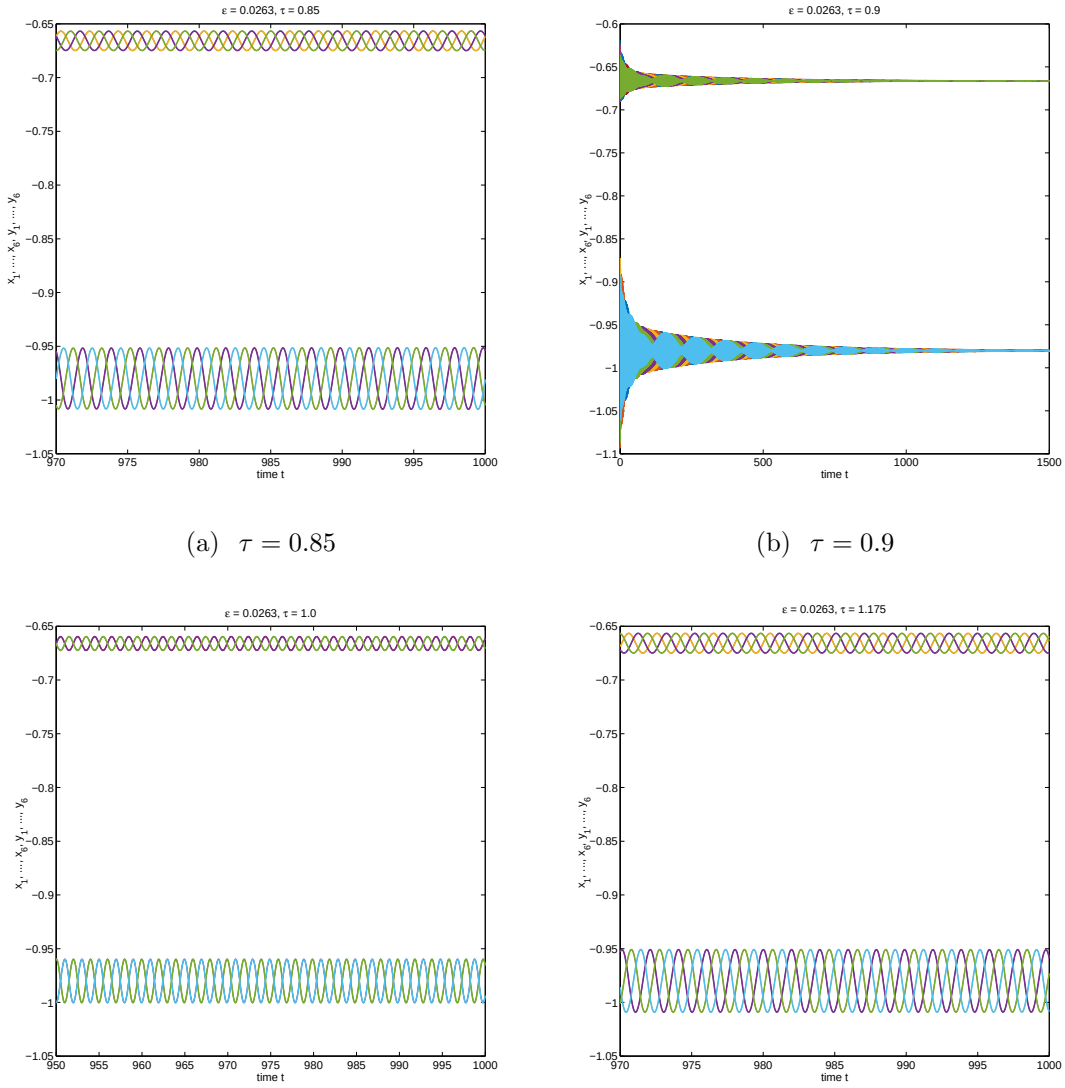

(a) $\tau = 0.85$

(b) $\tau = 0.9$

(c) $\tau = 1.0$

(d) $\tau = 1.175$

Figure 5.6: Numerical simulations showing stable behaviour for $\epsilon = 0.0263$ and τ values as shown. (a) 3-cluster periodic orbit. (b) Equilibrium point, E^*. (c) 2-cluster periodic orbit. (d) 3-cluster periodic orbit.

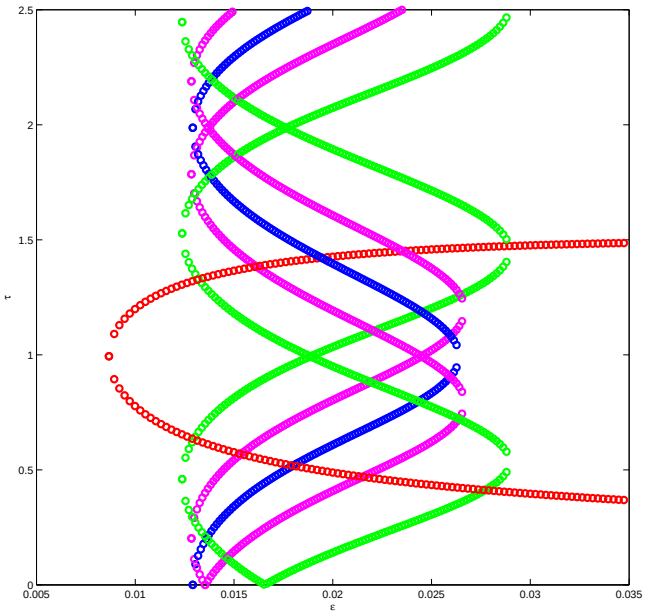

(a) $\tau = 0.98$

Figure 5.7: Normal form calculation for the Hopf bifurcation of (5.17) with $N = 6$ neurons for $a = 0.98$ considering ϵ as a bifurcation parameter. The stars and empty circles indicate supercritical and subcritical, respectively, Hopf bifurcation which produce a stable periodic solution. The plus sign indicates that an unstable periodic solutions is bifurcating from the critical Hopf bifurcation ϵ value.

(a) $\epsilon = 0.4$

E^*	1-cluster	Other
0.4 - 1.4, 2.6 - 3.2, 4.9, 5.0	0.1 - 0.3, 1.5 - 1.7, 2.4 - 2.5, 3.3 - 4.8	1.8 - 2.3

(b) $\epsilon = 0.0285$

E^*	1-cluster	6-cluster
0.7 - 1.3	0.1 - 0.4, 1.5 - 1.7	0.5, 0.6, 1.4

(c) $\epsilon = 0.0266$

E^*	6-cluster	3-cluster
0.9 - 1.1	0.6, 0.7, 1.3, 1.4	0.8

(d) $\epsilon = 0.0263$

E^*	3-cluster	2-cluster
0.9, 0.925, 1.125	0.825, 0.85, 0.875, 1.175, 1.2	0.95, 0.975, 1.0, 1.025

Table 5.1: Summary of numerical simulations for $\tau = 0.1, 0.2, \cdots, 5.0$.

For $\tau = 1$, we have $\epsilon_c = 0.0263$. The theory predicts that the equilibrium point E^* is stable for $\epsilon > 0.0263$, and stable 2-cluster periodic solutions are predicted for $\epsilon \lessapprox 0.0263$. These predictions are confirmed by the numerical simulations. See Figure 5.8. The simulations also show that as decreasing of ϵ, the amplitude of 2-cluster solutions are increasing. For the summary in Table 5.1 we can see that when $\tau = 1$ and $\epsilon > 0.0263$, E^* is stable.

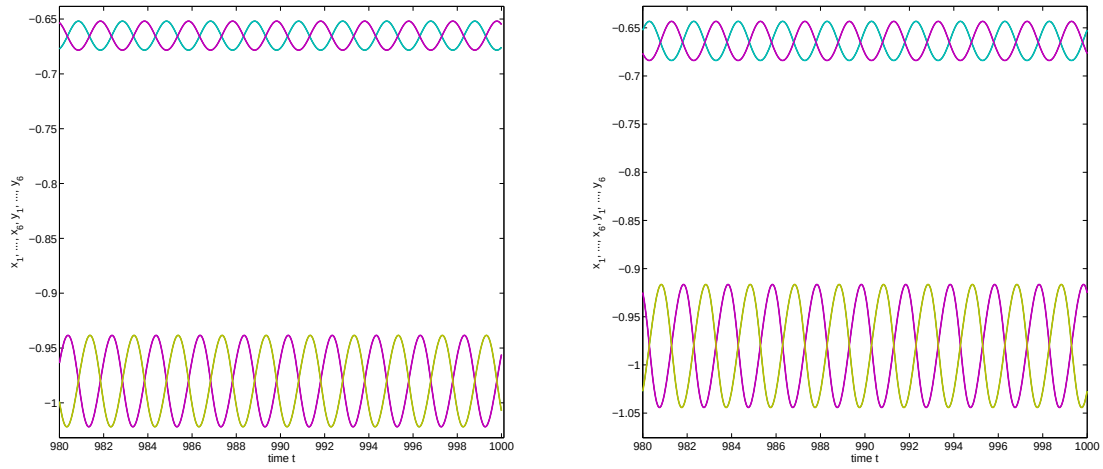

(a) $\epsilon = 0.026$ (b) $\epsilon = 0.0255$

Figure 5.8: Numerical simulations stable behaviour for $\tau = 1$ and ϵ values as shown.

For $\tau = 0.6$, we have $\epsilon_c = 0.0286$. The theory predicts that the equilibrium point E^* is stable for $\epsilon > 0.0286$, and stable 6-cluster solutions bifurcate for $\epsilon \lessapprox 0.0286$. These predictions are confirmed by the numerical simulation. See Figure 5.9 (a), (b), and (c). From Figure 5.2 (a) we see that as decreasing of ϵ reaches another critical point points at $\epsilon_c = 0.0246$. The simulation shows that the 6-cluster solution is still stable at $\epsilon = 0.023$.

5.5 Application to a Morris-Lecar network

In this section, we apply the theory to the model we considered in chapter 4 section 4.4, a network of N identical delay-coupled Morris-Lecar neurons. We write the model here for completeness

$$\begin{aligned} v_i' &= I_{app} - g_{Ca}C_\infty(v_i)(v_i - v_{Ca}) - g_K m_i(v_i - v_K) - g_L(v_i - v_L) \\ &\quad - \epsilon \sum_{j=1}^{N} w_{ij} s(v_j(t-\tau))(v_i(t) - E_{syn}) \triangleq F(v_i, m_i), \quad i = 1, \cdots, N \\ m_i' &= \varphi\lambda(v_i)(m_\infty(v_i) - m_i), \end{aligned} \tag{5.46}$$

where $i = 1, \ldots, N$ and

$$\begin{aligned} C_\infty(v) &= \frac{1}{2}(1 + \tanh((v - \nu_1)/\nu_2)), \ \lambda(v) = \cosh((v - \nu_3)/2\nu_4), \\ m_\infty(v) &= \frac{1}{2}(1 + \tanh((v - \nu_3)/\nu_4)), \ s(v) = \frac{1}{2}(1 + \tanh(10v)). \end{aligned}$$

In the following, we systematically study the Hopf bifurcations of this delay-coupled Morris-Lecar system to determine the oscillation patterns induced by coupling delay.

5.5.1 Stability and Hopf bifurcations induced by the time delay

It is clear from the symmetry of (5.46) that it has an equilibrium point $E^* = (v^*, m^*, \cdots, v^*, m^*)^T$, where

$$F(v^*, m^*) = 0 \text{ and } m^* = m_\infty(v^*). \tag{5.47}$$

The linearization of (5.46) at E^* is given by (5.2) with

$$A_1 = \begin{pmatrix} f_{10} & f_{01} \\ g_{10} & g_{01} \end{pmatrix}, \ A_2 = 0, \ B = \begin{pmatrix} h_{01} & 0 \\ 0 & 0 \end{pmatrix},$$

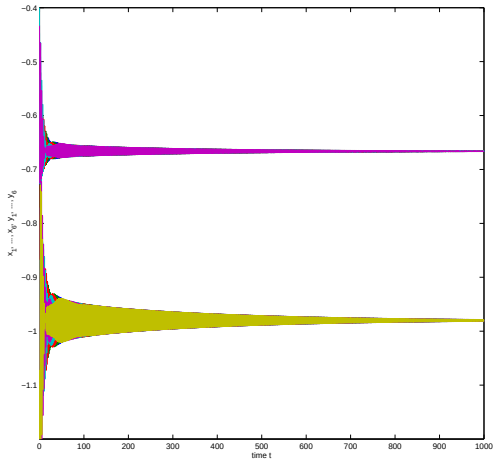

(a) $\epsilon = 0.029$

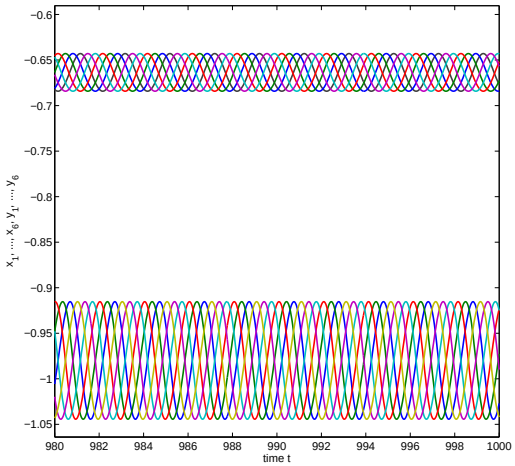

(b) $\epsilon = 0.028$

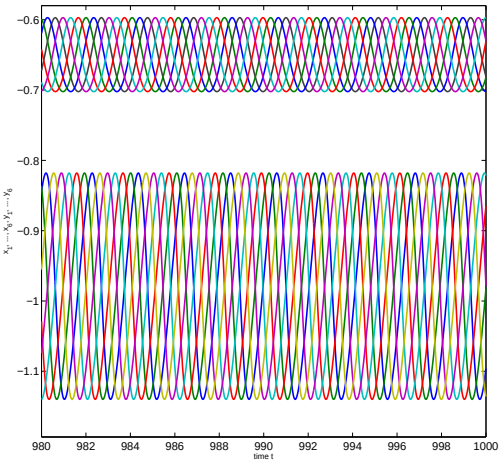

(c) $\epsilon = 0.025$

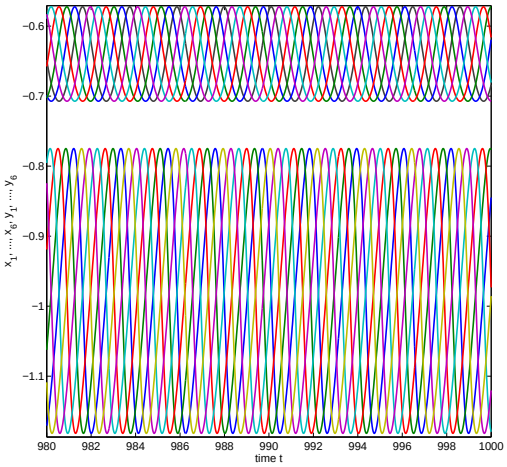

(d) $\epsilon = 0.023$

Figure 5.9: Numerical simulations showing stable behaviour in the FitzHugh-Nagumo model (5.17) for $\tau = 0.6$ and ϵ values as shown.

where

$$
\begin{aligned}
f_{10} &= -g_{Ca}C_{\infty}(v^*) - \frac{1}{2\nu_2}g_{Ca}(v^* - v_{Ca})[1 - \tanh^2\frac{v^* - \nu_1}{\nu_2}] - g_k m^* - g_L - \epsilon s(v^*)\bar{w},\\
f_{01} &= -g_k(v^* - v_k),\\
h_{01} &= -5\epsilon(v^* - E_{syn})(1 - \tanh^2(10v^*)),\\
g_{10} &= \frac{\varphi}{2\nu_4}\cosh\frac{v^* - \nu_3}{2\nu_4}(1 - \tanh^2\frac{v^* - \nu_3}{\nu_4}),\\
g_{01} &= -\varphi\lambda(v^*).
\end{aligned}
$$

It follows that the characteristic equaiton of the linearization is given by (5.4) with

$$\Delta_k(\lambda, \tau) = (\lambda - f_{10})(\lambda - g_{01}) - f_{01}g_{10} - (\lambda - g_{01})h_{01}e^{-\lambda\tau}\delta_k,$$

and δ_k is defined as in section 5.2.

In the decoupled case, i.e., when $\epsilon = 0$, the individual dynamics of the independent neuron is determined by the internal parameters. One can show that the equilibrium point is asymptotically stable if $f_{10} + g_{01} < 0$ and $f_{10}g_{01} - f_{01}g_{10} > 0$, and unstable otherwise.

In the following, we investigate how the coupling strength ϵ and the coupling time delay affect the stability of this equilibrium point and Hopf bifurcations induced by the coupling time delay. To begin, we first study the distribution of roots of the characteristic equation (5.4). Using the notation from section 5.2, we have

$$L(i\omega_k, \tau) = -\omega_k^2 - i(f_{10} + g_{01})\omega_k + f_{10}g_{01} - f_{01}g_{10},\ H(i\omega_k, \tau) = (g_{01} - i\omega_k)h_{01}$$

Lemma 6. *Assume that $\tau = 0$, $k \in \mathcal{I}_N$, and define*

$$
\begin{aligned}
H_{1,k} &= f_{10} + g_{01} + h_{01}\alpha_k;\\
H_{2,k} &= (f_{10} + g_{01} + h_{01}\alpha_k)^2(f_{10}g_{01} - f_{01}g_{10} + h_{01}g_{01}\alpha_k) + (f_{10} + g_{01} + h_{01}\alpha_k)h_{01}^2 g_{01}\beta_k^2\\
H_{3,k} &= f_{10}g_{01} - f_{01}g_{10} + h_{01}g_{01}\alpha_k
\end{aligned}
$$

This leads to the following

1. *All $2N$ roots of (5.4) have negative real parts if $H_{1,k} < 0$ and $H_{2,k} > 0$ are satisfied for all $k \in \mathcal{I}_N$;*

2. *At least one root of (5.4) has positive real part if $H_{1,k} \geq 0$ or $H_{2,k} \leq 0$ (and both are not zero at the same time) for same $k \in \mathcal{I}_N$;*

3. *If $H_{1,k}=0$ and $H_{3,k}>0$ for $k=0$ or $\frac{N}{2}$ (N even), (5.4) has a pair of pure imaginary roots $\pm i\sqrt{f_{10}g_{01}-f_{01}g_{10}+h_{01}g_{01}\alpha_k}$;*

4. *If $H_{1,k}=H_{2,k}=0$ for $k\in\mathcal{I}_N$ and $k\neq 0$, $\frac{N}{2}$(N even), (5.4) has two pairs of pure imaginary roots $\pm i\frac{h_{01}\beta_k+\sqrt{h_{01}^2\beta_k^2+4(f_{10}g_{01}-f_{01}g_{10}+h_{01}g_{01}\alpha_k)}}{2}$.*

Proof. When $\tau=0$, the characteristic equation is in the form of (5.4) with

$$\Delta_k(\lambda,\tau)=(\lambda-f_{10})(\lambda-g_{01})-f_{01}g_{10}-(\lambda-g_{01})h_{01}\delta_k,$$

$k=0,1,\cdots N-1$, which is a 2N-degree polynomial. The results is a direct result by considering the real parts of the roots of the above polynomial.

□

Lemma 7. *For $k\in\mathcal{I}_N$, and $j\in Z_0^+$, define $\omega_k^{\pm}$ and $\tau_{k,j}^{\pm}$ as follows*

$$\begin{aligned}
\omega_k^{\pm}&=\frac{\sqrt{2}}{2}\sqrt{B_k\pm\sqrt{B_k^2-4C_k}},\\
\tau_{k,j}^{\pm}&=\frac{1}{\omega_k^{\pm}}\left(2\pi j-\psi_k^{\pm}+\arccos(\frac{\omega_k^2-f_{10}g_{01}+f_{01}g_{10}}{h_{01}\|\delta_k\|\sqrt{\omega_k^2+g_{01}^2}})\right),\ \textit{if}\ \frac{(f_{10}+g_{01}\omega_k)}{h_{01}}<0;\\
&=\frac{1}{\omega_k^{\pm}}\left(2\pi(j+1)-\psi_k^{\pm}-\arccos(\frac{\omega_k^2-f_{10}g_{01}+f_{01}g_{10}}{h_{01}\|\delta_k\|\sqrt{\omega_k^2+g_{01}^2}})\right),\ \textit{if}\ \frac{(f_{10}+g_{01}\omega_k)}{h_{01}}>0;
\end{aligned}\tag{5.48}$$

with $B_k=h_{01}^2\|\delta_k\|^2-f_{10}^2-g_{01}^2-2f_{01}g_{10}$, $C_k=(f_{01}g_{10}-f_{10}g_{01})^2-g_{01}^2h_{01}^2\|\delta_k\|^2$, and

$$\psi_k^{\pm}=\arg((g_{01}h_{01}-i\omega_k^{\pm}h_{01})\delta_k).\tag{5.49}$$

Note that $\omega_{N-k}^{\pm}=-\omega_k^{\pm}$ and $\psi_{N-k}=-\psi_k$, which imply $\tau_{N-k,-j-1}^{+}=\tau_{k,j}^{+}$ and $\tau_{N-k,-j-1}^{-}=\tau_{k,j}^{-}$.

1. *If $\omega_k^{\pm}$ in (5.48) exists, the equation $\Delta_k=0$ has purely imaginary roots $i\omega_k^{\pm}$ at $\tau=\tau_{k,j}^{\pm}$ and the equation $\Delta_{N-k}=0$ has purely imaginary roots $-i\omega_k^{\pm}$ at $\tau=\tau_{N-k,j}^{\pm}$.*

2. *If we let $\lambda(\tau)=\eta(\tau)+i\omega(\tau)$ be a solution of the equation $\Delta_k=0$ satisfying $\eta(\tau_{k,j}^{\pm})=0$ and $\omega(\tau_{k,j}^{\pm})=\omega_k^{\pm}$, then we have*

$$Re\left(\frac{d\lambda}{d\tau}\Big|_{\tau=\tau_{k,j}^{+}}\right)>0,\quad Re\left(\frac{d\lambda}{d\tau}\Big|_{\tau=\tau_{k,j}^{-}}\right)<0.$$

Note that by the nonlinearity of $F(v^*, m^*)$, we can not solve for v^* or m^*. Therefore, we could not determine how the existence and stability of Hopf bifurcation depend on the coupling strength, ϵ. However, we are able to calculate these conditions numerically for a specific set of parameters. As an example in section 5.5.3 we consider a system of $N = 6$ neurons with coupling matrix $W = \text{circ}(0, 1, \frac{1}{2}, \frac{1}{3}, \frac{1}{4}, \frac{1}{5})$, as in the Fitzhugh-Nagumo example.

5.5.2 Direction and stability for Hopf bifurcation

In this section, we derive the normal form of Hopf bifurcation of (5.46) by taking the time delay τ as bifurcation parameter. Using the same notation as in section 5.4.2, we define $u(t) = (v_1(t), m_1(t), \cdots, v_N(t), m_N(t))^T$. The Taylor expansion of (5.46) truncated at the cubic term is as follows

$$u' = N_0 u(t) + N_1 u(t-\tau) + f(u(t)), \tag{5.50}$$

with

$$N_0 = \begin{Bmatrix} M & 0 & \cdots & 0 \\ 0 & M & \cdots & 0 \\ \vdots & \vdots & \ddots & \vdots \\ 0 & 0 & \cdots & M \end{Bmatrix}, \; N_1 = h_{01} \begin{Bmatrix} 0 & \bar{w_1} & \bar{w_2} & \cdots & \bar{w_{N-1}} \\ \bar{w_{N-1}} & 0 & \bar{w_1} & \cdots & \bar{w_{N-2}} \\ \vdots & \vdots & \vdots & \ddots & \vdots \\ \bar{w_1} & \bar{w_2} & \bar{w_3} & \cdots & 0 \end{Bmatrix},$$

with

$$M = \begin{bmatrix} f_{10} & f_{01} \\ g_{10} & g_{01} \end{bmatrix}, \; \bar{w_i} = \begin{bmatrix} w_i & 0 \\ 0 & 0 \end{bmatrix}, \; i = 1, \cdots, N-1.$$

For an odd i, we have

$$\begin{aligned} (f(u(t)))_i &= f_{20}u_i^2 + f_{11}u_i u_{i+1} + h_{11}u_i \sum_{j=1}^{N} w_{ij} u_{2j-1}(t-\tau) + h_{02} \sum_{j=1}^{N} w_{ij} u_{2j-1}^2(t-\tau) \\ &\quad + f_{20}u_i^3 + h_{12}u_i \sum_{j=1}^{N} w_{ij} u_{2j-1}^2(t-\tau) + h_{03} \sum_{j=1}^{N} w_{ij} u_{2j-1}^3(t-\tau), \\ (f(u(t)))_{i+1} &= g_{20}u_i^2 + g_{11}u_i u_{i+1} + g_{30}u_i^3 + g_{21}u_i^2 u_{i+1}, \end{aligned}$$

where

$$f_{20} = -\frac{g_{Ca}}{2\nu_2}(1-\tanh^2(\frac{v^*-\nu_1}{\nu_2}))(1+(v^*-v_{Ca})\tanh(\frac{v^*-\nu_1}{\nu_2})),$$

$$f_{11} = -g_k,$$

$$f_{30} = \frac{g_{Ca}}{6\nu_2^3}(1-\tanh^2(\frac{v^*-\nu_1}{\nu_2}))\Big(3\nu_2\tanh(\frac{v^*-\nu_1}{\nu_2}) + (v^*-v_{Ca})(1-\sinh^2(\frac{v^*-\nu_1}{\nu_2}))(1-\tanh^2(\frac{v^*-\nu_1}{\nu_2}))\Big),$$

$$g_{20} = \frac{\phi}{16\nu_4^2}\Big((4\nu_4\sinh(\frac{v^*-\nu_3}{2\nu_4}) - 8\cosh(\frac{v^*-\nu_3}{2\nu_4}))(1-\tanh(\frac{v^*-\nu_3}{\nu_4})) + \cosh(\frac{v^*-\nu_3}{2\nu_4})(1+\tanh(\frac{v^*-\nu_3}{\nu_4}) - m^*)\Big),$$

$$g_{11} = -\frac{\phi}{2\nu_4}\sinh(\frac{v^*-\nu_3}{2\nu_4}),$$

$$g_{30} = \frac{\phi}{96\nu_4}\Big(\sinh(\frac{v^*-\nu_3}{2\nu_4})(1+\tanh(\frac{v^*-\nu_3}{\nu_4}) - m^*) + (1-\tanh^2(\frac{v^*-\nu_3}{\nu_4}))\big(6\cosh(\frac{v^*-\nu_3}{2\nu_4}) - 48\sinh^2(\frac{v^*-\nu_3}{\nu_4}) - 16(1-4\sinh^4(\frac{v^*-\nu_3}{\nu_4}))(1-\tanh^2(\frac{v^*-\nu_3}{\nu_4}))\big)\Big),$$

$$g_{21} = -\frac{\phi}{8\nu_4^2}\cosh(\frac{v^*-\nu_3}{\nu_4}),$$

$$h_{11} = -5(1-\tanh^2(10v^*)),$$

$$h_{02} = 50\epsilon(v^*-E_{syn})\tanh(10v^*)(1-\tanh^2(10v^*)),$$

$$h_{03} = \frac{500}{3}\epsilon(v^*-E_{syn})(1-2\sinh^2(10v^*))(1-\tanh^2(10v^*))(1-\tanh^2(10v^*)),$$

$$h_{12} = 50\epsilon\tanh(10v^*)(1-\tanh^2(10v^*)).$$

We seek a second-order uniform expansion of the solution of equation (5.50) in the neighborhood of $\tau = \tau_k$ in the form

$$u(t,\zeta) = \zeta u_1(T_0,T_2) + \zeta^2 u_2(T_0,T_2) + \zeta^3 u_3(T_0,T_2), \tag{5.51}$$

and let

$$\tau = \tau_k + \zeta^2\tau_2. \tag{5.52}$$

Here T_0, T_2, and ζ are defined as in section 5.4.2. Substituting (5.51) and (5.52) into (5.50) and collecting terms of like powers of ζ, we end up with the same equations for $u_1(T_0,T_2)$,

$u_2(T_0,T_2)$ and $u_3(T_0,T_2)$ as in (5.27)(5.28) and (5.29). By further calculation, the solutions of $u_1(T_0,T_2)$, $u_2(T_0,T_2)$ and $u_3(T_0,T_2)$ in (5.51) have similar forms as those for the FHN model.

The general solution of $u_1(T_0,T_2)$ in (5.51) is

$$u_1(T_0,T_2) = A_k(T_2)\mathbf{p_k}e^{i\omega_k T_0} + \bar{A}_k(T_2)\bar{\mathbf{p}}_{\mathbf{k}}e^{-i\omega_k T_0}, \tag{5.53}$$

where $\mathbf{p_k}$ is given by

$$\mathbf{p_k} = ((i\omega_k - g_{01}), g_{10}, (i\omega_k - g_{01})\rho_k, g_{10}\rho_k, \cdots, (i\omega_k - g_{01})\rho_k^{N-1}, g_{10}\rho_k^{N-1})^T, \tag{5.54}$$

with $\rho_k = e^{\frac{i2\pi}{N}k}$. The general solution of $u_2(T_0,T_2)$ is

$$u_2(T_0,T_2) = A_k^2 e^{2i\omega_k T_0}(\Gamma_1,\Gamma_2,\cdots,\Gamma_1\rho_k^{2(N-1)},\Gamma_2\rho_k^{2(N-1)})^T + A\bar{A}(\Gamma_3,\Gamma_4,\cdots,\Gamma_3,\Gamma_4)^T, \tag{5.55}$$

with

$$\begin{aligned}
\Gamma_1 &= \frac{\eta_1 + \frac{f_{01}}{2i\omega_k - g_{01}}\eta_2}{2i\omega_k - f_{01} - \frac{f_{01}g_{10}}{2i\omega_k - g_{01}} - h_{01}e^{-2i\omega_k\tau_k}(w_1\rho_k^2 + \cdots + w_{N-1}\rho_k^{2(N-1)})},\\
\Gamma_2 &= \frac{\Gamma_1 g_{10} + \eta_2}{2i\omega_k - g_{01}},\\
\Gamma_3 &= \frac{g_{10}\eta_3 - f_{01}\eta_4}{f_{01}g_{10} - f_{10}g_{10} - g_{10}h_{01}\bar{w}},\\
\Gamma_4 &= -\frac{g_{10}\eta_3 - f_{01}\eta_4}{f_{01}g_{10} - f_{10}g_{01} - g_{01}h_{01}\bar{w}}
\end{aligned}$$

where

$$\begin{aligned}
\eta_1 &= (i\omega_k - g_{01})^2\left(f_{20} + \frac{f_{11}g_{10}}{i\omega_k - g_{01}} + h_{11}\delta_k e^{-i\omega_k\tau_k} + h_{02}e^{-2i\omega_k\tau_k}(w_1\rho_k^2 + \cdots + w_{N-1}\rho_k^{2(N-1)})\right),\\
\eta_2 &= (i\omega_k - g_{01})\left(g_{20}(i\omega_k - g_{01}) + g_{11}g_{10}\right),\\
\eta_3 &= (\omega_k^2 + g_{01}^2)\left(f_{20} - \frac{f_{11}g_{10}}{i\omega_k + g_{01}} + h_{11}\bar{\delta}_k e^{i\omega_k\tau_k} + h_{01}\bar{w}\right),\\
\eta_4 &= (\omega_k^2 + g_{01}^2)g_{20} + (i\omega_k - g_{01})g_{10}g_{11}.
\end{aligned}$$

Finally, substituting (5.53) and (5.55) into the equation of $u_3(T_0,T_2)$ and solving for $u_3(T_0,T_2)$, we obtain the normal form of (5.50) for taking τ as bifurcation parameter

$$A_k' = D_1\tau_2 A_k + D_2 A_k^2\bar{A}_k, \tag{5.56}$$

with

$$D_1 = -\frac{i\omega_k(i\omega_k - g_{01})^2 h_{01}\delta_k e^{-i\omega_k\tau_k}}{(i\omega_k - g_{01})^2(1+\tau_k\delta_k h_{01}e^{-i\omega_k\tau_k}) + f_{01}g_{10}},$$
$$D_2 = \frac{(i\omega_k - g_{01})\eta_5 + f_{01}\eta_6}{(i\omega_k - g_{01})^2(1+\tau_k\delta_k h_{01}e^{-i\omega_k\tau_k}) + f_{01}g_{10}}$$

where

$$\begin{aligned}
\eta_5 &= 2f_{20}\big((i\omega_k - g_{01})(\Gamma_3+\bar{\Gamma}_3) - (i\omega_k+g_{01})\Gamma_1\big) + f_{11}\big((i\omega_k-g_{01})(\Gamma_4+\bar{\Gamma}_4) - (i\omega_k+g_{01})\Gamma_2\big)\\
&+ h_{11}\big((i\omega_k-g_{01})(\Gamma_3+\bar{\Gamma}_3)\bar{w} - (i\omega_k+g_{01})\Gamma_1 e^{-2i\omega_k\tau_k}(w_1\rho_k^2+\cdots+w_{N-1}\rho_k^{2(N-1)})\big)\\
&+ h_{11}\big((i\omega_k-g_{01})(\Gamma_3+\bar{\Gamma}_3)\delta_k e^{-i\omega_k\tau_k} - (i\omega_k+g_{01})\bar{\delta}_k\Gamma_1 e^{i\omega_k\tau_k}\big) + f_{11}\big(g_{10}(\Gamma_3+\bar{\Gamma}_3)+g_{10}\Gamma_1\big)\\
&+ 2h_{02}\big((i\omega_k-g_{01})(\Gamma_3+\bar{\Gamma}_3)\delta_k e^{-i\omega_k\tau_k} - (i\omega_k+g_{01})\delta_k\Gamma_1 e^{-i\omega_k\tau_k}\big)\\
&- 3f_{30}\big((i\omega_k-g_{01})^2(i\omega_k+g_{01})\big) - 3h_{03}\big((i\omega_k-g_{01})^2(i\omega_k+g_{01})\delta_k e^{-i\omega_k\tau_k}\big)\\
&- h_{12}(i\omega_k-g_{01})^2(i\omega_k+g_{01})\big(2\bar{w}+e^{-2i\omega_k\tau_k}(w_1\rho_k^2+\cdots+w_{N-1}\rho_k^{2(N-1)})\big),\\
\eta_6 &= 2g_{20}\big((i\omega_k-g_{01})(\Gamma_3+\bar{\Gamma}_3) - (i\omega_k+g_{01})\Gamma_1\big) + g_{11}\big((i\omega_k-g_{01})(\Gamma_4+\bar{\Gamma}_4) - (i\omega_k+g_{01})\Gamma_2\big)\\
&+ g_{11}\big(g_{10}(\Gamma_3+\bar{\Gamma}_3)+g_{10}\Gamma_1\big) - 3g_{30}\big((i\omega_k-g_{01})^2(i\omega_k+g_{01})\big)\\
&+ g_{21}(i\omega_k-g_{01})\big((i\omega_k-g_{01})g_{01} - 2(i\omega_k+g_{01})g_{10}\big).
\end{aligned}$$

Let $A_k = r_k e^{i\theta_k}$, substituting these expressions into (5.56), we have

$$\begin{aligned}
r_k' &= d_1\tau_2 r_k + d_2 r_k^3\\
\theta_k' &= d_3\tau_2 + d_4 r_k^2,
\end{aligned} \tag{5.57}$$

where $d_1 = \text{Real}(D_1), d_2 = \text{Real}(D_2), d_3 = \text{Imag}(D_1), d_4 = \text{Imag}(D_2)$. Therefore, we can determine the direction of the Hopf bifurcation (supercritical when $d_1 d_2 < 0$, and subcritical when $d_1 d_2 > 0$) and the stability of the bifurcating periodic solutions (stable when $d_2 < 0$, and unstable when $d_2 > 0$)

5.5.3 Example: Morris Lecar network with 6 neurons

In this section, we numerically investigate the Hopf bifurcation induced by the time delay for a network of six Morris-Lecar oscillators. We adopt the parameters for v_{Ca}, v_k, v_L, g_K, g_L, ϕ, ν_1, ν_2, ν_3, ν_4 fixed as in Table 4.1, $g_{Ca} = 1$, $I_{app} = 0.25$, and two sets of E_{syn} values: $E_{syn} = 0$ and $E_{syn} = -0.5$. In addition, the coupling matrix W is taking as $W = circ(0, 1, \frac{1}{2}, \frac{1}{3}, \frac{1}{4}, \frac{1}{5})$.

We first investigate the behavior of (5.46) with $N = 6$, $E_{syn} = 0$ and the other parameters as described above. We start with the existence of E^*, and its dependence on parameters. Figure 5.10 is produced by XPPAUT, and shows the dependence of E^* with respect to ϵ and I_{app}, respectively. Figure 5.10 shows the dependence of v^* with respect to ϵ and I_{app}. We can see that for a fixed I_{app} value, E^* exists and is stable for $\epsilon < -0.5104$ unstable for $\epsilon < -0.5104$. $\epsilon = -0.5104$ is a Hopf bifurcation point which we investigate further later. Similarly, for a fixed ϵ values, system (5.46) undergoes SNIC bifurcation with respect to I_{app}. Furthermore, the solid black curve of Figure 5.11 represents the fold or saddle node of equilibria bifurcation in the (I_{app}, ϵ)-plane.

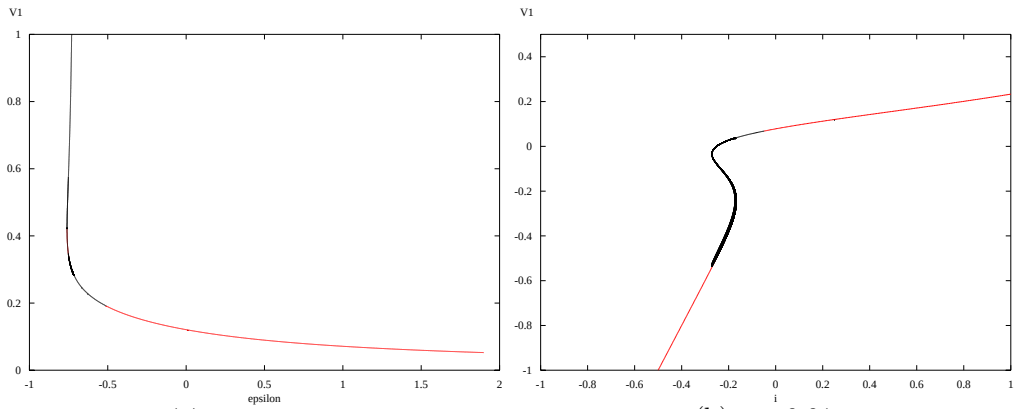

(a) $I_{app} = 0.25$ (b) $\epsilon = 0.01$

Figure 5.10: Bifurcation diagram of the inphase equilibrium point E^* of system (5.46) with respect to (a) ϵ and (b) I_{app}.

According to Lemma 6 and 7 and eigenvalue calculation, we obtain the Hopf bifurcation curves in the (I_{app}, ϵ) plane, which are shown by the red, green, blue and magenta curves in Figure 5.11. Therefore, E^* is the only equilibrium point in the region outside the area bounded by the cusp bifurcation curve and the Hopf bifurcation curves, and it is stable in that region. In the region inside the Hopf bifurcation curves, E^* may be stable or experience stability switch. Furthermore, Hopf bifurcation occurs at critical values of $\tau^{\pm}_{k,j}$. There are three equilibrium points in the region bounded by the fold bifurcation and Hopf bifurcation curves. Notice that SNIC bifurcations occur near the fold points.

To investigate further, we fix I_{app}, and plot the Hopf bifurcation curves in (ϵ, τ) plane (Figure 5.12 (a)). The red, green, magenta, blue, curves shows the Hopf bifurcation curves for $k = 0, 1, \cdots, 3$, which corresponding to 1-cluster, 6-cluster, 3-cluster, and 2-cluster Hopf bifurcations, respectively. The thin (thick) dashed curves correspond to $\tau^{-}_{k,j}$ ($\hat{\tau}^{-}_{k,j}$),

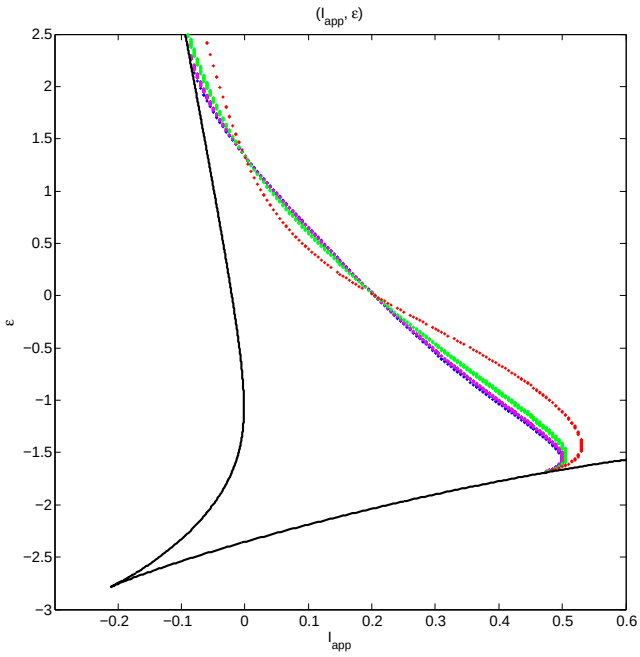

Figure 5.11: Two parameter (I_{app}, ϵ) bifurcation diagram. for the Morris-Lecar model (5.46) with $N = 6$, and $\tau = 0$.

while the thin (thick) solid curves correspond to $\tau^+_{k,j}$ ($\hat{\tau}^+_{k,j}$). By Lemma 7, we can determine how many pairs of positive eigenvalues there are at each region for fixed ϵ, or τ values. Furthermore, from the normal form calculation, we obtain Figure 5.12. The "$*$" indicates the cases where $d_1 > 0$ and $d_2 < 0$; "o" indicates the cases where $d_1 < 0$ and $d_2 < 0$; and "$+$" indicates the cases where $d_2 > 0$. That is, the system undergoes supercritical Hopf bifurcations near E^* at "$*$" points, and subcritical Hopf bifurcations at "o" points. It is observed that d_2 is always negative, and d_1 is negative along $\tau^-_{k,j}$ ($\hat{\tau}^-_{k,j}$), and positive along $\tau^+_{k,j}$ ($\hat{\tau}^+_{k,j}$). This indicates that the equilibrium point is stable in the shaded region, and stable 1, 2, 3, 6-cluster periodic solutions are bifurcating through supercritical Hopf bifurcation along the solid curves and subcritical Hopf bifurcation along the dashed curves.

In the following, we illustrate how the coupling time delay affects the stability of the

equilibrium point E^* and the cluster periodic solutions arising in the Hopf bifurcation for some values of ϵ. All the numerical simulations are performed with initial conditions as follows

$$v_i(t) = 0.2RD,$$
$$m_i(t) = 0.8RD,$$

where RD is any random number between $[0, 1]$. Here 0.2 (0.8) is chosen because the v^* (w^*) of stable equilibrium point is roughly between $(0, 0.2)$ $((0.3, 0.8))$

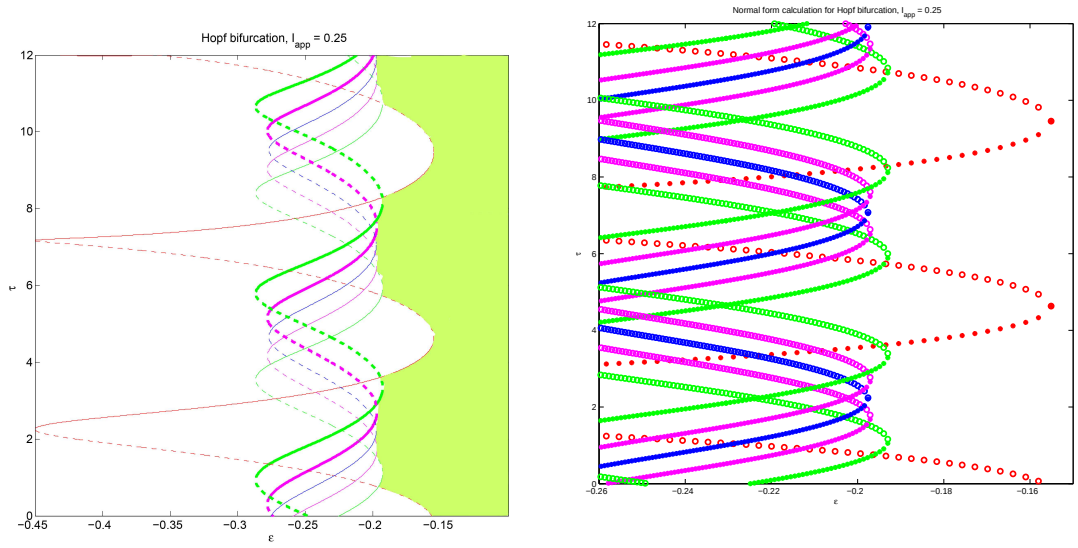

(a) (b)

Figure 5.12: Hopf bifurcation diagram in the (ϵ, τ) plane with $I_{app} = 0.25$.

Take $\epsilon = -0.18$. The critical values of the coupling delay are

$$0 < \tau^-_{0,1}(0.553) < \tau^+_{0,1}(3.798) < \tau^-_{0,2}(5.529) < \tau^+_{0,2}(8.486) < \tau^-_{0,3}(10.51) \cdots$$

The theory predicts that the equilibrium point E^* is stable for $\tau \in (0.553, 3.298) \cup (5.529, 8.486) \cup (10.51, 13.180)$, and unstable for $\tau \in (0, 0.553) \cup (3.798, 5.529) \cup (8.486, 10.51)$. Furthermore, by the normal form calculation, there is a supercritical Hopf bifurcation at $3.798, 8.486$, and subcritical Hopf bifurcation at $0.553, 5.529$ and 10.51. This is confirmed by the numerical simulations. The simulations are carried out for $\tau = 0.5, 1.0, 1.5, \cdots, 12.0$. See Table 5.2 and Figure 5.13. The simulation also shows that a stable 3, 6-cluster solution

E^*	1-cluster	Other
1.0 - 3.5, 6.0 - 8.0, 11.0 - 12.0	4.0 - 5.0	0.5, 5.5, 9.0 - 10.5

Table 5.2: Summary of numerical simulations for $\epsilon = -0.18$ and $\tau = 0.5, 1.0, \cdots, 12.0$.

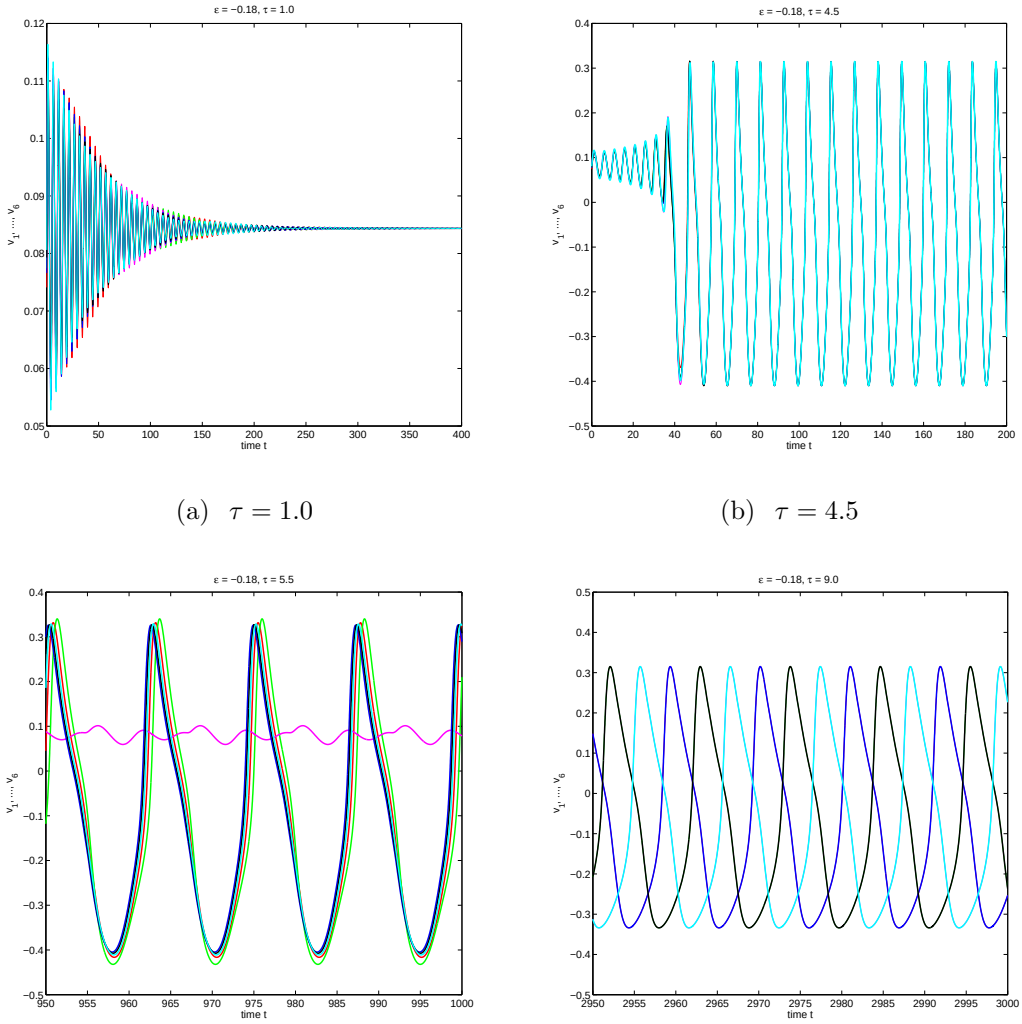

(a) $\tau = 1.0$

(b) $\tau = 4.5$

(c) $\tau = 5.5$

(d) $\tau = 9.0$

Figure 5.13: Numerical simulations showing stable behaviour for $\epsilon = -0.18$ and τ values as shown. (a) Stable E^*. (b) In-phase periodic orbit. (c) Nonsymmetric solution. (d) Stable 3-cluster periodic orbit. The y-axis shows only $v_1, \cdots, v_6$ for clarity.

exist for $\tau = 9.0$ and $\tau = 10, 10.5$, respectively. And nonsymmetric cluster solutions exist such as Figure 5.13(c) exist for $\tau = 0.5, 5.5$.

When $\epsilon = -0.195$, the critical values of the coupling time delays are

$$\tau_{0,1}^{-}(0.739) < \tau_{1,1}^{-}(0.840) < \tau_{1,1}^{-}(1.390) < \hat{\tau}_{1,1}^{+}(3.049)$$

The theory predicts that the equilibrium point is stable for $\tau \in (0.739, 0.84) \cup (1.391, 3.049)$. Stable 1-cluster solutions exist for $\tau \lessapprox 0.739$, and stable 6-cluster solutions exist for $\tau \gtrapprox 0.84, 3.049$ and $\tau \lessapprox 1.391$. Figure 5.14(a, b, c) confirm the prediction, while nonsymmetric cluster solution appears for $\tau = 3.1$. In the simulation, we observe that it is difficult to get the predicted symmetric cluster solutions by random initial conditions. The above plots are chosen from various simulations from random initial conditions. We conjecture that the multistability of different cluster solutions is created by the saddle node on an invariant circle at the solid black curve in Figure 5.11 associated with the Hopf bifurcation.

In this part, we focus on $E_{syn} = -0.5$. According to Lemma 6 and 7 and eigenvalue calculation, we obtain the Hopf bifurcation curves in the (ϵ, τ)-plane for various values of I_{app} (Figure 5.15). The equilibrium point E^* is stable in the shaded region to the right of the Hopf bifurcation curves. Note that the region of stability for E^* look similar for the four I_{app} values, but the Hopf bifurcation curves move to the left as I_{app} decreases. Furthermore, by the normal form calculation, we are able to calculate the sign of d_1, d_2 at every critical τ value along the Hopf bifurcation curves. Figure 5.16 shows an example of the normal form calculation. We observed that on the region where stable Hopf bifurcating periodic solutions may occur, d_2 is always negative, and d_1 is negative along $\tau_{k,j}^{-}$ ($\hat{\tau}_{k,j}^{-}$) and positive along $\tau_{k,j}^{+}$ ($\hat{\tau}_{k,j}^{+}$).

In the following, we illustrate how the coupling time delay affects the stability of E^* and the Hopf bifurcating cluster solutions by considering $I_{app} = 0.25$.

Considering $\epsilon = 0.04$, the sequence of τ bifurcation values is

$$0 < \tau_{0,1}^{+}(1.46) < \tau_{0,1}^{-}(3.16) < \tau_{0,2}^{+}(6.12) < \tau_{0,2}^{-}(8.36)\tau_{0,3}^{+}(10.78), \cdots,$$

The theory predicts that the equilibrium point E^* is stable for $\tau \in (0, 1.46) \cup (3.16, 6.12) \cup (8.38, 10.78)$, while stable 1-cluster solutions exist for $\tau \gtrapprox 1.46, 6.12, 10.78$ and $\tau \lessapprox 3.16, 8.36$. Simulations for $\tau = 0.1, 0.2, \cdots, 12.0$ are carried out. For $\tau = 0.1, 0.2, \cdots, 1.3, 3.4, 3.5, \cdots, 6.0, 8.6, 8.7, \cdots, 10.7$, we find that the equilibrium point E^* is stable, which is as predicted theoretically (See Figure 5.17 (a) for example). And for $\tau = 1.5, 1.6, \cdots, 2.7, 10.8$, we find that 1-cluster solutions exist as expected (See Figure 5.17 (b) for example). However, for all the other τ values, the simulation results does not match with prediction, and all the simulation solutions are nonsymmetric (See Figure 5.17 (c, d) for example).

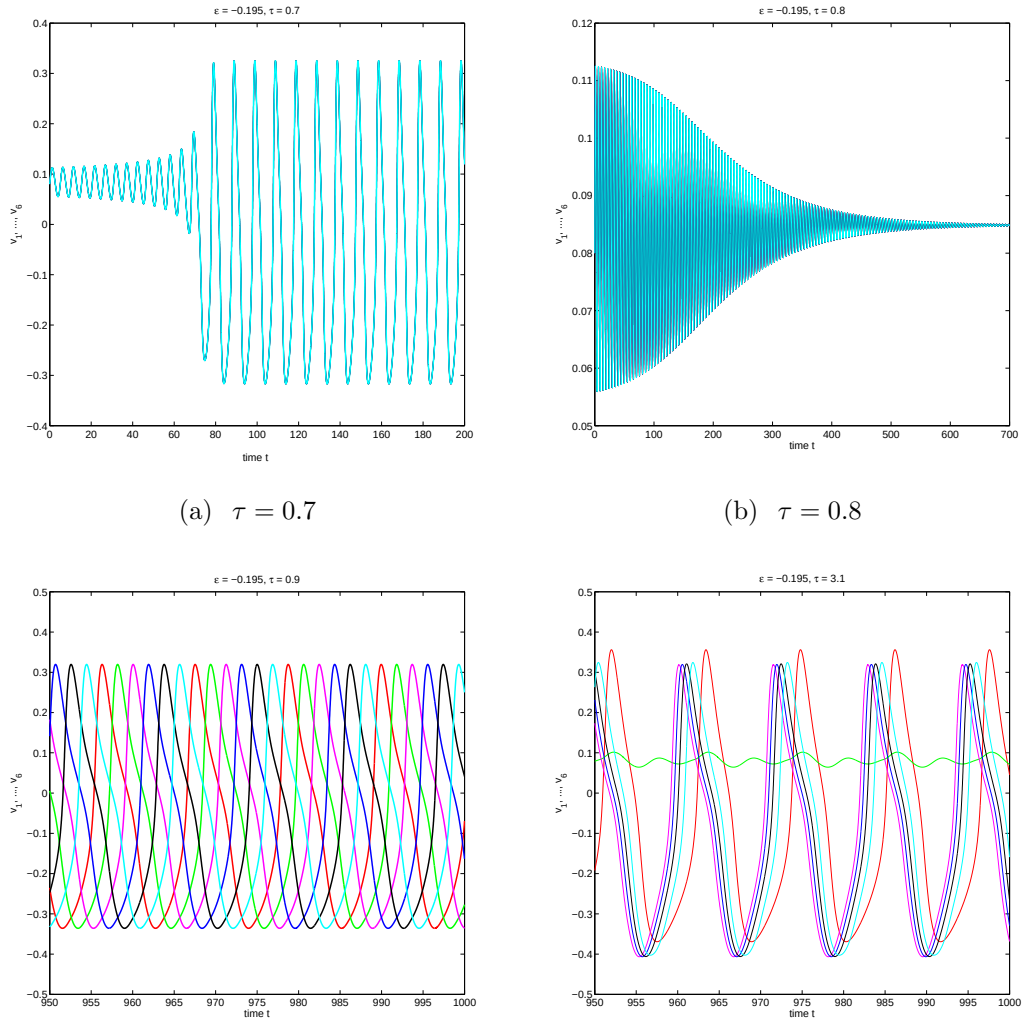

(a) $\tau = 0.7$

(b) $\tau = 0.8$

(c) $\tau = 0.9$

(d) $\tau = 3.1$

Figure 5.14: Numerical simulations showing stable behaviour for $\epsilon = -0.195$ and τ values as shown. (a) Stable in-phase periodic orbit. (b) Stable E^*. (c) Stable 6-cluster periodic orbit (d) Nonsymmetric cluster solutions. The y-axis shows only $v_1, \cdots, v_6$ for clarity.

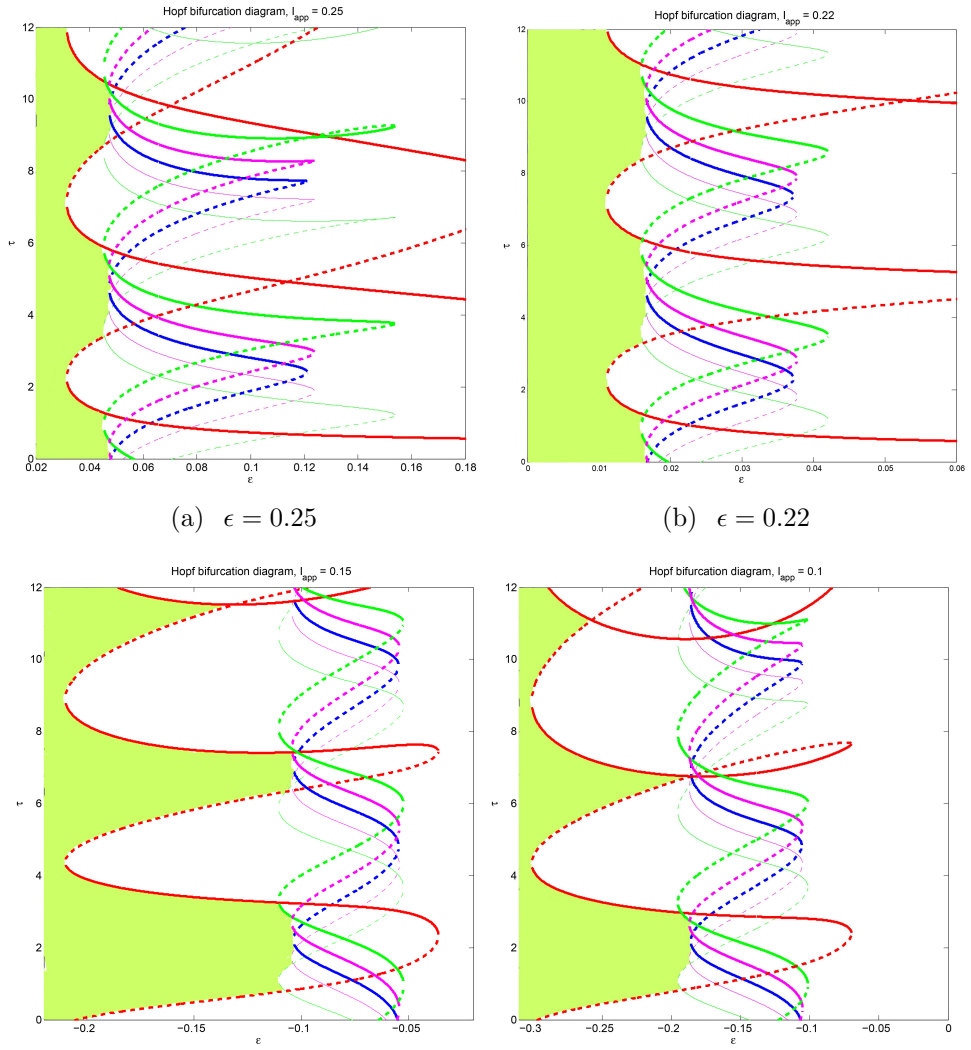

(a) $\epsilon = 0.25$ (b) $\epsilon = 0.22$

(c) $\epsilon = 0.15$ (d) $\epsilon = 0.10$

Figure 5.15: Hopf bifurcation curves for system (5.46) with $N = 6$ and I_{app} values as shown. Red, green, magenta, blue curves are Hopf bifurcation curves for $k = 0, 1, 2, 3$ which correspond to 1-cluster, 6-cluster, 3-cluster and 2-cluster periodic solutions, respectively. Thin (thick) dashed curves corresponds to $\tau^-_{k,j}$ ($\hat{\tau}^-_{k,j}$). Thin (thick) solid curves corresponds to $\tau^+_{k,j}$ ($\hat{\tau}^+_{k,j}$).

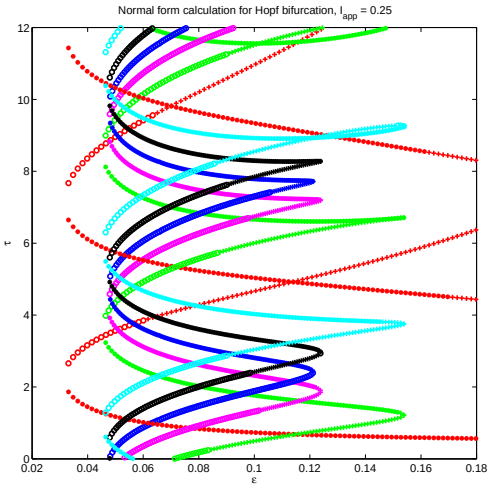

Figure 5.16: Normal form calculation for the Hopf bifurcation of (5.46) with $N = 6$ for $I_{app} = 0.25$ considering τ as the bifurcation parameter. The stars and empty circles indicate supercritical and subcritical, respectively, Hopf bifurcation which produce a stable periodic solution. The plus sign indicates that an unstable periodic solution is bifurcating from the critical Hopf bifurcation value.

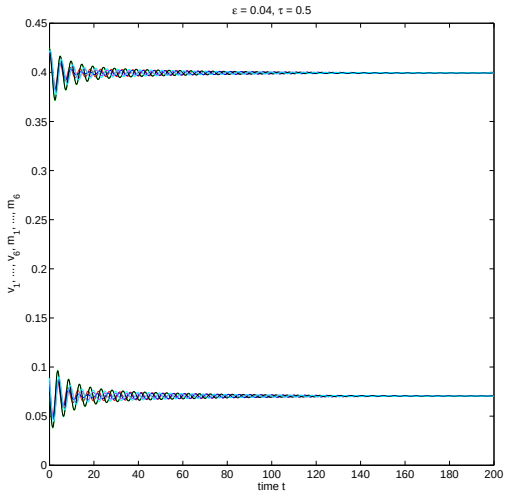

(a) $\tau = 0.5$

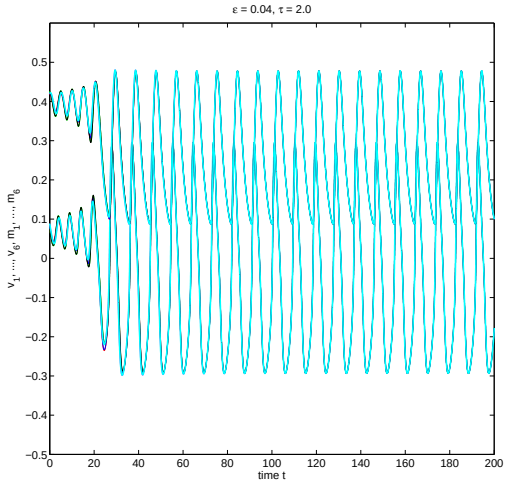

(b) $\tau = 2.0$

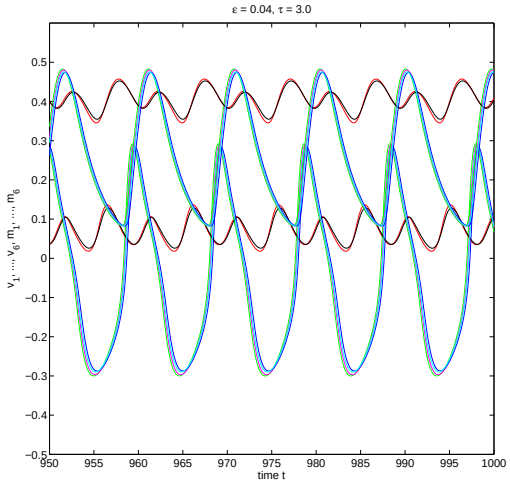

(c) $\tau = 3.0$

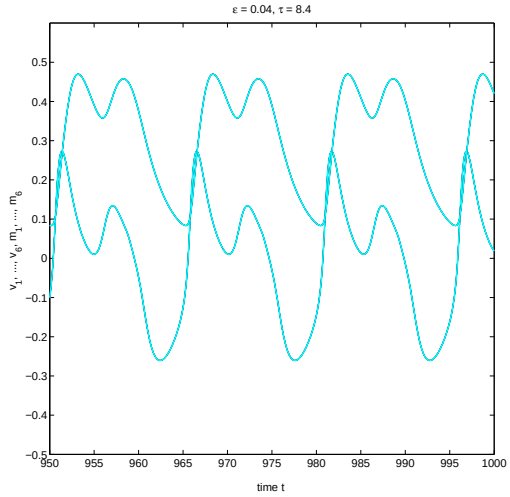

(d) $\tau = 8.4$

Figure 5.17: Numerical simulations showing stable behavior for $\epsilon = 0.04$ and τ values as shown. (a) Stable equilibrium point E^*. (b) Stable 1-cluster periodic solution. (c) Nonsymmetric cluster solution. (d) Stable 1-cluster periodic solution, not Hopf bifurcating periodic solutions.

We then consider $\epsilon = 0.046$. In this case, the τ bifurcation values are

$$0 < \hat{\tau}^+_{1,0}(0.69) < \hat{\tau}^-_{1,0}(1.20) < \tau^+_{0,1}(1.26) < \tau^+_{1,1}(3.33) < \tau^-_{0,1}(3.43) < \tau^-_{1,1}(3.94) < \hat{\tau}^+_{1,1}(5.57)$$

The theory predicts that the equilibrium point E^* is stable when $\tau \in (0, 0.69) \cup (1.20, 1.26) \cup (3.94, 5.57)$, stable 1-cluster solutions exist for $\tau \gtrapprox 1.26$, and stable 6-cluster solutions exist for $\tau \gtrapprox 0.69, 5.57$ and $\tau \lessapprox 1.20$. Numerical simulations are performed for $\tau = 0.1, 0.2, \cdots, 6.0$, and the simulation results are summarized in Table 5.3. As above, we observe the coexisting stable of symmetric cluster solutions and nonsymmetric cluster solutions.

E^*	6-cluster	1-cluster	Other
0.1 - 0.7, 3.9 - 4.9, 5.3 - 5.5	0.9 - 1.2	1.6 - 2.8, 3.1, 3.2	All other values

Table 5.3: Summary of numerical simulations for $\epsilon = 0.046$ and $\tau = 0.1, 0.2, \cdots, 6.0$.

5.6 Conclusion

In this chapter, we investigated Hopf bifurcations of a general network of N globally coupled identical nodes with time delayed coupling. We derived expressions for all delay induced Hopf bifurcations from a symmetric equilibrium point and used symmetric bifurcation theory to determine the cluster periodic solutions which are created by these bifurcations. Our results apply to most typical neural network models, including both biophysical (conductance-based) and artificial networks.

We applied our results to two particular models: a network of FitzHugh-Nagumo neurons with delayed, diffusive coupling and a network of Morris-Lecar neurons with delayed, synaptic coupling.

For the FitzHugh-Nagumo model, we completely described the delay independent stability of the symmetric equilibrium point and the delay induced Hopf bifurcations, and gave explicit expressions for the critical delay values, showing how these depend on other parameters, including the coupling strength and the parameter (a) that induces oscillations in the uncoupled neural model. Further, using the method of multiple scales, we explicitly derived the normal forms at Hopf bifurcation critical points, which determine the direction of Hopf bifurcation and stability of bifurcating periodic orbits.

Due to the nonlinearity of the Morris-Lecar model, we were unable to give explicit expressions. However, we numerically described the delay independent stability of the

symmetric equilibrium points for various sets of parameter values and the delay induced Hopf bifurcations. Again, normal forms at Hopf bifurcation critical points are calculated by the method of multiple scales, and the direction of Hopf bifurcation and stability of bifurcating periodic solutions are numerically calculated.

We illustrated our results for specific parameter values in the two example models, focussing on the case of 6 neurons. We presented curves of Hopf bifurcations in the parameter space consisting of the coupling delay and coupling strength and studied how these curves change as the parameter a (I_{app}) is varied. We showed that Hopf bifurcations leading to stable cluster solutions could occur both in the case where the neurons are intrinsically oscillating and when they are not. Theoretical results, confirmed by numerical simulations, indicate that increasing the time delay can cause the stable solution to switch between the equilibrium solution and $1, 2, 3$ or $6-$ cluster periodic orbits.

We note that symmetric bifurcations exist in the coupled system with no delay, but occur in a strict ordering in parameter space. The delay causes variation in the ordering of the curves, allowing for bifurcation of stable solutions of all cluster types. Further, this reordering gives rise to intersection points of the various Hopf bifurcations, which correspond to co-dimension two Hopf-Hopf bifurcation points. Such points, which are quite common in delay systems [4, 123], can lead to coexistence of multiple stable periodic solutions or tori [52]. Indeed, in other numerical simulations we have found stable torus solutions (Figure 5.18(a)) and parameter values where two or more stable symmetric cluster solutions co-exist (not shown). As previously noted, other solutions not predicted by our results occur (see Figure 5.18(b)). The origin of such solutions is a topic for future work.

For the FitzHugh-Nagumo model, the delay-induced Hopf bifurcations in the case study we considered are linked to supercritical Hopf bifurcations in the uncoupled neurons. This can be seen as follows. Taking $\tau^{\pm}_{k,0}$ to zero, implies that $\epsilon(\alpha_k - \bar{w}) + 1 - a^2 = 0$, which is the Hopf bifurcation condition for the nondelayed system (see Lemma 4 and Figure 5.2). Further, as ϵ goes to zero we obtain the Hopf bifurcation condition in the uncoupled neuron, $1 - a^2 = 0$. Thus the cluster patterns can be thought of as emanating from an interaction of the delay with the intrinsic oscillation mechanism of the neurons. In neural models exhibiting Type II excitability, where oscillations are created by a subcritical Hopf bifurcations, we expect that a similar mechanism for creating cluster patterns can occur. For the network of Morris-Lecar oscillators, the parameters that we choose such that a saddle node on an invariant circle (SNIC) bifurcations occur for a single oscillator. That is, oscillations are created by the SNIC bifurcations. Interaction of the Hopf bifurcation and SNIC bifurcation causes complexities in the solution patterns. However, delay induced cluster patterns are still observed ([115]). In general, since most Type I model neurons have a Hopf bifurcation involved in the destruction of limit cycles we conjecture that the

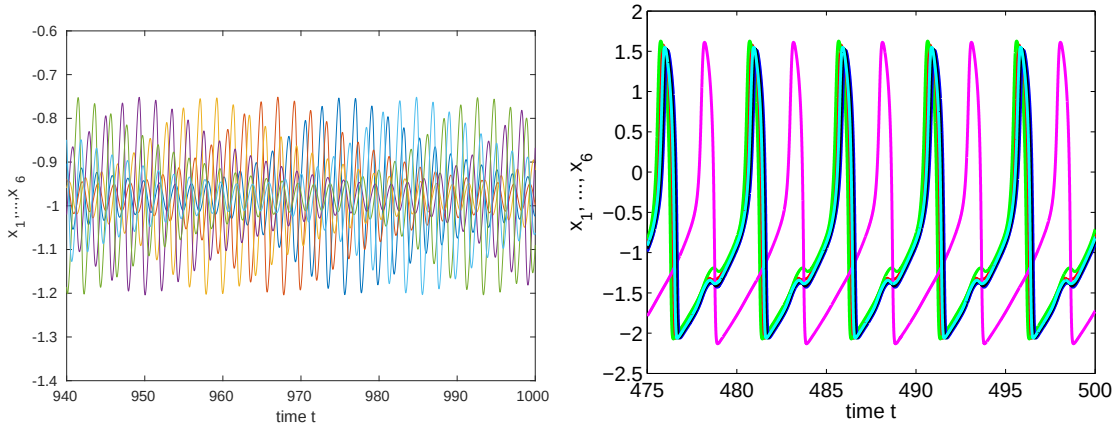

(a) $\epsilon = 0.021, \tau = 1.4$ (b) $\epsilon = 0.04, \tau = 2.2$

Figure 5.18: Numerical simulations showing stable solutions not predicted by theory. (a) Torus. (b) Non-symmetric cluster periodic orbit.

mechanism we have discussed may still come into play.

Chapter 6

Discussion and future directions

In this thesis, we study clustering behaviour in networks with time delayed, circulant coupling.

The analysis in chapter 4 is an extension to the work of [91, 82, 76]. It determines the existence and stability for all symmetric cluster solutions of networks of arbitrary size with time delay coupling. Our work provides explicit dependence of the eigenvalues that determine stability of symmetric cluster states on the coupling strength and time delay. An important question that arises in this analysis is how small the coupling strength ϵ should be to guarantee the accuracy of the phase model prediction. The question is answered numerically for the specific network of Morris-Lecar oscillators. Another question is whether these results can be applied to networks with arbitrary global coupling. The answer is positive but several new problems arise. First, the stability conditions become more complicated and difficult to calculate. Intuitively, we utilize the circulant property of the coupling matrix W in the stability analysis of clustering solutions. For a coupling matrix without any symmetry, the existence conditions of symmetric cluster solutions will remain the same while the stability conditions will be more complicated and highly depend on the coupling matrix.

In chapter 5, we investigate the stability of the steady state and Hopf bifurcation induced by the time delay. The relation between the critical values of delay τ and patterns of Hopf bifurcating cluster solutions are found explicitly. For the FitzHugh-Nagumo model, the regions that are asymptotically stable, globally stable and absolute unstable are determined in the plane of the excitability parameter a and the coupling strength ϵ. Furthermore, we use the method of multiple time scales to calculate the normal form of the Hopf bifurcation at critical τ (ϵ) values. We find that just by decreasing the coupling strength, the dynamics of the system can change from the equilibrium point to any symmetric clus-

ter solutions. By increasing the time delay, the dynamics of the system can switch from the equilibrium point to symmetric cluster solutions and back to the equilibrium point or other symmetric cluster solutions, and so on.

The stability of clustering behaviour in this thesis supports the hypothesis that cluster solutions play a role in neural assembly. First, the variation of stability with coupling is one of the key results. For example, our numerical studies of a network of six Morris-Lecar oscillators for $\epsilon = 0.01$ (Tables 4.3 and 4.4) show that there exist stable 2-cluster solutions and stable 3-cluster solutions with bi-directional coupling and $\tau \in (4.18, 8.00)$, while with homogeneous coupling the 3-cluster states lose stability and leave only the 2-cluster solutions. Thus switching from bi-directional coupling to homogeneous coupling gives a mechanism that the system can switch from 3-cluster solutions to 2-cluster equations, i.e., reorganizing which neurons spikes together. On the other hand, the simulation studies in Figures 4.8 and 4.9 suggests another way of producing neural assembly, which is via varying the inputs to the neurons. In Figures 4.8 and 4.9, we can get different cluster solutions without varying the network connections. Thus, it is possible for networks to possess multiple stable solutions with the same number of clusters but with different grouping of neurons.

The work in this thesis also provide actual evidence that the axonal conduction delays play a more important role in time dependencies than generally recognized. It is well known that axonal conduction delays are very precisely timed. They vary greatly in the mammalian nervous system, from less than 0.1 milliseconds in very short axons to greater than 0.1 milliseconds in very long non-myelinated central axons [111]. However, it is usually thought that they cannot give rise to delays more than 10 milliseconds. Therefore, the impact of axonal conduction time is usually neglected. On the contrary, we show that axonal conduction delays have a profound influence on the clustering behaviour. Take the Morris-Lecar networks as a example. Based on the non-dimensionalization procedure, we get that the dimensionless time delay τ in the thesis corresponds to a time delay of 5 $\times\tau$ milliseconds. That is, $\tau = 1$ corresponds to 5 milliseconds and $\tau = 2$ corresponds to 10 milliseconds. Recall that in section 2.4 we discuss that the time delay τ here include two parts: the axonal conduction delay and the processing delay. By the Hopf bifurcation analysis in section 5.5.3, we see that by increasing the time delay from 0 to 10 milliseconds, the simple system with six Morris-Lecar neurons switches between the equilibrium, 6-cluster solutions, 3-cluster solutions and 2-cluster solutions for different coupling strength. For networks with more neurons, the time delay can lead to more complex dynamic behaviour.

For future study, we would like to extend our work in the following directions.

1. Extend all the results to networks with time delayed, general global coupling.

2. Extend all the results to networks with different oscillators instead of identical elements.

3. Extend the stability analysis for general synchronization solutions in section 4.3.3 to any symmetric cluster solutions.

4. Seek the existence and stability conditions for non-symmetric cluster solutions.

5. Extend the Hopf bifurcation analysis for networks with more symmetry, for example, networks with bidirectional coupling (D_N symmetry) and global homogeneous coupling (S_N symmetry).

References

[1] P. Ashwin and J.W. Swift. The dynamics of n weakly coupled identical oscillators. *J. Nonlinear Sci.*, 2:69–108, 1992.

[2] M. Bartos, I. Vida, M. Frotscher, J.R.P. Geiger, and P. Jonas. Rapid signaling at inhibitory synapses in a dentate gyrus interneuron network. *J. Neurosci.*, 21:2687–2698, 2001.

[3] M. Bartos, I. Vida, M. Frotscher, A. Meyer, H. Monyer, J.R.P. Geiger, and P. Jonas. Fast synaptic inhibition promotes synchronized gamma oscillations in hippocampal interneuron networks. *Proc. Natl. Acad. Sci.*, 99(20):13222–13227, 2002.

[4] J. Bélair and S. A. Campbell. Stability and bifurcations of equilibria in a multiple-delayed differential equation. *SIAM J. Appl. Math.*, 54(5):1402–1424, 1994.

[5] K.B. Blyuss. The effects of symmetry on the dynamics of antigenic variation. *J. Mathematical Biology*, pages 1–23, 2013.

[6] K.B. Blyuss. Analysis of symmetries in models of multi-strain infections. *J. Mathematical Biology*, 69(6-7):1431–1459, 2014.

[7] K.B. Blyuss and Y.N. Kyrychko. Symmetry breaking in a model of antigenic variation with immune delay. *Bulletin of Mathematical Biology*, 74(10):2488–2509, 2012.

[8] P. Bressloff and S. Coombes. Symmetry and phase-locking in a ring of pulse-coupled oscillators with distributed delays. *Physica D*, 126:99–122, 1999.

[9] P. Bressloff and S. Coombes. Travelling waves in chains of pulse-coupled integrate-and-fire oscillators with distributed delays. *Physica D*, 130:232–254, 1999.

[10] E. Brown, P. Holmes, and J. Moehlis. Globally coupled oscillator networks. In E. Kaplan, J. Marsden, and K. Sreenivasan, editors, *Perspectives and Problems in*

Nonlinear Science: A Celebratory Volume in Honor of Larry Sirovich, pages 183–215. Springer, New York, NY, 2003.

[11] S.D. Bungay and S.A. Campbell. Patterns of oscillation in a ring of identical cells with delayed coupling. *International J. Bifurcation and Chaos*, 17(9):3109–3125, 2007.

[12] P.L. Buono and J.A. Collera. Symmetry-breaking bifurcations in rings of delay-coupled semiconductor lasers. *SIAM J. Applied Dynamical Systems*, 14(4):1868–1898, 2015.

[13] N. Burić, I. Grozdanović, and N. Vasović. Type I vs type II excitable systems with delayed coupling. *Chaos, Solitons and Fractals*, 23:1221–1233, 2005.

[14] N. Burić and D. Todorović. Dynamics of Fitzhugh-Nagumo excitable systems with delayed coupling. *Phys. Rev. E*, 67:066222, 2003.

[15] N. Burić and D. Todorović. Bifurcations due to small time-lag in coupled excitable systems. *Int. J. Bifurc. Chaos*, 15(5):1775–1785, 2005.

[16] S.A. Campbell. Time delays in neural systems. In R. McIntosh and V. K. Jirsa, editors, *Handbook of Brain Connectivity*. Springer-Verlag, New York, 2007.

[17] S.A. Campbell, R. Edwards, and P. van den Dreissche. Delayed coupling between two neural network loops. *SIAM J. Applied Mathematics*, 65(1):316–335, 2004.

[18] S.A. Campbell and I. Kobelevskiy. Phase models and oscillators with time delayed coupling. *Dynamics of Discrete and Continuous Systems*, 38(8):2653–2673, 2012.

[19] S.A. Campbell, I. Ncube, and J. Wu. Multistability and stable asynchronous periodic oscillations in a multiple-delayed neural system. *Physica D*, 214(2):101–119, 2006.

[20] S.A. Campbell and Z. Wang. Phase models and clustering in networks of oscillators with delayed coupling. *arXiv preprint arXiv:1607.05759*, 2016.

[21] S.A. Campbell, Y. Yuan, and S.D. Bungay. Equivariant Hopf bifurcation in a ring of identical cells with delayed coupling. *Nonlinearity*, 18(6):2827, 2005.

[22] J.D. Cao and L.L. Li. Cluster synchronization in an array of hybrid coupled neural networks with delay. *Neural Networks*, 22(4):335–342, 2009.

[23] J. Carr. *Applications of Center Manifold Theory*. Springer-Verlag, New York, 1981.

[24] C-U. Choe, T. Dahms, P. Hövel, and E. Schöll. Controlling synchrony by delay coupling in networks: From in-phase to splay and cluster states. *Phys. Rev. E*, 81(2):025205, 2010.

[25] J.A. Connor and C.F. Stevens. Prediction of repetitive firing behaviour from voltage clamp data on an isolated neurone soma. *The Journal of Physiology*, 213(1):3153, 1971.

[26] S.M. Crook, G.B. Ermentrout, M.C. Vanier, and J.M. Bower. The role of axonal delay in synchronization of networks of coupled cortical oscillators. *J. Comp. Neurosci.*, 4:161–172, 1997.

[27] M.A. Dahlem, G.Hiller, A. Panchuk, and Schöll E. Dynamics of delay-coupled excitable neural systems. *International Journal of Bifurcaion and Chaos*, 19:745–753, 2009.

[28] T. Dahms, J. Lehnert, and E. Schöll. Cluster and group synchronization in delay-coupled networks. *Phys. Rev. E*, 86(1):016202, 2012.

[29] P.J. Davis. *Circulant matrices*. Wiley, New York, 1979.

[30] A. Destexhe, Z.F. Mainen, and T.J. Sejnowski. Kinetic models of synaptic transmission. In C. Koch and I. Segev, editors, *Methods in Neuronal Modeling: From Synapses to Networks*, chapter 1. MIT Press, Cambridge, MA, 1998.

[31] F. Dörfler and F. Bullo. Synchronization in complex networks of phase oscillators: A survey. *Automatica*, 50(6):1539–1564, 2014.

[32] G. Dragoi and G. Buzsáki. Temporal encoding of place sequences by hippocampal cell assemblies. *Neuron*, 50(1):145–157, 2006.

[33] M.G. Earl and S.H. Strogatz. Synchronization in oscillator networks with delayed coupling: a stability criterion. *Physical Review E*, 67:036204, 2003.

[34] A.K. Engel, P. Fries, and W. Singer. Dynamic predictions: oscillations and synchrony in top–down processing. *Nature Reviews Neuroscience*, 2(10):704–716, 2001.

[35] K. Engelborghs, T. Luzyanina, and G. Samaey. DDE-BIFTOOL v. 2.00: a MATLAB package for bifurcation analysis of delay differential equations. Technical Report TW-330, Department of Computer Science, K.U. Leuven, Leuven, Belgium, 2001.

[36] G.B. Ermentrout. An introduction to neural oscillators. In F. Ventriglia, editor, *Neural Modelling and Neural Networks*, pages 79–110. Pergamon, Oxford, UK, 1994.

[37] G.B. Ermentrout. Type I membranes, phase resetting curves, and synchrony. *Neural Comput.*, 8:979–1001, 1996.

[38] G.B. Ermentrout. *Simulating, analyzing, and animating dynamical systems: a guide to XPPAUT for researchers and students*, volume 14. SIAM, Philadephia, PA, 2002.

[39] G.B. Ermentrout and N. Kopell. Frequency plateaus in a chain of weakly coupled oscillators I. *SIAM J. Applied Math.*, 15:215–237, 1984.

[40] G.B. Ermentrout and N. Kopell. Multiple pulse interactions and averaging in couple neural oscillators. *J. Math. Biol.*, 29:195–217, 1991.

[41] G.B. Ermentrout and D.H. Terman. *Mathematical Foundations of Neuroscience*. Springer, New York, NY, 2010.

[42] M. Farkas. *Periodic Motions*. Springer Science + Business Media, LLC, New York, 1994.

[43] R. FitzHugh. Impulses and physiological states in theoretical models of nerve membrane. *Biophysical J.*, 1:445–466, 1961.

[44] J. Foss, A. Longtin, B. Mensour, and J. Milton. Multistability and delayed recurrent feedback. *Phys. Rev. Lett.*, 76:708–711, 1996.

[45] J. Foss and J. Milton. Multistability in recurrent neural loops arising from delay. *J. Neurophysiol.*, 84:975–985, 2000.

[46] J. Foss, F. Moss, and J. Milton. Noise, multistability and delayed recurrent loops. *Phys. Rev. E*, 55:4536–4543, 1997.

[47] R.F. Galán. The phase oscillator approximation in neuroscience: an analytical framework to study coherent activity in neural networks. In *Coordinated Activity in the Brain*, pages 65–89. Springer, 2009.

[48] R.F. Galán, G.B. Ermentrout, and N.N. Urban. Predicting synchronized neural assemblies from experimentally estimated phase-resetting curves. *Neurocomputing*, 69(10):1112–1115, 2006.

[49] D. Golomb and J. Rinzel. Clustering in globally coupled inhibitory neurons. *Physica D*, 72:259–282, 1994.

[50] M. Golubitsky, I. Stewart, and D. G. Schaeffer. *Singularities and Groups in Bifurcation Theory*. Springer-Verlag, New York, 1988.

[51] R.M. Gray. *Toeplitz and circulant matrices: A review*. Now Publishers Inc, 2006.

[52] J. Guckenheimer and P.J. Holmes. *Nonlinear Oscillations, Dynamical Systems and Bifurcations of Vector Fields*. Springer-Verlag, New York, 1983.

[53] S. Guo, L. Huang, and L. Wang. Linear stability and Hopf bifurcation in a two neuron network with three delays. *Internat. J. Bifur. Chaos*, 14:27992810, 2004.

[54] S.J. Guo and L.H. Huang. Hopf bifurcating periodic orbits in a ring of neurons with delays. *Physica D*, 183(1):19–44, 2003.

[55] S.J. Guo and L.H. Huang. Stability of nonlinear waves in a ring of neurons with delays. *J. Differential Equations*, 236(2):343–374, 2007.

[56] S.J. Guo and J.H. Wu. *Bifurcation Theory of Functional Differential Equations*. Springer, New York, 2013.

[57] J.K. Hale. *Theory of Functional Differential Equations*. Springer-Verlag, New York, 1977.

[58] J.K. Hale and S.M. Verduyn Lunel. *Introduction to Functional Differential Equations*. Springer Verlag, New York, 1993.

[59] D. Hansel, G. Mato, and C. Meunier. Phase dynamics for weakly coupled Hodgkin-Huxley neurons. *Europhys. Lett.*, 23(5):367–372, 1993.

[60] D. Hansel, G. Mato, and C. Meunier. Synchrony in excitatory neural networks. *Neural Computation*, 7:307–337, 1995.

[61] K.D. Harris, J. Csicsvari, H. Hirase, G. Dragoi, and G. Buzsáki. Organization of cell assemblies in the hippocampus. *Nature*, 424(6948):552–556, 2003.

[62] J.L. Hindmarsh and R.M. Rose. A model of neuronal bursting using three coupled first order differential equations. *Proceedings of the Royal Society of London B*, 221(1222):87102, 1984.

[63] A.L. Hodgkin and A.F. Huxley. A quantitative description of membrane current and its application to conduction and excitation in nerve. *J. Physiology*, 117:500–544, 1952.

[64] F.C. Hoppensteadt and E.M. Izhikevich. *Weakly connected neural networks*. Springer-Verlag, New York, 1997.

[65] E.M. Izhikevich. Phase models with explicit time delays. *Phys. Rev. E*, 58:905–908, 1998.

[66] Z.P. Kilpatrick and G.B. Ermentrout. Sparse gamma rhythms arising through clustering in adapting neuronal networks. *PLoS computational biology*, 7(11):e1002281, 2011.

[67] S. Kim, S. H. Park, and C.S. Ryu. Multistability in coupled oscillator systems with time delay. *Phys. Rev. Lett.*, 79:2911–2914, 1997.

[68] I. Kobelevskiy. Bifurcation analysis of a system of Morris-Lecar neurons with time delayed gap junctional coupling. Master's thesis, University of Waterloo, 2008.

[69] N. Kopell and G.B. Ermentrout. Coupled oscillators and the design of central pattern generators. *Math. Biosci.*, 90:87–109, 1988.

[70] N. Kopell and G.B. Ermentrout. Mechanisms of phase-locking and frequency control in pairs of coupled neural oscillators. In B Fiedler, editor, *Handbook of Dynamical Systems, vol 2: Toward Applications*, pages 3–54. Elsevier, Amsterdam, 2002.

[71] M. Krupa, S. Gielen, and B. Gutkin. Adaptation and shunting inhibition leads to pyramidal/interneuron gamma with sparse firing of pyramidal cells. *J. Computational Neuroscience*, 37(2):357–376, 2014.

[72] Y. Kuang. *Delay Differential Equations with Applications in Population Dynamics.* Academic Press, Boston San Diego, New York, 1993.

[73] Y. Kuramoto. Cooperative dynamics of oscillator community. A study based on lattice of rings. *Prog. Theor. Phys. Suppl.*, 79:223–240, 1984.

[74] Y.A. Kuznetsov. *Elements of Applied Bifurcation Theory.* Springer-Verlag, New York, 2004.

[75] G. Laurent and H. Davidowitz. Encoding of olfactory information with oscillating neural assemblies. *Science*, 265(5180):1872–1875, 1994.

[76] Y.-X. Li. Clustering in neural networks with heterogeneous and asymmetrical coupling strengths. *Physica D*, 180:210–234, 2003.

[77] Y.-X. Li, Y.-Q. Wang, and R. Miura. Clustering in small networks of excitatory neurons with heterogeneous coupling strengths. *J. Computational Neuroscience*, 14:139–159, 2003.

[78] T. Luzyanina. Synchronization in an oscillator neural network model with time-delayed coupling. *Network: Computation in Neural Systems*, 6:43–59, 1995.

[79] J. Ma and J. Wu. Multistability in spiking neuron models of delayed recurrent inhibitory loops. *Neural Comp.*, 19:2124–2148, 2007.

[80] J.F. Ma and J.H. Wu. Multistability and gluing bifurcation to butterflies in coupled networks with non-monotonic feedback. *Nonlinearity*, 22(6):1383, 2009.

[81] J.G. Mancilla, T.J. Lewis, D.J. Pinto, J. Rinzel, and B.W. Connors. Synchronization of electrically coupled pairs of inhibitory interneurons in neocortex. *J. Neuroscience*, 27(8):2058–2073, 2007.

[82] J. Miller, H. Ryu, Z. Teymuroglu, X. Wang, V. Booth, and S.A. Campbell. Clustering in inhibitory neural networks with nearest neighbor coupling. In T. Jackson and A. Radunskaya, editors, *Applications of Dynamical Systems in Biology and Medicine*, pages 99–121. Springer, New York, 2015.

[83] R.E. Mirollo and S.H. Strogatz. Synchronization of pulse-coupled biological oscillators. *SIAM J. Appl. Math.*, 50(6):1645–1662, 1990.

[84] C. Morris and H. Lecar. Voltage oscillations in the barnacle giant muscle fibre. *Biophysical J.*, 35:193–213, 1981.

[85] J. Nagumo, S. Arimoto, and S. Yoshizawa. An active pulse transmission line simulating nerve axon. *Proceeding IRE*, 50:2061–2070, 1962.

[86] A.H. Nayfeh. *Perturbation Methods*. Wiley-Interscience, New York, 1973.

[87] A.H. Nayfeh. *Introduction to Perturbation Techniques*. Wiley-Interscience, New York, 1981.

[88] A.H. Nayfeh. Order reduction of retarded nonlinear system: the method of multiple scales versus center manifold reduction. *Nonlinear Dynamics*, 51:483–500, 2008.

[89] I. Ncube, S.A. Campbell, and J. Wu. Change in criticality of synchronous Hopf bifurcation in a multiple-delayed neural system. *Fields Inst. Commun.*, 36:17–193, 2003.

[90] E. Niebur, H.G. Schuster, and D.M. Kammen. Collective frequencies and metastability in networks of limit-cycle oscillators with time delay. *Physical Review Letters*, 67:2753–2756, 1991.

[91] K. Okuda. Variety and generality of clustering in globally coupled oscillators. *Physica D*, 63:424–436, 1993.

[92] G. Orosz. Decomposing the dynamics of delayed networks: equilibria and rhythmic patterns in neural systems. In *10th IFAC Workshop on Time Delay Systems*, pages 173–178, 2012.

[93] G. Orosz. Decomposing the dynamics of delayed Hodgkin-Huxley neurons. In *Delay Systems*, pages 343–357. Springer, 2014.

[94] G. Orosz. Decomposition of nonlinear delayed networks around cluster states with applications to neurodynamics. *SIAM J. Applied Dynamical Systems*, 13(4):1353–1386, 2014.

[95] A. Panchuk, D.P. Rosin, P. Hövel, and E. Schöll. Synchronization of coupled neural oscillators with heterogeneous delays. *International J. Bifurcation and Chaos*, 23(12), 2013.

[96] D. Paré, R. Curro'Dossi, and M. Steriade. Neural basis of the parkinsonian, resting tremor: a hypothesis and its implication for treatment. *Neuroscience*, 35(2):217–226, 1990.

[97] E. Pastalkova, V. Itskov, A. Amarasingham, and G. Buzsáki. Internally generated cell assembly sequences in the rat hippocampus. *Science*, 321(5894):1322–1327, 2008.

[98] M. Radice. A diagram of the neuron highlighting the chain structure between the axon and dendrite. http://mikerbio.weebly.com/structure--function.html.

[99] J. Rinzel and G.B. Ermentrout. Analysis of neural excitability and neural oscillations. In C. Koch and I. Segev, editors, *Methods in Neuronal Modeling: From synapses to networks*, pages 251–291. MIT Press, Cambridge, MA, 1989.

[100] Y. Sakurai. Hippocampal and neocortical cell assemblies encode memory processes for different types of stimuli in the rat. *J. Neuroscience*, 16(8):2809–2819, 1996.

[101] F. Saraga, L. Ng, and F.K. Skinner. Distal gap junctions and active dendrites can tune network dynamics. *J. Neurophysiology*, 95(3):1669–1682, 2006.

[102] E. Schöll, G. Hiller, P. Hövel, and M.A. Dahlem. Time-delay feedback in neurosystems. *Philosophical Transactions Royal Society A*, 367:1079–10956, 2009.

[103] H.G. Schuster and P. Wagner. Mutual entrainment of two limit cycle oscillators with time delayed coupling. *Prog. Theor. Phys.*, 82(5):939–945, 1989.

[104] M.A. Schwemmer and T.J. Lewis. The theory of weakly coupled oscillators. In N.W. Schultheiss, A.A. Prinz, and R.J. Butera, editors, *Phase Response Curves in Neuroscience*, pages 3–31. Springer, New York, NY, 2012.

[105] G.C. Sethia, A. Sen, and F.M. Atay. Clustered chimera states in delay-coupled oscillator systems. *Physical review letters*, 100(14):144102, 2008.

[106] G.C. Sethia, A. Sen, and F.M. Atay. Phase-locked solutions and their stability in the presence of propagation delays. *Pramana*, 77(5):905–915, 2011.

[107] Y. Song and J. Xu. Inphase and antiphase synchronization in a delay-coupled system with applications to a delay-coupled Fitzhugh-Nagumo system. *IEEE Transactions on Neural Networks and Learning Systems*, 23(10):1659–1670, 2012.

[108] T. Splettstoesser. Schematic of a synapse. https://commons.wikimedia.org/wiki/File:SynapseSchematic_en.svg.

[109] G. Stépán. *Retarded dynamical systems: stability and characteristic functions*. Longman Scientific and Technical, England, 1989.

[110] G. Strang. *Introduction to Applied Mathematics*. Wellesley Cambridge Press, Wellesley, MA, 1986.

[111] H.A. Swadlow and S.G. Waxman. Axonal conduction delays. *Scholarpedia*, 7(6):1451, 2012.

[112] A. Takamatsu, T. Fujii, and I. Endo. Time delay effect in a living coupled oscillator system with plasmodium of *physarum polycephalum*. *Phys. Rev. E*, 85(9):2026–2029, 2000.

[113] G.J. Tee. Eigenvectors of block circulant and alternating circulant matrices. *Res. Lett. Inf. Math. Sci.*, 8:123–142, 2005.

[114] X. Wang and G. Buzsáki. Gamma oscillation by synaptic inhibition in a hippocampal interneuronal network model. *The journal of Neuroscience*, 16(20):64026413, 1996.

[115] Z. Wang and S.A Campbell. Phase models and clustering in networks of oscillators with delayed, all-to-all coupling. In *12th IFAC Workshop on Time Delay Systems*, pages 105–110, 2015.

[116] M. Wehr, G. Laurent, et al. Odour encoding by temporal sequences of firing in oscillating neural assemblies. *Nature*, 384(6605):162–166, 1996.

[117] S. Wiggins. *Introduction to Applied Nonlinear Dynamical Systems and Chaos*. Springer-Verlag, New York, 1990.

[118] H.G. Winful and S.S. Wang. Dynamics of phaselocked semiconductor laser arrays. *Applied Physics Letters*, 52(21):1774–1776, 1988.

[119] H.G. Winful and S.S. Wang. Stability of phase locking in coupled semiconductor laser arrays. *Applied Physics Letters*, 53(20):1894–1896, 1988.

[120] J.H. Wu. Symmetric functional-differential equations and neural networks with memory. *Trans. Amer. Math. Soc.*, 350(12):4799–4838, 1998.

[121] M.K.S. Yeung and S.H. Strogatz. Time delay in the Kuramoto model of coupled oscillators. *Phys. Rev. Lett.*, 82:648–651, 1999.

[122] J.Y. Ying and Y. Yuan. Pattern formation in a symmetrical network with delay. *Nonlinear Analysis: Real World Applications*, 14(2):1102–1113, 2013.

[123] J.Y. Ying and Y. Yuan. Codimension one and two bifurcations in a symmetrical ring network with delay. *J. Mathematical Analysis and Applications*, 425(2):1155–1176, 2015.

[124] P. Yu. Computation of normal forms via a perturbation technique. *J. Sound Vibr.*, 211:19–38, 1998.

[125] P. Yu, Y.T. Ding, and W.H. Jiang. Equivalence of the MTS method and CMR method for differential equations associated with semisimple singularity. *International Journal of Bifurcation and Chaos*, 24:1450003, 2014.

[126] T. Zahid and F.K. Skinner. Predicting synchronous and asynchronous network groupings of hippocampal interneurons coupled with dendritic gap junctions. *Brain Research*, 1262:115–129, 2009.

[127] S.F. Zou, Y.M. Chen, and J.H. Wu. Delay for the capacity-simplicity dilemma in associative memory attractor networks. *Neural Networks*, 29:37–51, 2012.